REFERENCES

Adelôdun, A.A. (2014) Effect of basicity on amination of activated carbon pellets modified for CO_2 adsorption. Purity, Utility Reaction, and Environment, 3(1), 17.

Alkhabbaz, M.A., Khunsupat, R., and Jones, C.W. (2014) Guanidinylated poly(allylamine) supported on mesoporous silica for CO_2 capture from flue gas. Fuel, 121, 79-85.

Al-Muhtaseb, S.A. and Ritter, J.A. (2003) Preparation and properties of resorcinol–formaldehyde organic and carbon gels. Advanced Materials, 15(2), 101-114.

Amrita. 'Comparison between physisorption and chemisorption." Vlab.amrita.edu. 6 June 2014 <http://amrita.vlab.co.in/?sub=2&brch=190&sim=606& nt=1>

Ardanuy, M., Rodríguez-Pérez, M.Á., de Saja, J.A., and Velasco, J.I. (2012) Foaming behavior, cellular structure and physical properties of polybenzoxazine foams. Polymers for Advanced Technologies, 23(5), 841-849.

Berger, A.H. and Bhown, A.S. (2011) Comparing physisorption and chemisorption solid sorbents for use separating CO_2 from flue gas using temperature swing adsorption. Energy Procedia, 4, 562-567.

Blackman, J.M., Patrick, J.W., and Snape, C.E. (2006) An accurate volumetric differential pressure method for the determination of hydrogen storage capacity at high pressures in carbon materials. Carbon, 44(5), 918-927.

Brooks, C. and Media, D. " Calculate Theoretical Percent" Classroom. 11 June 2015 < http://classroom.synonym.com/calculate-theoretical-percent-2826 .html>

Burhenne, L. and Aicher, T. (2014) Benzene removal over a fixed bed of wood char: The effect of pyrolysis temperature and activation with CO_2 on the char reactivity. Fuel Processing Technology, 127, 140-148.

Burg, P., Fydrych, P., Cagniant, D., Nanse, G., Bimer, J., and Jankowska, A. (2002) The characterization of nitrogen-enriched activated carbons by IR, XPS and LSER methods. Carbon, 40, 1521–1531.

Casco, M.E., Martínez-Escandell, M., Silvestre-Albero, J., and Rodríguez-Reinoso, F. (2014) Effect of the porous structure in carbon materials for CO_2 capture at atmospheric and high-pressure. Carbon, 67, 230-235.

CCS Masters. "CO_2 capture and separation." Capture Ready. 17 Apr 2014 <http: //www.captureready.com/en/Channels/OverViews/showDetail.asp?ClassID =1.>

Chaisuwan, T. (2011) Porous materials from polybenzoxazine. In Ishida, H. and Agag, T. Amsterdam (Eds.), Handbook of Benzoxazine Resins (pp. 457- 468). Leicestershire: Elsevier Science.

Chaisuwan, T., Komalwanich, T., Luangsukrerk, S., and Wongkasemjit, S. (2010) Removal of heavy metals from model wastewater by using polybenzoxazine aerogel. Desalination, 256(1–3), 108-114.

Choi, S., Drese, J.H., and Jones, C.W. (2009) Adsorbent materials for carbon dioxide capture from large anthropogenic point sources. ChemSusChem, 2(9), 796-854.

Cook, P.J. (2012). Clean Energy, Climate and Carbon. Canberra: CSIRO Pub- lishing.

Cotet, L.C., Danciu, V., Cosoveanu, V., Popesc, I.C., Roig, A., and Molins, E. (2007) Synthesis of meso- and macroporous carbon aerogels. Revue Roumaine de Chimie, 52(11), 6.

Coutinho, D.F., Sant, S., Shakiba, M., Wang, B., Gomes, M.E., Neves, N.M., Reis, R.L. and Khademhosseini, A. (2012) Microfabricated photocrosslinkable polyelectrolyte-complex of chitosan and methacrylated gellan gum. Journal of Materials Chemistry, 22(33), 17262-17271.

Danish, M., Hashim, R., Ibrahim, M.N.M., and Sulaiman, O. (2014) Optimized pre- paration for large surface area activated carbon from date (Phoenix dactylifera L.) stone biomass. Biomass and Bioenergy, 61, 167-178.

Davis, M.E. (2002) Ordered porous materials for emerging applications. Chemical Engineering, 417, 813-821.

Drage, T.C., Arenillas, A., Smith, K.M., Pevida, C., Piippo, S., and Snape, C.E. (2007) Preparation of carbon dioxide adsorbents from the chemical activation of urea–formaldehyde and melamine–formaldehyde resins. Fuel, 86(1–2), 22-31.

Fu, K., Yue, Q., Gao, B., Sun, Y., and Zhu, L. (2013) Preparation, characterization and application of lignin-based activated carbon from black liquor lignin by steam activation. Chemical Engineering Journal, 228, 1074-1082.

Furmaniak, S., Kowalczyk, P., Terzyk, A.P., Gauden, P.A., and Harris, P.J.F. (2013) Synergetic effect of carbon nanopore size and surface oxidation on CO_2 capture from CO_2/CH_4 mixtures. Journal of Colloid and Interface Science, 397, 144-153.

He, H., Li, W., Lamson, M., Zhong, M., Konkolewicz, D., Hui, C.M., Yaccato, K., Rappold, T., Sugar, G., David, N.E., Damodaran, K., Natesakhawat, S., Nulwala, H., and Matyjaszewski, K. (2014) Porous polymers prepared via high internal phase emulsion polymerization for reversible CO_2 capture. Polymer, 55(1), 385-394.

Hirikamol, N. (2013) Polybenzoxazine Sorbents for CO_2 Capture. M.S. Thesis, The Petroleum and Petrochemical College, Chulalongkorn University, Bangkok, Thailand.

Hsu, S.H., Lin, Y.F., Chung, T.W., Wei, T.Y., Lu, S.Y., Tung, K.L., and Liu, K.T. (2013) Mesoporous carbon aerogel membrane for phospholipid removal from Jatropha curcas oil. Separation and Purification Technology, 109, 129-134.

Ishida, H. (2011) Overview and historical background of polybenzoxazine research. In Ishida, H. and Agag, T. Amsterdam (Eds.), Handbook of Benzoxazine Resins (pp. 3-81). Leicestershire: Elsevier Science.

Karl, T.R. and Trenberth, K.E. (2003) Modern Global Climate Change. Science, 302(5651), 1719-1723.

Katanyoota, P., Chaisuwan, T., Wongchaisuwat, A., and Wongkasemjit, S. (2010) Novel polybenzoxazine-based carbon aerogel electrode for supercapacitors. Materials Science and Engineering: B, 167(1), 36-42.

Kiskan, B. and Yagci, Y. (2014) Self-healing of poly(propylene oxide)-polybenzoxazine thermosets by photoinduced coumarine dimerization. Polymer Science Part A: Polymer Chemistry, 52(20), 2911-2918.

Kim, H.D. and Ishida, H. (2003). Model compounds study on the network structure of polybenzoxazines. Macromolecules, 36(22), 8320-8329.

Kwon, S.H., Lee, E., Kim, B.S., Kim, S.G., Lee, B.J., Kim, M.S., and Jung, J.C. (2014) Activated carbon aerogel as electrode material for coin-type EDLC cell in organic electrolyte. Current Applied Physics, 14(4), 603-607.

Larson, J.A., Liebowitz, J., and Coiera, E. (2011) Carbon Capture and Storage: Technologies, Policies, Economics, and Implementation Strategies. Riyadh : CRC Press.

Lee, K.B., Verdooren, A., Caram, H.S., and Sircar, S. (2007) Chemisorption of carbon dioxide on potassium-carbonate-promoted hydrotalcite. Journal of Colloid and Interface Science, 308(1), 30-39.

Lee, Y.J., Kim, G.-P., Bang, Y., Yi, J., Seo, J.G., and Song, I.K. (2014) Activated carbon aerogel containing graphene as electrode material for supercapacitor. Materials Research Bulletin, 50, 240-245.

Li, W., Reichenauer, G., and Fricke, J. (2002) Carbon aerogels derived from cresol–resorcinol–formaldehyde for supercapacitors. Carbon, 40(15), 2955-2959.

Liu, L. and Zhang, J. (2013) Triptycene-based microporous polymer with pending tetrazole moieties for CO_2-capture application. Macromolecular Rapid Communications, 34(23-24), 1833-1837.

Lorjai, P., Chaisuwan, T., and Wongkasemjit, S. (2009) Porous structure of polybenzoxazine-based organic aerogel prepared by sol–gel process and their carbon aerogels. Journal of Sol-Gel Science and Technology, 52(1), 56-64.

Lorjai, P., Wongkasemjit, S., and Chaisuwan, T. (2009) Preparation of polybenzoxazine foam and its transformation to carbon foam. Materials Science and Engineering: A, 527(1–2), 77-84.

Lorjai, P., Wongkasemjit, S., Chaisuwan, T., and Jamieson, A.M. (2011) Significant enhancement of thermal stability in the non-oxidative thermal degradation of bisphenol-A/aniline based polybenzoxazine aerogel. Polymer Degradation and Stability, 96(4), 708-718.

Marchal, V., Dellink, R., Vuuren, D.V., Christa, C., Chateau, J., Lanzi, E., Magne, B., and Vliet, J.V. (2011) OECD Environmental Outlook to 2050. (pp. 1-89) Paris: OECD Publishing.

McInerney, J. "Adsorption." CO2CRC. 17 Apr 2014 <http://www.co2crc.com.au/aboutccs/co2_capture_separation.html.>

Meng, L.Y. and Park, S.J. (2012) Investigation of Narrow Pore Size Distribution on Carbon Dioxide Capture of Nanoporous Carbons. Bulletin of the Korean Chemical Society, 33(11), 3749-3754.

Norby, P. "The different types of pores." Uio. 6 June 2014 <http://www.uio.no/studier/emner/matnat/kjemi/KJM5100/h06/undervisningsmateriale/16KJM5100_2006_porous_e.pdf.>

Pevida, C., Drage, T.C., and Snape, C.E. (2008) Silica-templated melamine–formaldehyde resin derived adsorbents for CO_2 capture. Carbon, 46(11), 1464-1474.

Plaza, M.G., Pevida, C., Arenillas, A., Rubiera, F., and Pis, J.J. (2007) CO_2 capture by adsorption with nitrogen enriched carbons. Fuel, 86(14), 2204-2212.

Plaza, M.G., Pevida, C., Arias, B., Fermoso, J., Arenillas, A., Rubiera, F., and Pis, J.J. (2008) Application of thermogravimetric analysis to the evaluation of aminated solid sorbents for CO_2 capture. Journal of Thermal Analysis and Calorimetry, 92(2), 601-606.

Plaza, M.G., Thurecht, K.J., Pevida, C., Rubiera, F., Pis, J.J., Snape, C.E., and Drage, T.C. (2013) Influence of oxidation upon the CO_2 capture performance of a phenolic-resin-derived carbon. Fuel Processing Technology, 110, 53-60.

Polarz, S. and Smarsly, B. (2002) Nanoporous materials. Journal of Nanoscience and Nanotechnology 2, 6, 581-612.

Qian, H., Zheng, J., and Zhang, S. (2013) Preparation of microporous polyamide networks for carbon dioxide capture and nanofiltration. Polymer, 54(2), 557-564.

Robertson, C. and Mokaya, R. (2013) Microporous activated carbon aerogels via a simple subcritical drying route for CO_2 capture and hydrogen storage. Microporous and Mesoporous Materials, 179, 151-156.

Sevilla, M., Valle-Vigón, P. and Fuertes, A.B. (2011) N-doped polypyrrole-based porous carbons for CO_2 capture. Advanced Functional Materials, 21(14), 2781-2787.

Smirnova, A., Wender, T., Goberman, D., Hu, Y.-L., Aindow, M., Rhine, W., and Sammes, N.M. (2009) Modification of carbon aerogel supports for PEMFC catalysts. International Journal of Hydrogen Energy, 34(21), 8992-8997.

Singh, U. and Kaushal, R.K. (2013) Treatment of waste water with low cost adsorbent-A Review. VSRD International Journal of Technical & Non-Technical Research, 4, 2319-2216.

Su, Y.C. and Chang, F.C. (2003) Synthesis and characterization of fluorinated polybenzoxazine material with low dielectric constant. Polymer, 44(26), 7989-7996.

Thubsuang, U., Ishida, H., Wongkasemjit, S., and Chaisuwan, T. (2014) Improvement in the pore structure of polybenzoxazine-based carbon xerogels through a silica templating method. Journal of Porous Materials, 21(4), 401-411.

Thubsuang, U., Ishida, H., Wongkasemjit, S., and Chaisuwan, T. (2015) Advanced and economical ambient drying method for controlled mesopore polybenzoxazine-based carbon xerogels: effects of non-ionic and cationic surfactant on porous structure. (submitted).

Tseng, H.-H., Itta, A.K., Weng, T.-H., and Li, Y.-L. (2013) SBA-15/CMS composite membrane for H_2 purification and CO_2 capture: Effect of pore size, pore volume, and loading weight on separation performance. Microporous and Mesoporous Materials, 180, 270-279.

Venkatesan, S. (2013) Adsorption. In Ramaswamy, S., Huang, H.J., and Ramarao, B.V. (Eds.), Separation and Purification Technologies in Biorefineries (pp. 103-148). New York: John Wiley.

Wang, D., Wang, X., Ma, X., Fillerup, E., and Song, C. (2014) Three-dimensional molecular basket sorbents for CO_2 capture: Effects of pore structure of supports and loading level of polyethylenimine. Catalysis Today, 23?, 100-107.

Wang, X., Wang, X., Liu, L., Bai, L., An, H., Zheng, L., and Yi, L. (2011) Preparation and characterization of carbon aerogel microspheres by an inverse emulsion polymerization. Journal of Non-Crystalline Solids, 357(3), 793-797.

Wei, L., Gao, Z., Jing, Y., and Wang, Y. (2013) Adsorption of CO_2 from simulated flue gas on pentaethylenehexamine-loaded mesoporous silica support adsorbent. Industrial & Engineering Chemistry Research, 52(42), 14965-14974.

Wickramaratne, N.P., Xu, J., Wang, M., Zhu, L., Dai, L., and Jaroniec, M. (2014) Nitrogen enriched porous carbon spheres: attractive materials for supercapacitor electrodes and CO_2 adsorption. Chemistry of Materials, 26(9), 2820-2828.

Yan, X., Zhang, L., Zhang, Y., Qiao, K., Yan, Z., and Komarneni, S. (2011) Amine-modified mesocellular silica foams for CO_2 capture. Chemical Engineering Journal, 168(2), 918-924.

Yu, C.H., Huang, C.H., and Tan, C.S. (2012) A review of CO_2 capture by absorption and adsorption. Aerosol and Air Quality Research, 12, 745-769.

Zeleňák, V., Badaničová, M., Halamová, D., Čejka, J., Zukal, A., Murafa, N., and Goerigk, G. (2008) Amine-modified ordered mesoporous silica: Effect of pore size on carbon dioxide capture. Chemical Engineering Journal, 144(2), 336-342.

Zhang, T., Yan, H., Fang, Z., E, Y., Wu, T., and Chen, F. (2014) Superhydrophobic and conductive properties of carbon nanotubes/polybenzoxazine nano-composites coated ramie fabric prepared by solution-immersion process. Applied Surface Science, 309, 218-224.

Zhu, C., Wei, Y., Zhang, J., Geng, P., and Lu, Z. (2014) Preparation of poly-siloxane oligomers bearing benzoxazine side groups and tunable properties of their thermosets. Journal of Applied Polymer Science. 131(21), DOI: 10.1002/app.40960.

Zúñiga, C., Lligadas, G., Ronda, J.C., Galià, M., and Càdiz, V. (2012) Self-foaming diphenolic acid benzoxazine. Polymer. 53(15), 3089-3095.

APPENDICES

Appendix A Calculation for Benzoxazine Synthesis Ratio

In this research, two kinds of benzoxazine monomer were prepared from three main precursors which were phenol, formaldehyde, and amine (e.g., diethylenetriamine (DETA) and pentaethylenehexamine (PEHA)). This synthesis process was suggested from the previous study of Hirikamol (2013). In detailed, there was a 2:4:1 mole ratio for phenol, formaldehyde, and amine, respectively, which was synthesized in the solution of chloroform. In all tests, the consumption of benzoxazine monomer was 80 g for each batch. Moreover, both synthesis reactions of benzoxazines were shown in Equations A1 and A2 (Hirikamol, 2013).

Molecular weight of phenol	= 94.11
Molecular weight of formaldehyde	= 30.03
Molecular weight of DETA	= 103.17
Molecular weight of PEHA	= 232.37
Density of formaldehyde	= 1.09 g/mL
Density of DETA	= 0.955 g/mL
Density of PEHA	= 0.95 g/mL

Amine: Diethylenetriamine (DETA)

$$2 \bigcirc^{OH} + 4CH_2O + H_2N \sim\!\!\sim^{NH}\!\!\sim\!\!\sim NH_2 \longrightarrow \text{(benzoxazine)} \tag{A1}$$
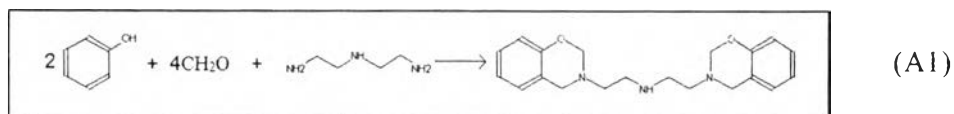
Molecular weight of benzoxazine $= (20 \times C) + (3 \times N) + (2 \times O) + (25 \times H)$

$\qquad\qquad\qquad\qquad\qquad\quad = (20 \times 12) + (3 \times 14) + (2 \times 16) + (25 \times 1)$

$\qquad\qquad\qquad\qquad\qquad\quad = 339$

Benzoxazine	339 g	= 1 mol
	80 g	= 0.24 mol
Phenol	= 0.24×2	= 0.48 mol
Formaldehyde	= 0.24×4	= 0.96 mol

DETA　　　　= 0.24×1　　= 0.24 mol

Use in gram:

Phenol　　　= 0.48×94.11　　= 45.17 g #

Use in mL:

Formaldehyde = 0.96×30.03　　= 28.83 g

But formaldehyde 37 wt% = (28.83×100) ÷ (37×1.09) = 71.49 mL #

DETA　　　= 0.24×103.17÷0.955　　= 25.93 mL #

Amine: Pentaethylenehexamine (PEHA)

(A2)
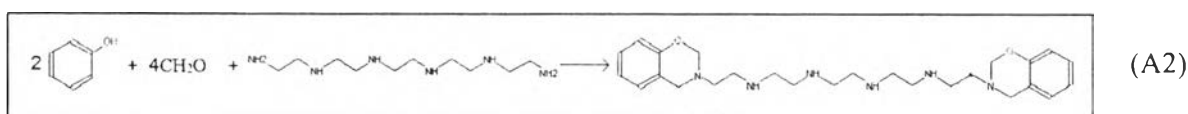
Molecular weight of benzoxazine　= (26×C) + (6×N) + (2×O) + (40×H)

= (26×12) + (6×14) + (2×16) + (40×1)

= 468

Benzoxazine　　468 g　= 1 mol

　　　　　　　80 g　= 0.171 mol

Phenol　　= 0.171×2　= 0.342 mol

Formaldehyde = 0.171×4　= 0.682 mol

PEHA　　= 0.171×1　= 0.171 mol

Use in gram:

Phenol　　= 0.342×94.11　　= 32.19 g #

Use in mL:

Formaldehyde = 0.682×30.03　　= 20.48 g

But formaldehyde 37 wt% = (20.48×100) ÷ (37×1.09) = 50.78 mL #

PEHA　　= 0.171×232.37÷0.95 = 41.83 mL #

Appendix B FTIR Spectra of Benzoxazine Monomers and Polybenzoxazines
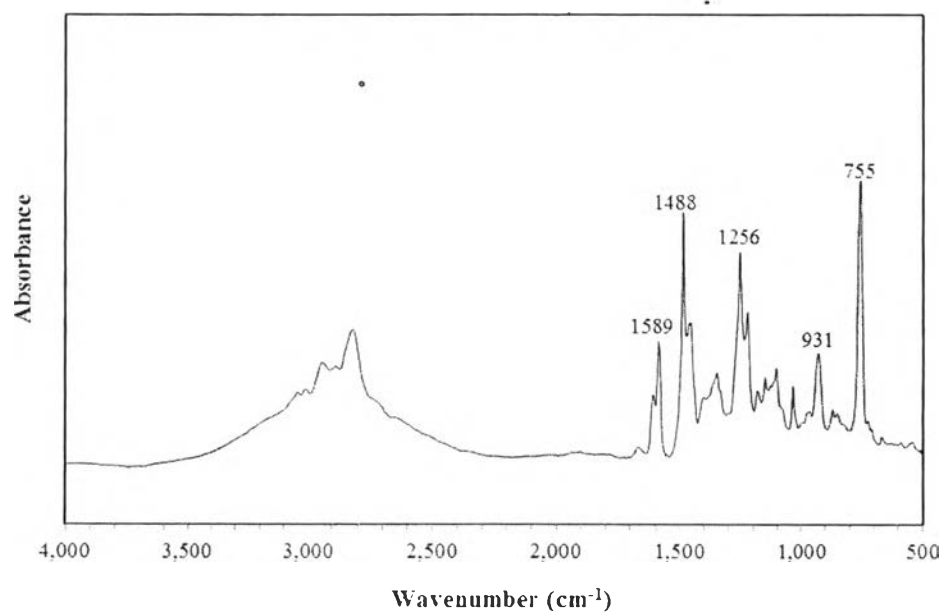
Figure B1 FT-IR spectrum of the benzoxazine monomer by DETA as reactant.
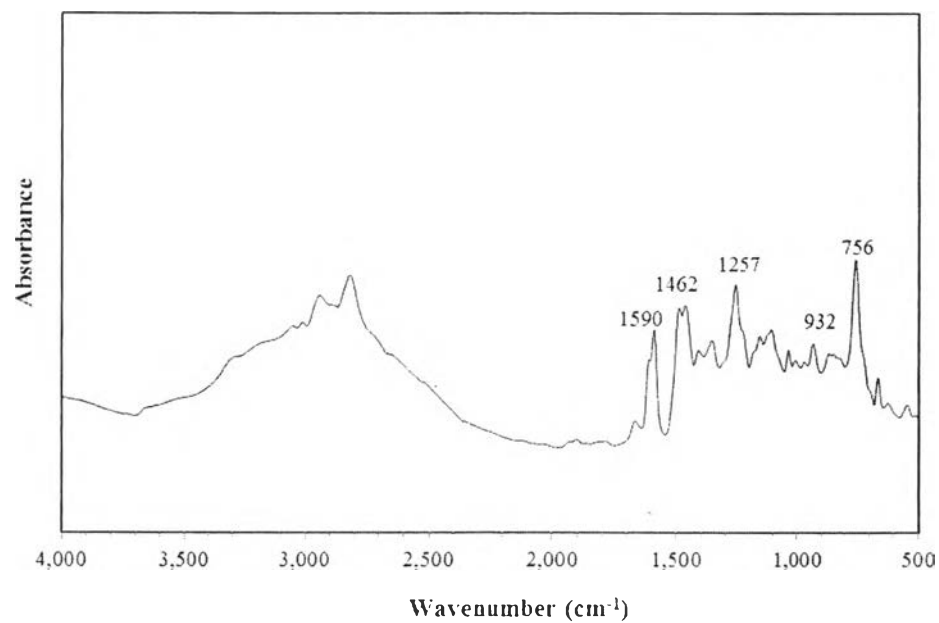
Figure B2 FT-IR spectrum of the benzoxazine monomer by PEHA as reactant.
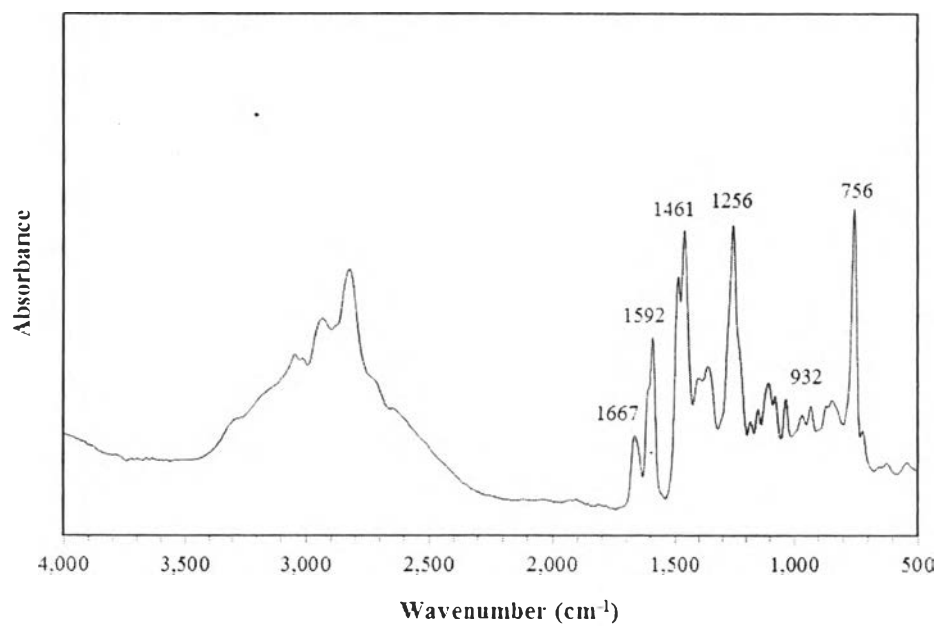
Figure B3 FT-IR spectrum of polybenzoxazine by DETA as reactant.
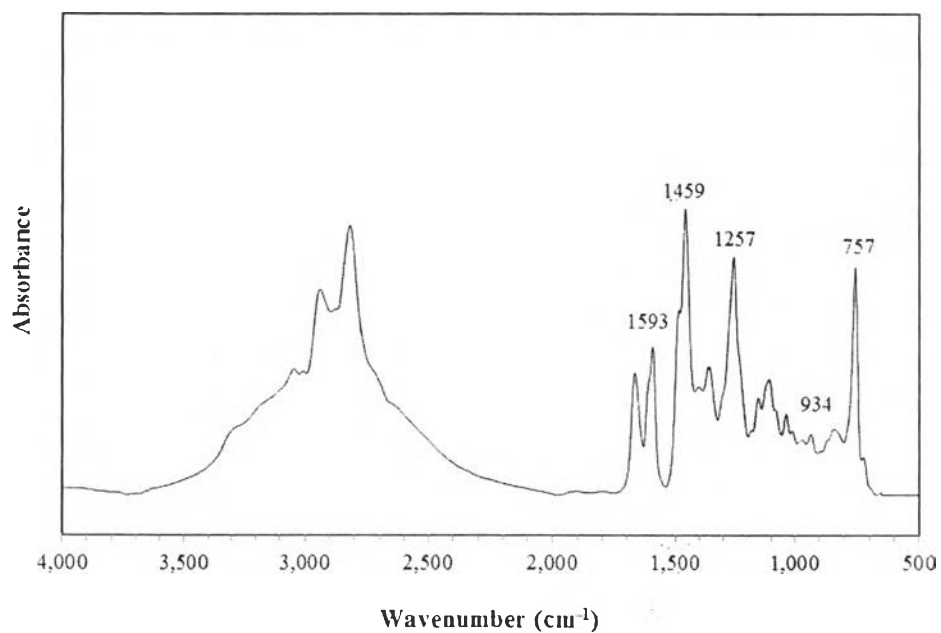
Figure B4 FT-IR spectrum of polybenzoxazine by PEHA as reactant.

Appendix C DSC Thermograms of all Materials
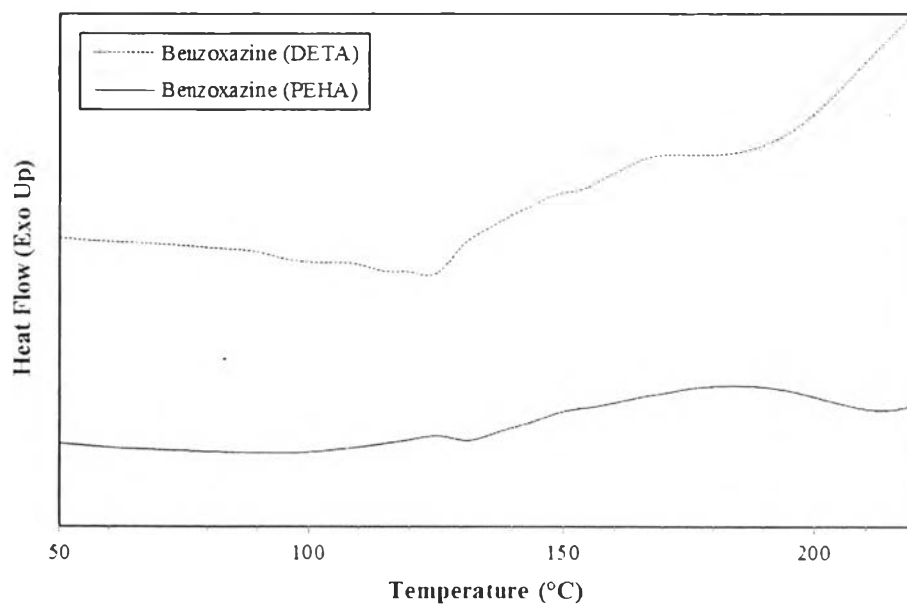
Figure C1 DSC thermograms of benzoxazine monomers by DETA and PEHA as reactants.
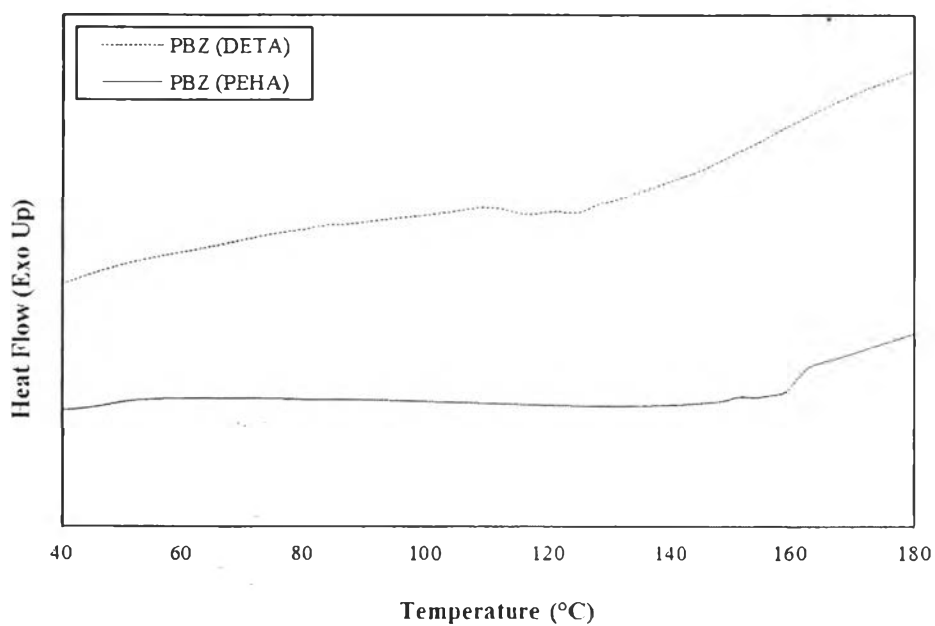
Figure C2 DSC thermograms of polybenzoxazines by DETA and PEHA as reactant.
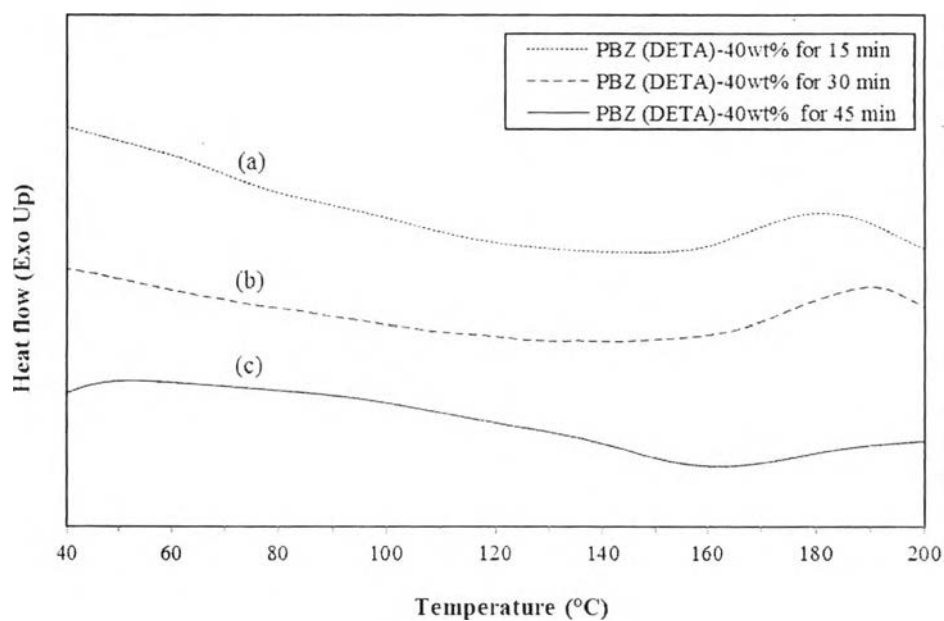
Figure C3 DSC thermograms of (a) DETA-40wt% derived aerogel at 180 °C for 15 min, (b) DETA-40wt% derived aerogel at 180 °C for 30 min, and (c) DETA-40wt% derived aerogel at 180 °C for 45 min.
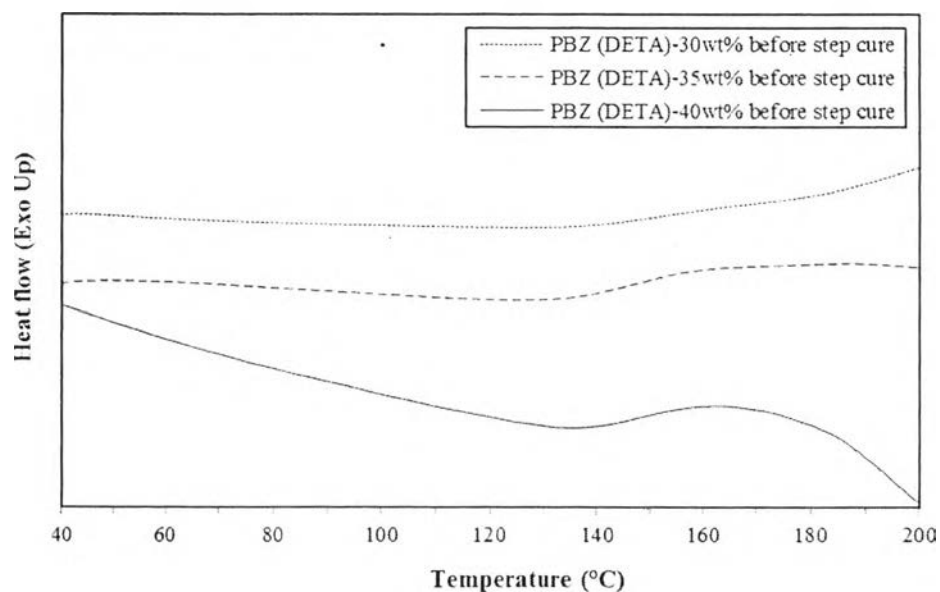
Figure C4 DSC thermograms of polybenzoxazine aerogels before curing step with DETA as reactant.
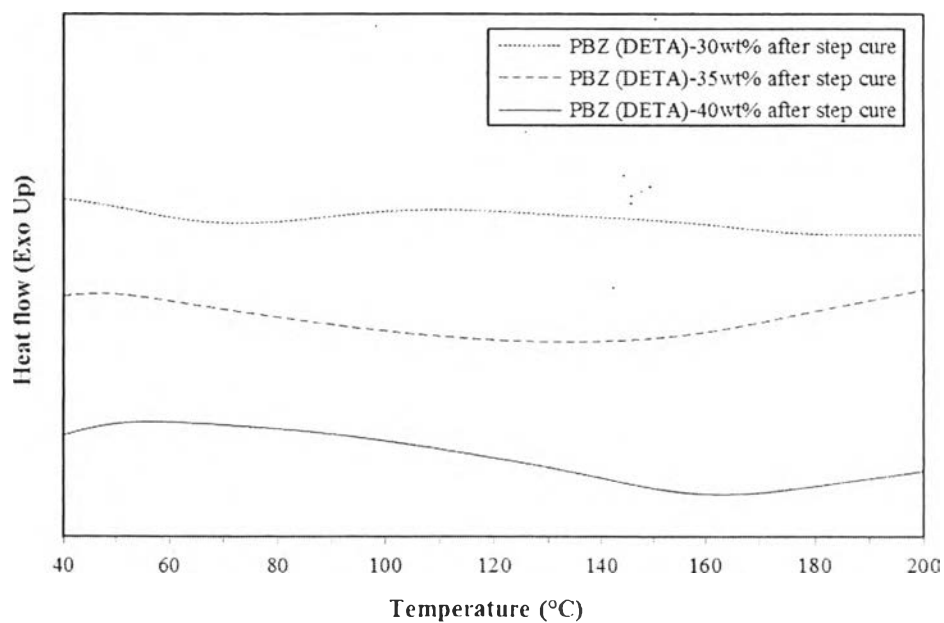
Figure C5 DSC thermograms of polybenzoxazine aerogels after curing step with DETA as reactant.
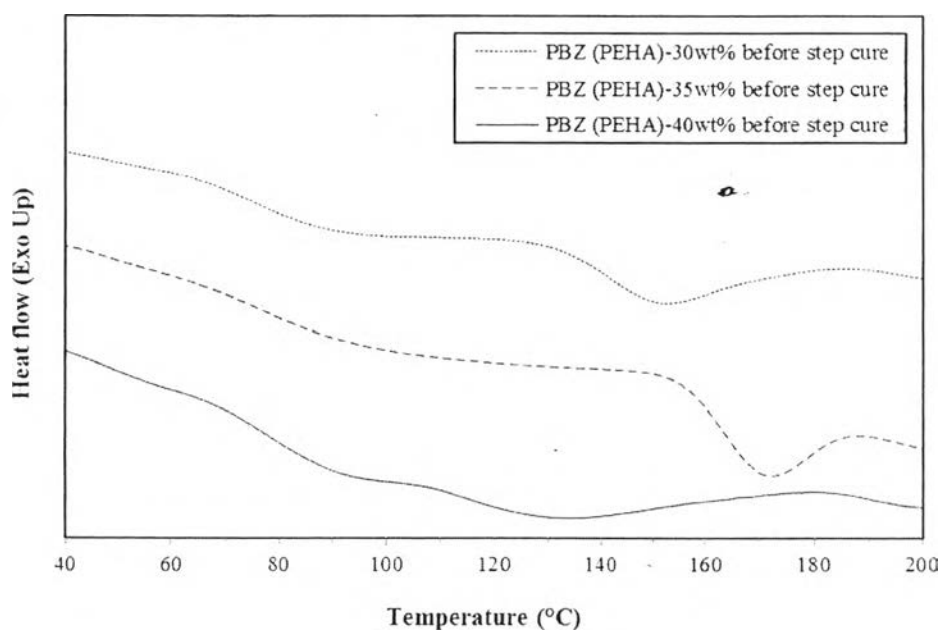
Figure C6 DSC thermograms of polybenzoxazine aerogels before curing step with PEHA as reactant.
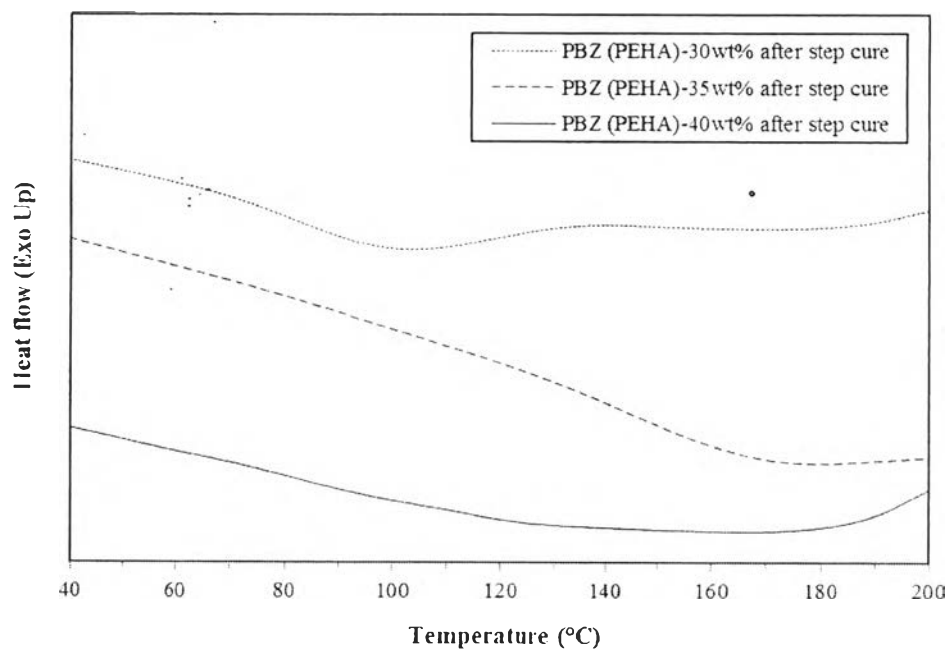
Figure C7 DSC thermograms of polybenzoxazine aerogels after curing step with PEHA as reactant.

Appendix D TGA Thermograms of all Materials
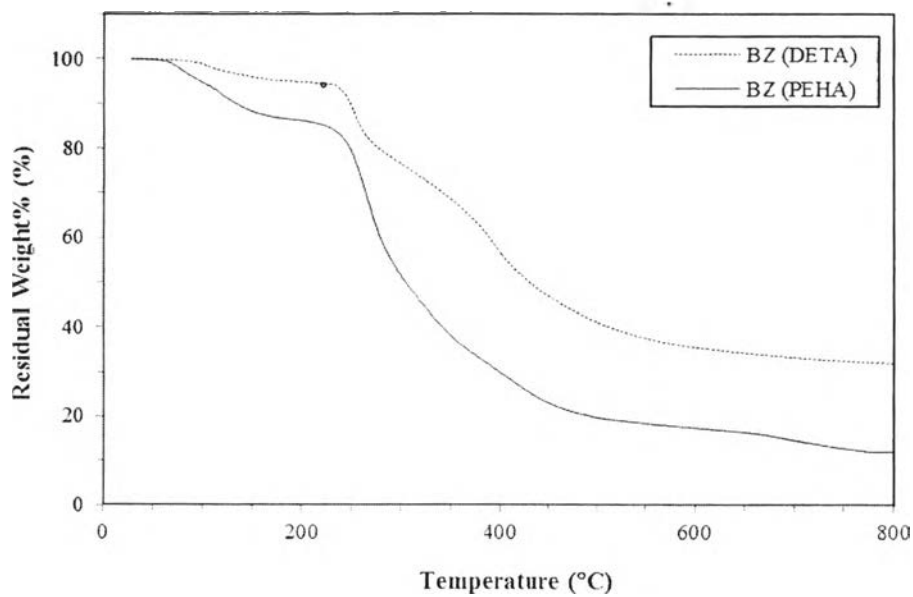
Figure D1 TGA thermograms of benzoxazine monomers with DETA and PEHA as amine reactants.
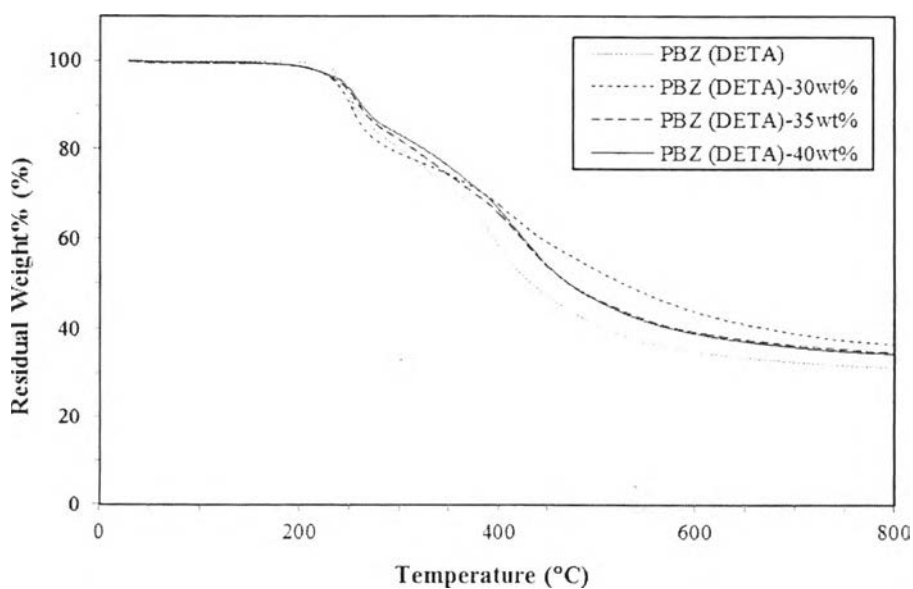
Figure D2 TGA thermograms of polybenzoxaine and polybenzoxazine aerogels with DETA as reactant.
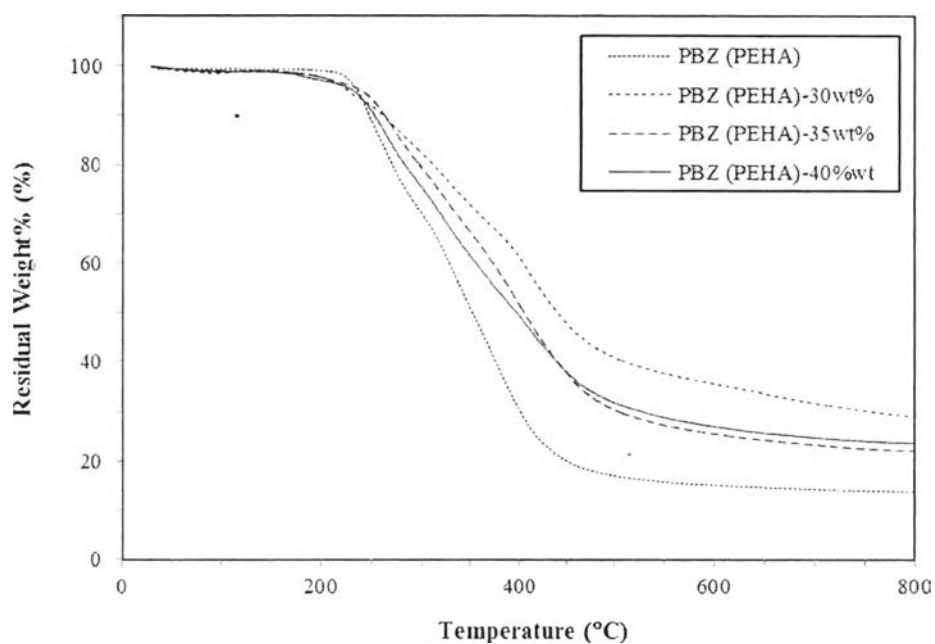
Figure D3 TGA thermograms of polybenzoxazine and polybenzoxazine aerogels with PEHA as reactant.
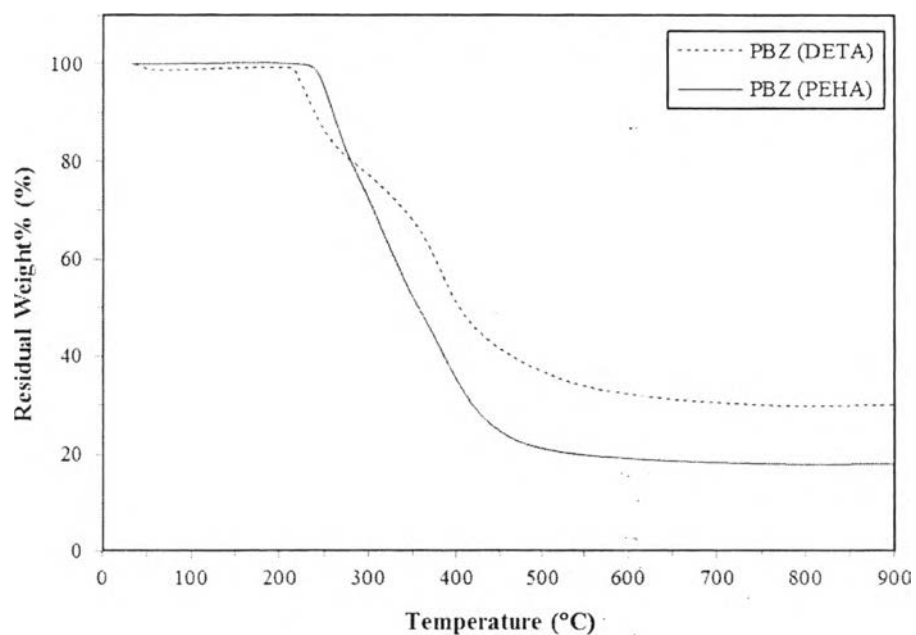
Figure D4 TGA thermograms of PBZs derived from DETA and PEHA after heating up to 900 °C (with a heating rate of 20 °C/min).
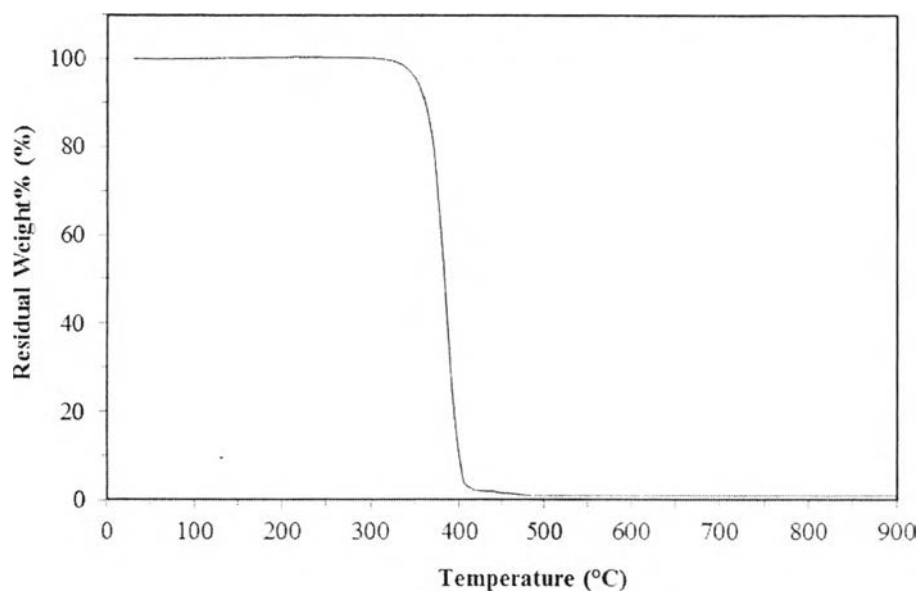
Figure D5 TGA thermograms of PEG-PPG-PEG block copolymer after heating up to 900 °C (with heating rate of 20 °C/min).
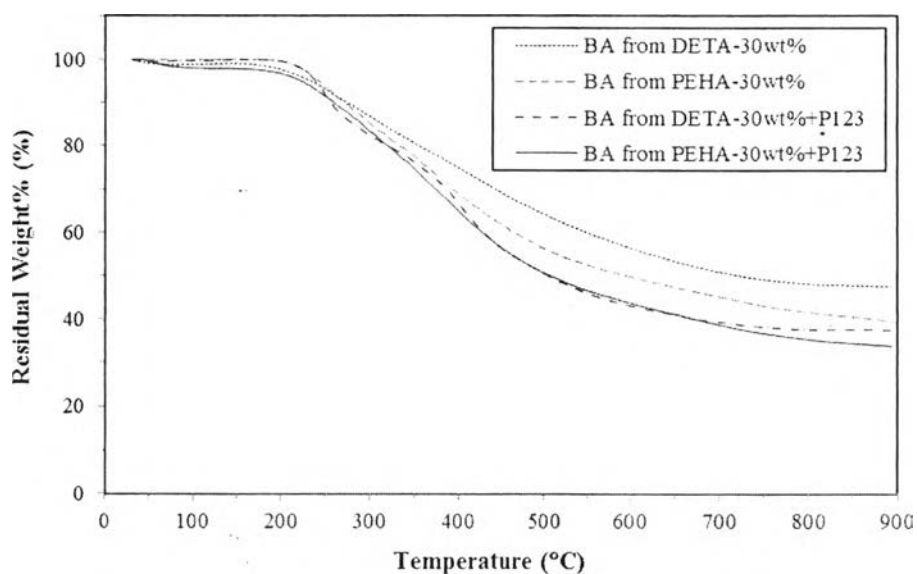
Figure D6 TGA thermograms of PBZ aerogels derived from DETA and PEHA with and without non-ionic surfactant (PEG-PPG-PEG block copolymer) after heating up to 900 °C (with heating rate of 20 °C/min).

Appendix E Calculation for Residual Weight of Polybenzoxazine

In this research, theoretical char yield of polybenzoxazine was calculated by dividing molecular weight of carbon compound by the total molecular weight of polybenzoxazine and multiplying by 100 as shown in Equations E1 and E2 (Brooks and Media, 2015).

Amine: Diethylenetriamine (DETA)
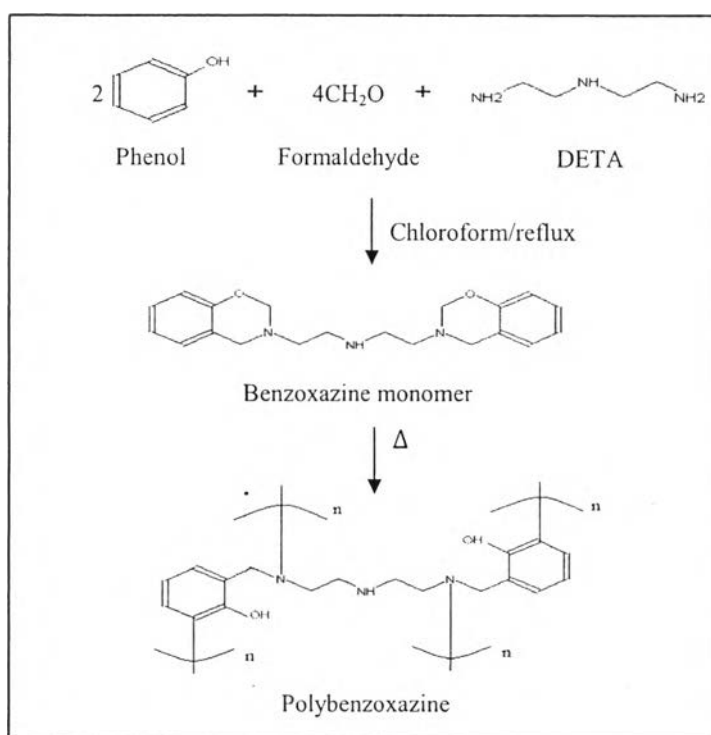
Molecular weight of PBZ (DETA) = $(18 \times C) + (3 \times N) + (2 \times O) + (21 \times H)$

$\qquad\qquad = (18 \times 12) + (3 \times 14) + (2 \times 16) + (21 \times 1)$

$\qquad\qquad = 311$

$$\% \text{ Char yield (DETA)} = \frac{\text{Molecular weight of carbon atom}}{\text{Molecular weight of polybenzoxazine (DETA)}} \times 100 \qquad (E1)$$

$$= \frac{216}{311} \times 100 \quad = \underline{69.45 \%} \text{ \#}$$

Amine: <u>Pentaethylenehexamine (PEHA)</u>
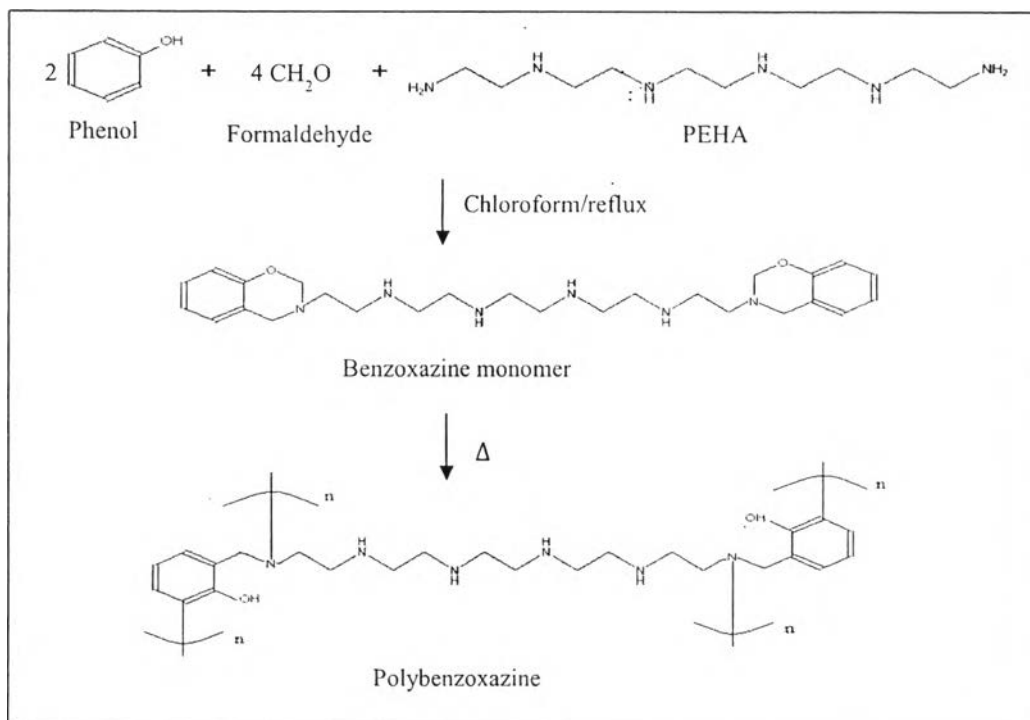
Molecular weight of PBZ (PEHA) $= (24 \times C) + (6 \times N) + (2 \times O) + (34 \times H)$

$\qquad\qquad\qquad\qquad\qquad\qquad = (24 \times 12) + (6 \times 14) + (2 \times 16) + (34 \times 1)$

$\qquad\qquad\qquad\qquad\qquad\qquad = 438$

$$\% \text{ Char yield (PEHA)} = \frac{\text{Molecular weight of carbon atom}}{\text{Molecular weight of polybenzoxazine (PEHA)}} \times 100 \qquad \text{(E2)}$$

$$= \frac{288}{438} \times 100 \quad = \underline{65.75\ \%}\ \#$$

Appendix F %Burn Off of Carbon Aerogels from Polybenzoxazine

Table F1   Comparison of %burn off of PBZ-derived carbon aerogels from two instruments (TG-DTA and Furnace)

Materials	%Burn Off (TG-DTA)	%Burn Off (Furnace)
BA from DETA-30 wt%	63.56 %	65.53 %
BA from DETA-35 wt%	65.39 %	65.62 %
BA from DETA-40 wt%	65.77 %	64.20 %
BA from PEHA-30 wt%	71.06 %	73.54 %
BA from PEHA-35 wt%	77.96 %	73.61 %
BA from PEHA-40 wt%	76.38 %	75.10 %

Appendix G XPS Spectra of all Materials

DETA-derived polybenzoxazine
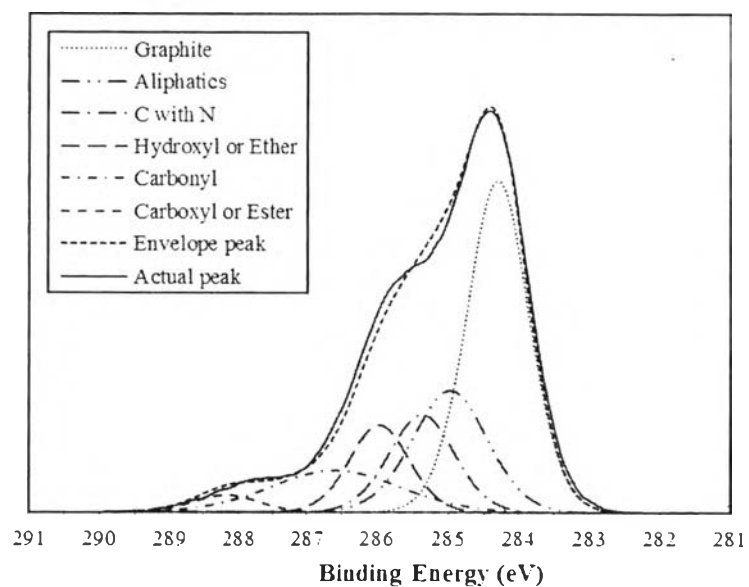
Figure G1 C1s XPS spectra of DETA-derived polybenzoxazine.
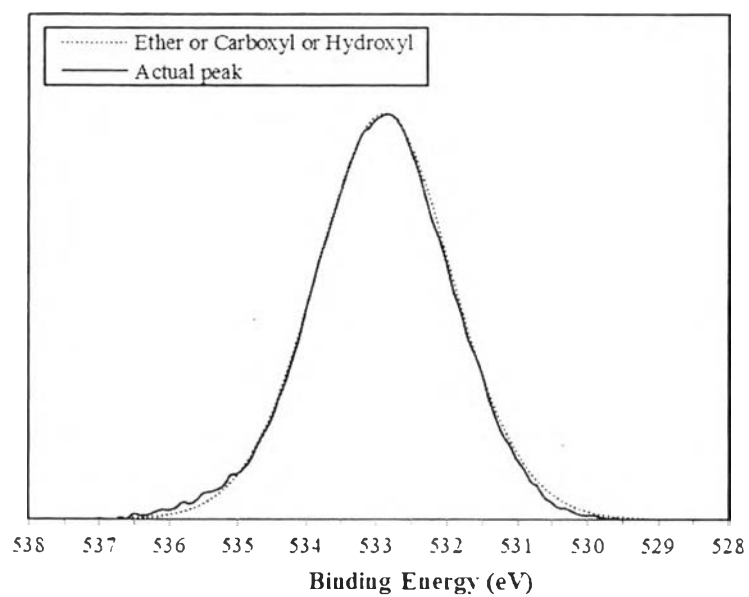
Figure G2 O1s XPS spectra of DETA-derived polybenzoxazine.
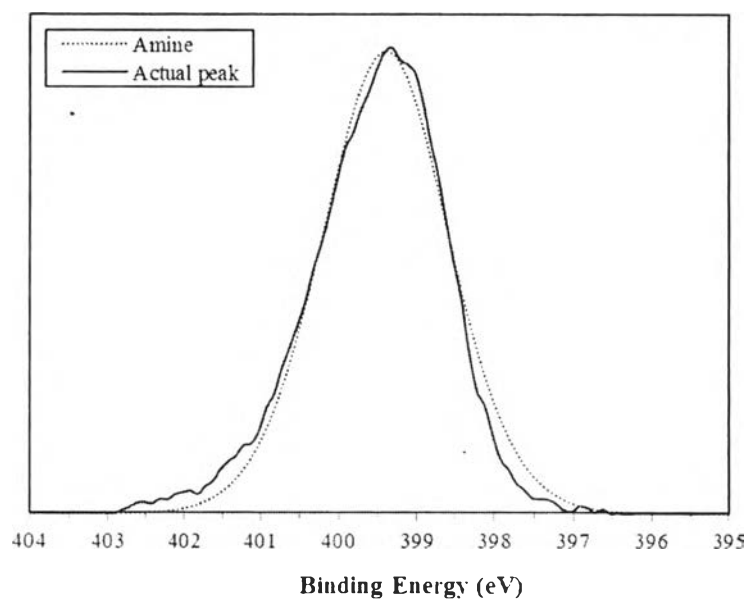
Figure G3 N1s XPS spectra of DETA-derived polybenzoxazine.

30 wt% DETA-derived PBZ organic aerogel
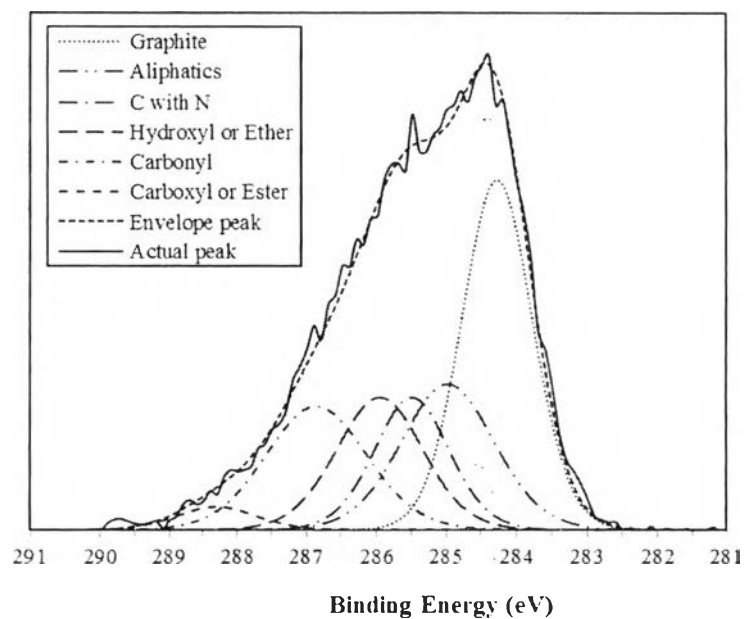
Figure G4 C1s XPS spectra of a 30 wt% DETA-derived PBZ organic aerogel.
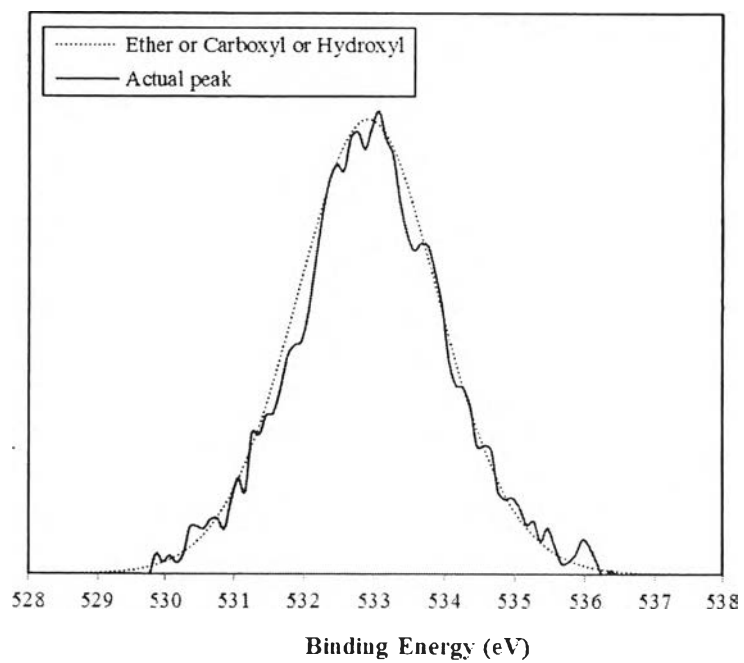
Figure G5 O1s XPS spectra of a 30 wt% DETA-derived PBZ organic aerogel.
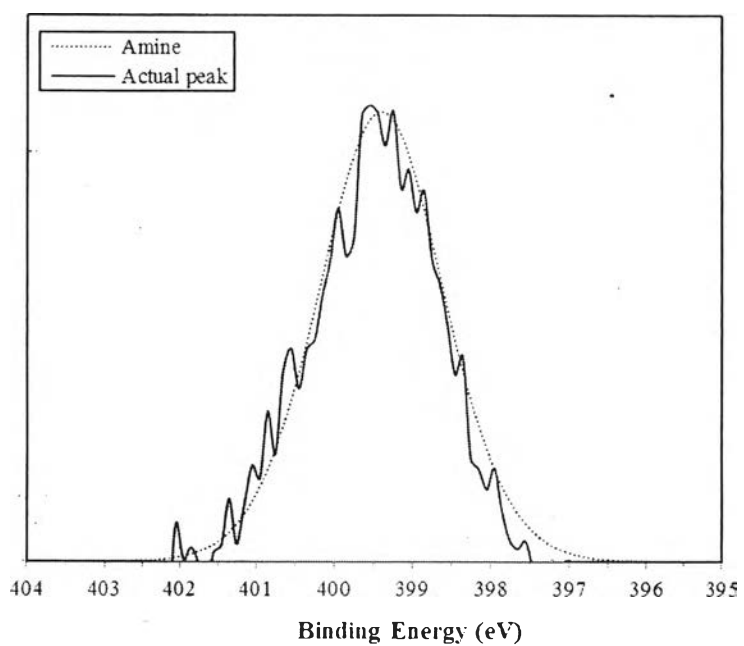
Figure G6 N1s XPS spectra of a 30 wt% DETA-derived PBZ organic aerogel.

35 wt% DETA-derived PBZ organic aerogel
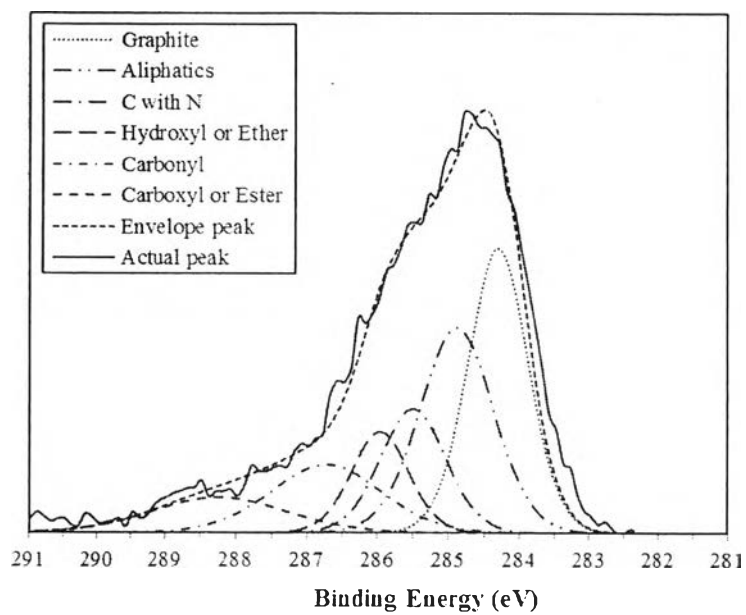
Figure G7 C1s XPS spectra of a 35 wt% DETA-derived PBZ organic aerogel.
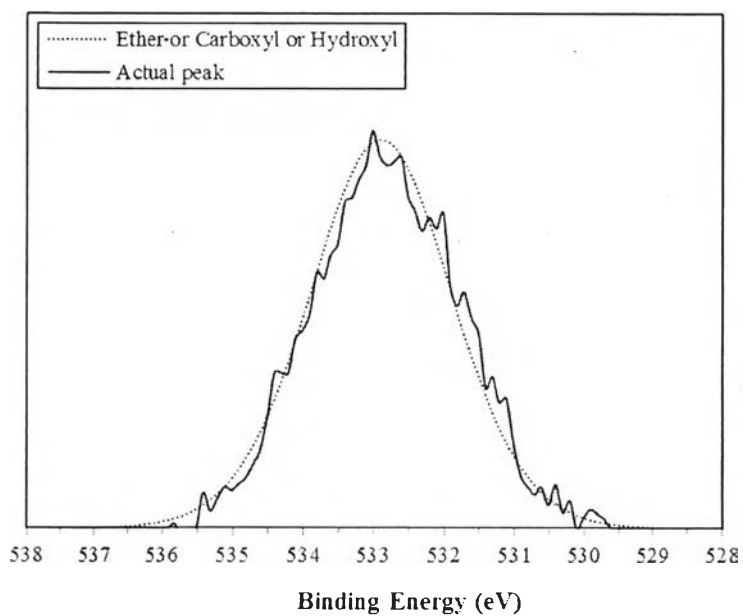
Figure G8 O1s XPS spectra of a 35 wt% DETA-derived PBZ organic aerogel.
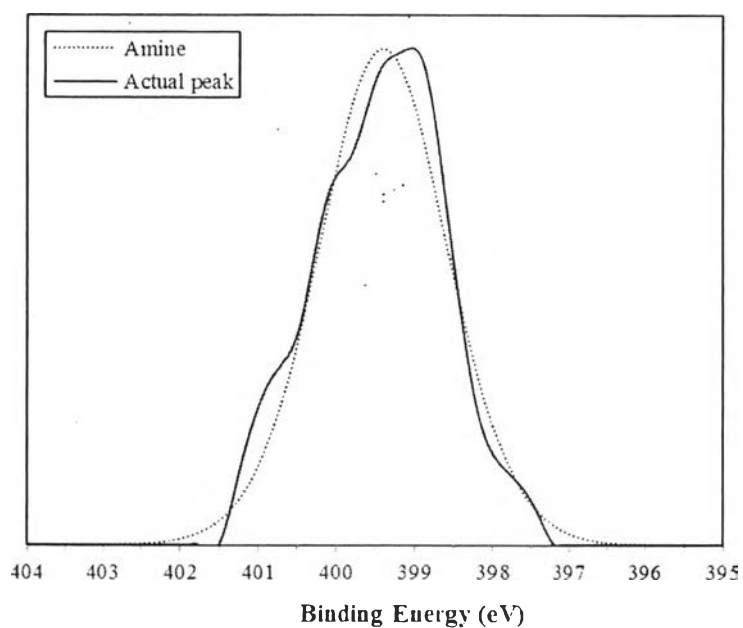
Figure G9 N1s XPS spectra of a 35 wt% DETA-derived PBZ organic aerogel.

40 wt% DETA-derived PBZ organic aerogel
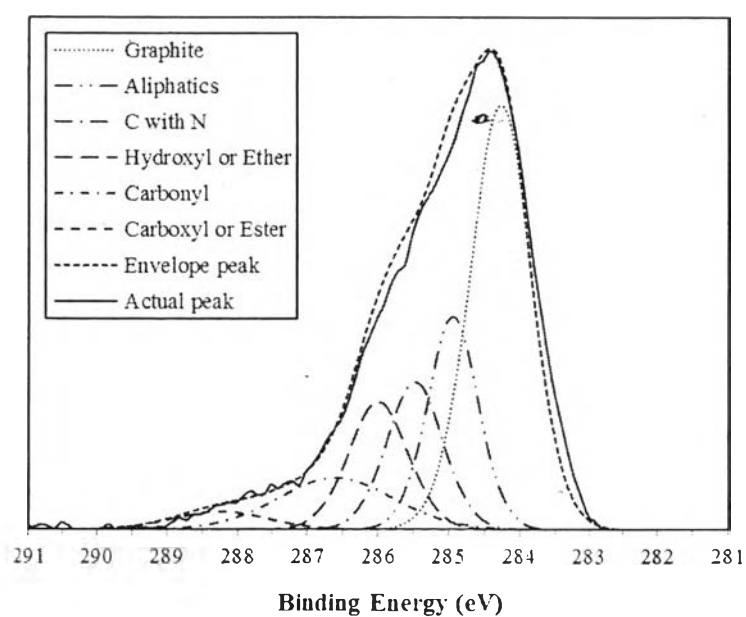
Figure G10 C1s XPS spectra of a 40 wt% DETA-derived PBZ organic aerogel.
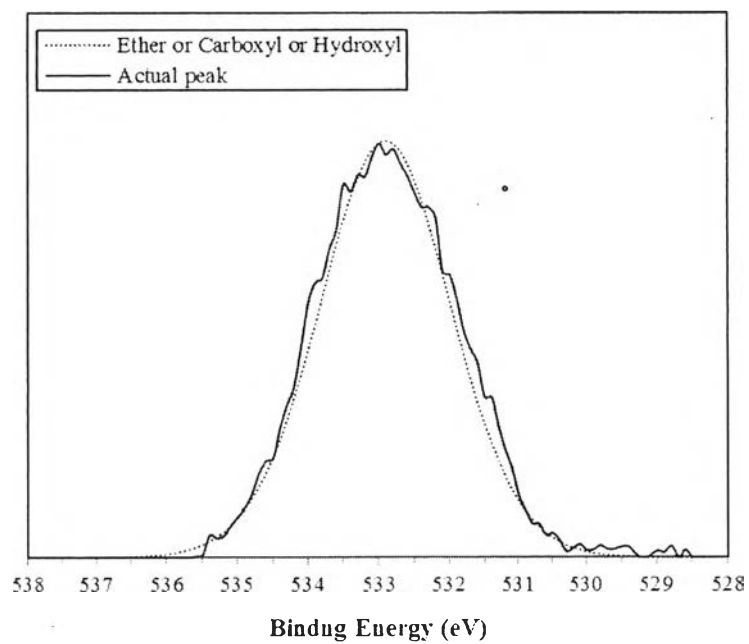
Figure G11 O1s XPS spectra of a 40 wt% DETA-derived PBZ organic aerogel.
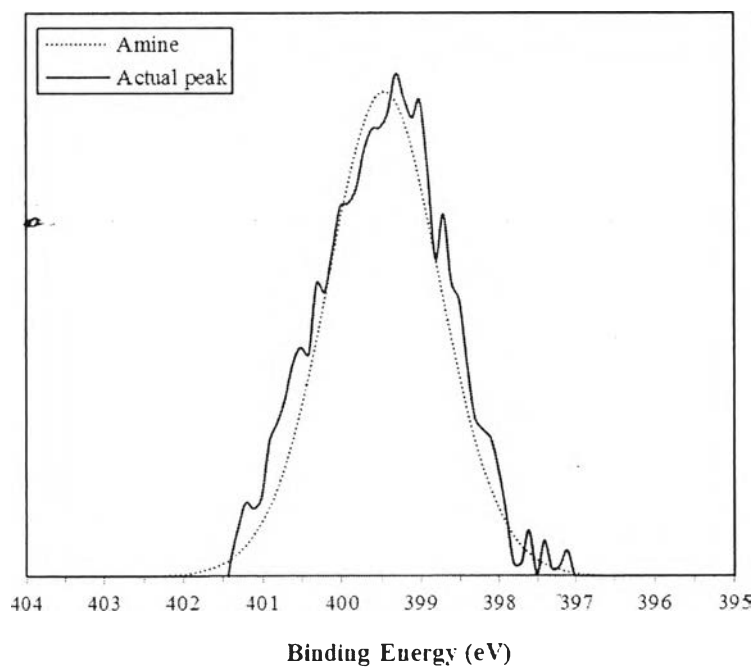
Figure G12 N1s XPS spectra of a 40 wt% DETA-derived PBZ organic aerogel.

PEHA-derived polybenzoxazine
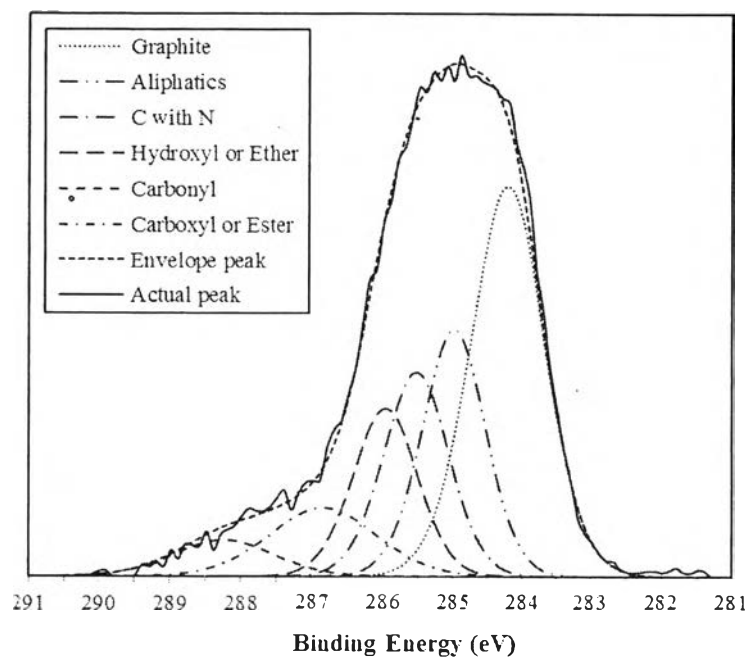
Figure G13 C1s XPS spectra of PEHA-derived polybenzoxazine.
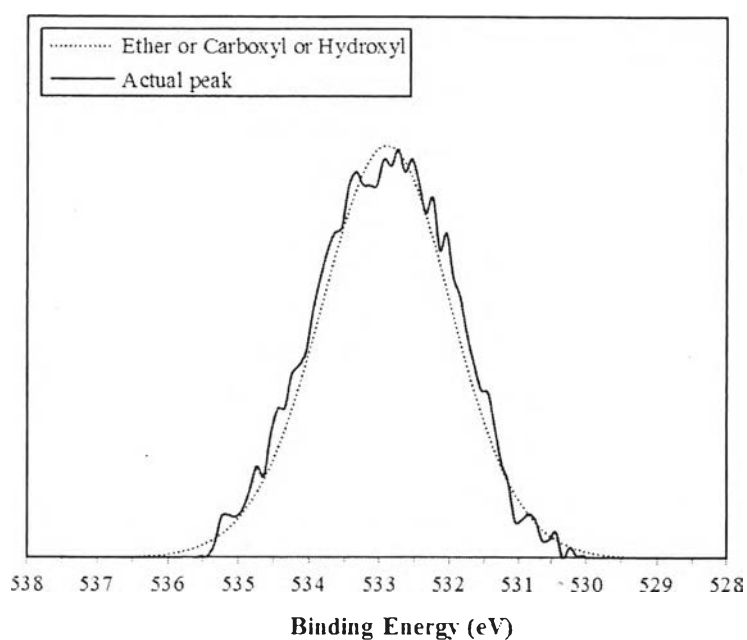
Figure G14 O1s XPS spectra of PEHA-derived polybenzoxazine.
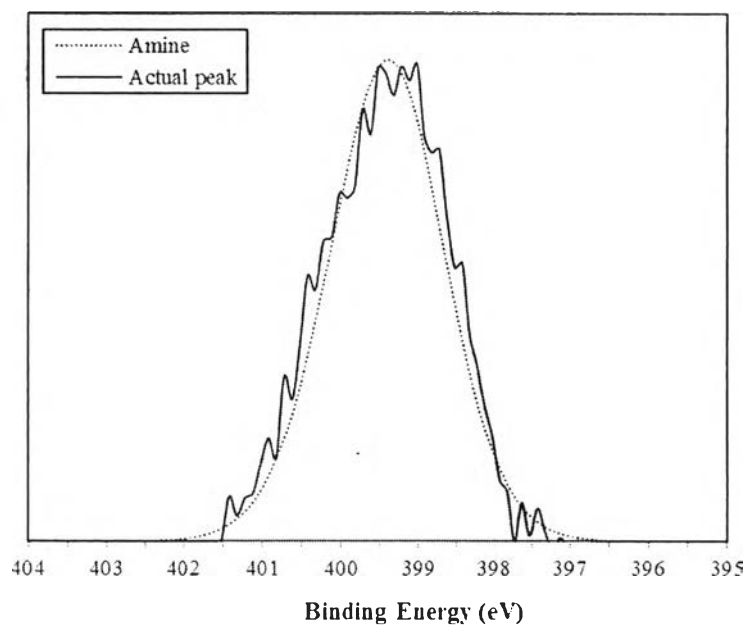
Figure G15 N1s XPS spectra of PEHA-derived polybenzoxazine.

30 wt% PEHA-derived PBZ organic aerogel
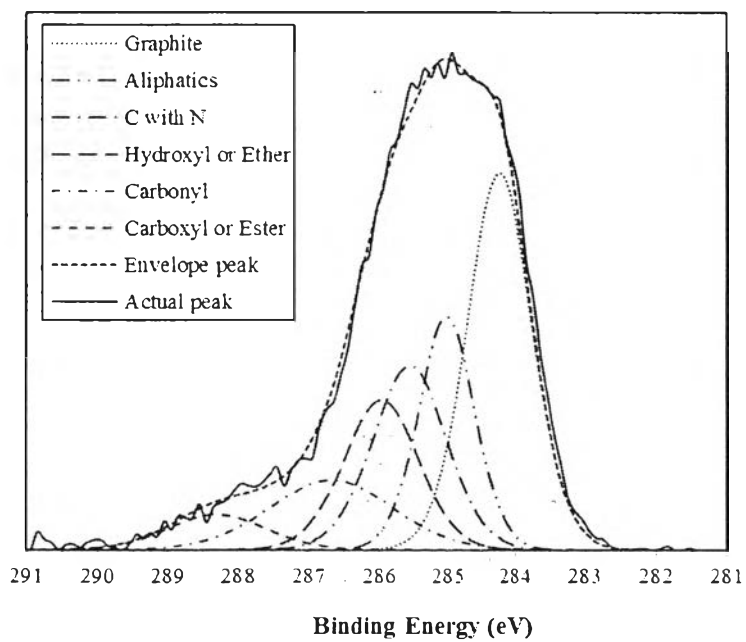
Figure G16 C1s XPS spectra of a 30 wt% PEHA-derived PBZ organic aerogel.
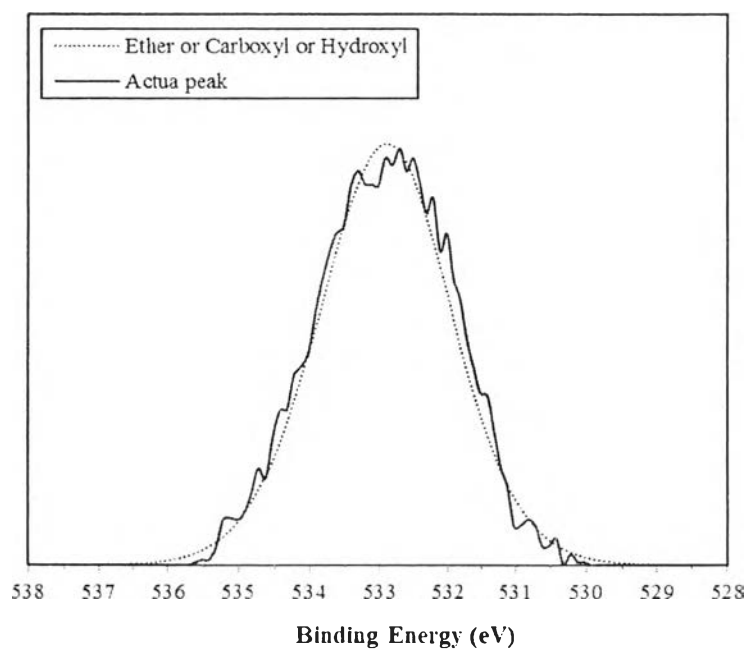
Figure G17 O1s XPS spectra of a 30 wt% PEHA-derived PBZ organic aerogel.
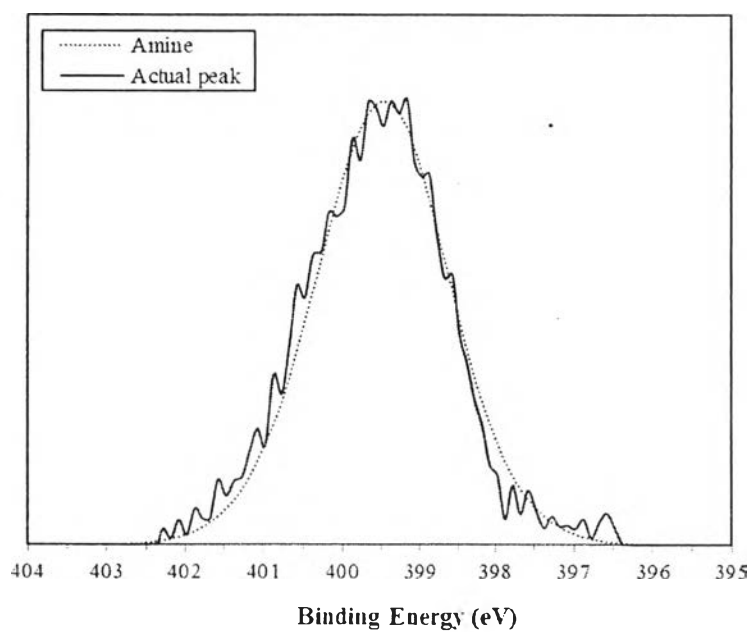
Figure G18 N1s XPS spectra of a 30 wt% PEHA-derived PBZ organic aerogel.
35 wt% PEHA-derived PBZ organic aerogel
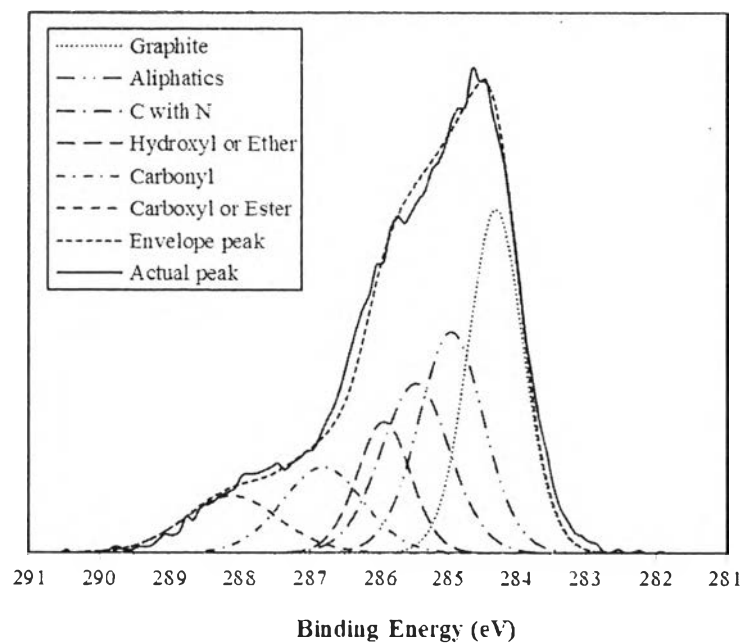
Figure G19 C1s XPS spectra of a 35 wt% PEHA-derived PBZ organic aerogel.
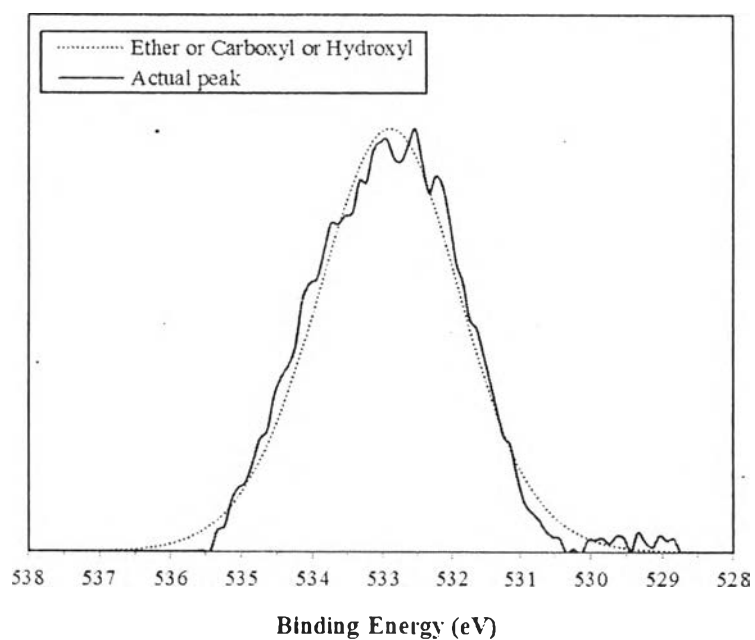
Figure G20 O1s XPS spectra of a 35 wt% PEHA-derived PBZ organic aerogel.
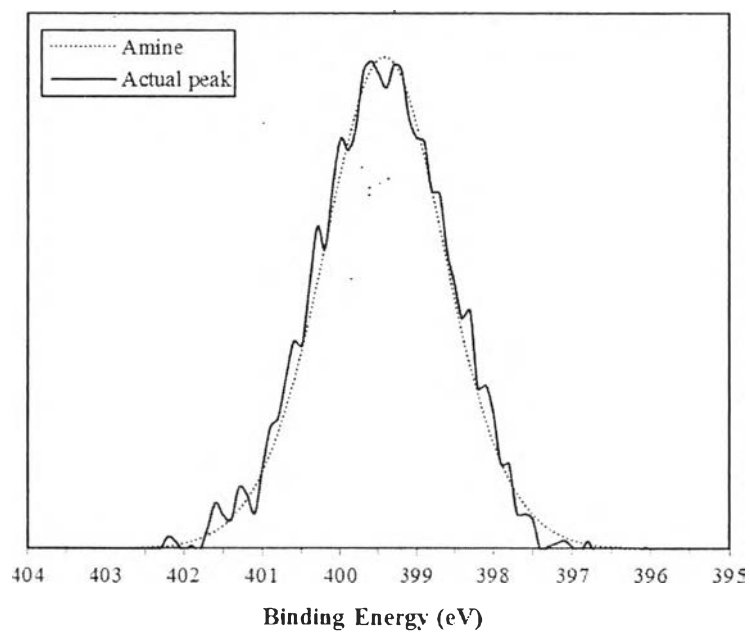
Figure G21 N1s XPS spectra of a 35 wt% PEHA-derived PBZ organic aerogel.

40 wt% PEHA-derived PBZ organic aerogel
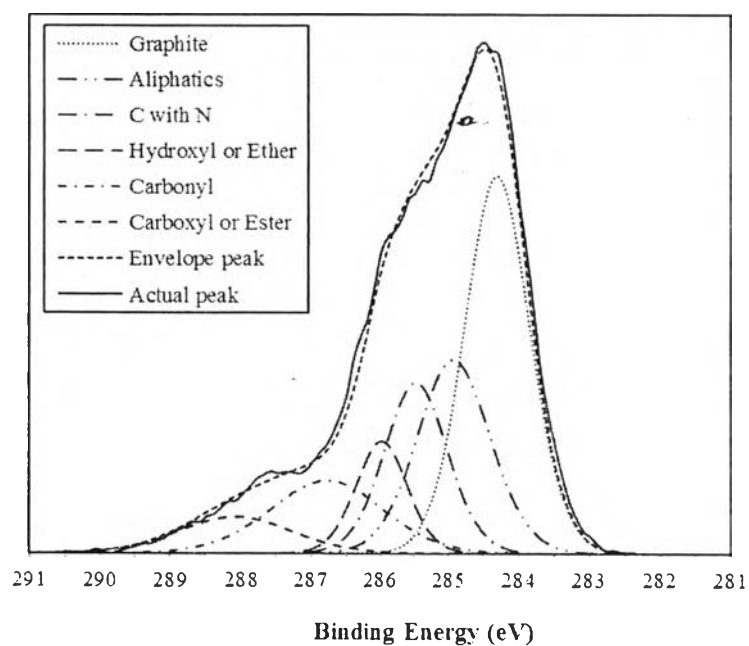
Figure G22 C1s XPS spectra of a 40 wt% PEHA-derived PBZ organic aerogel.
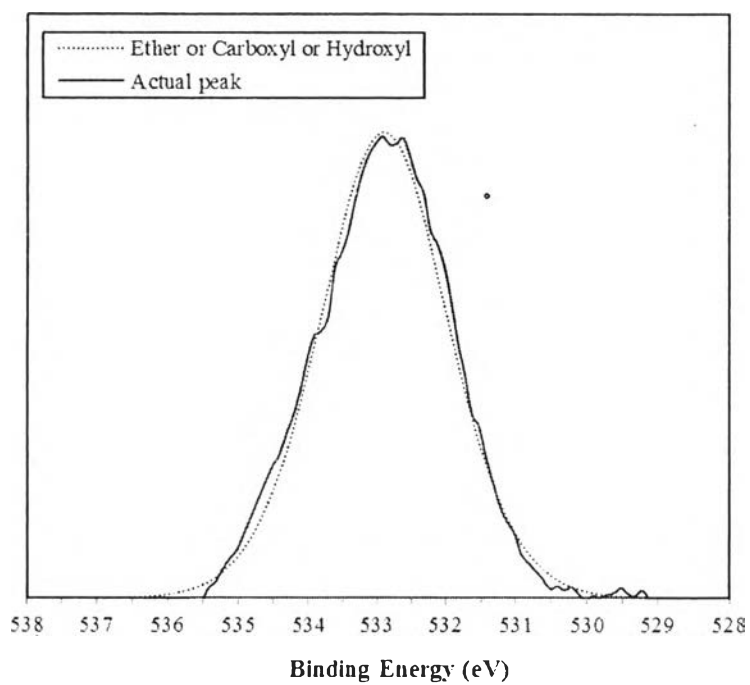
Figure G23 O1s XPS spectra of a 40 wt% PEHA-derived PBZ organic aerogel.
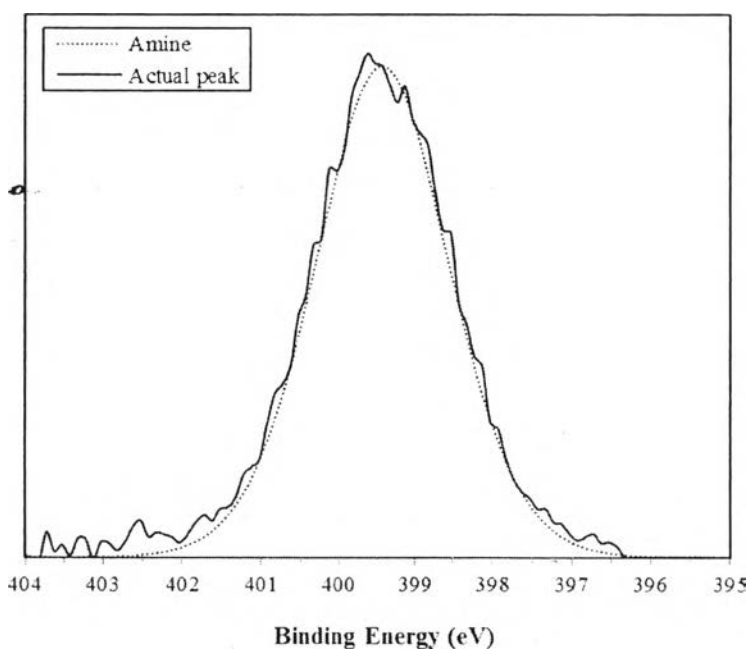
Figure G24 N1s XPS spectra of a 40 wt% PEHA-derived PBZ organic aerogel. Activated carbon from DETA-derived PBZ
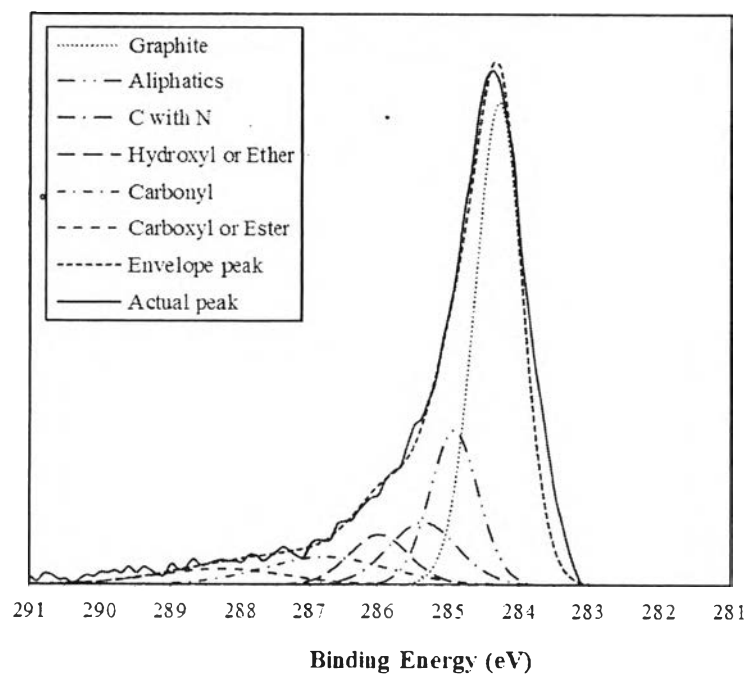
Figure G25 C1s XPS spectra of activated carbon from DETA-derived PBZ.
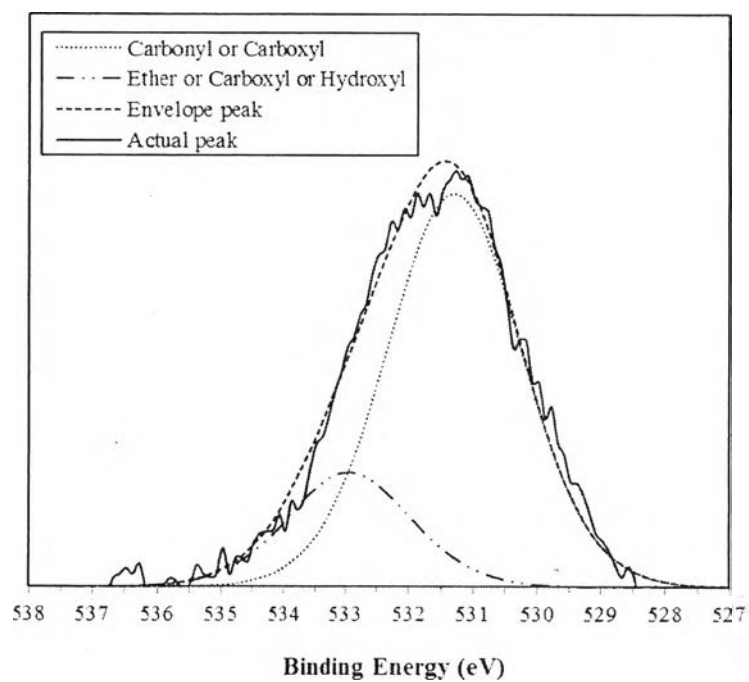
Figure G26 O1s XPS spectra of activated carbon from DETA-derived PBZ.
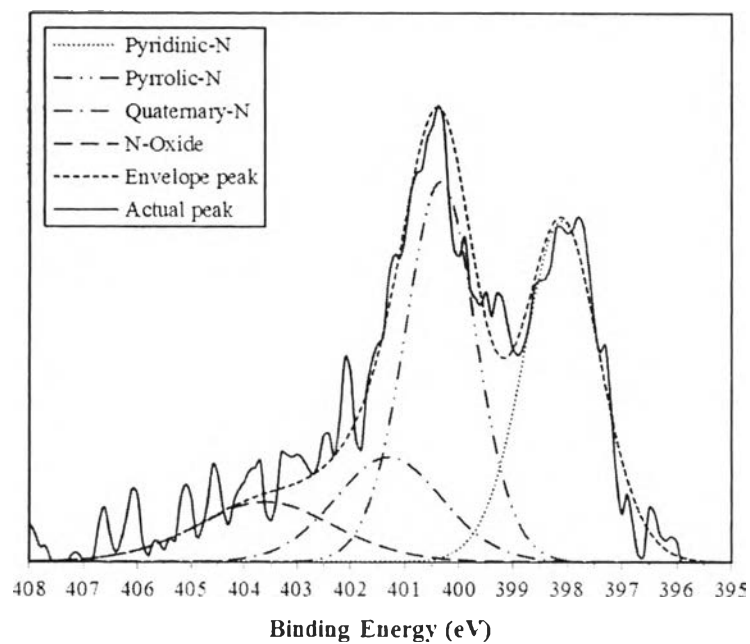
Figure G27 N1s XPS spectra of activated carbon from DETA-derived PBZ.

30 wt% DETA-derived PBZ carbon aerogel
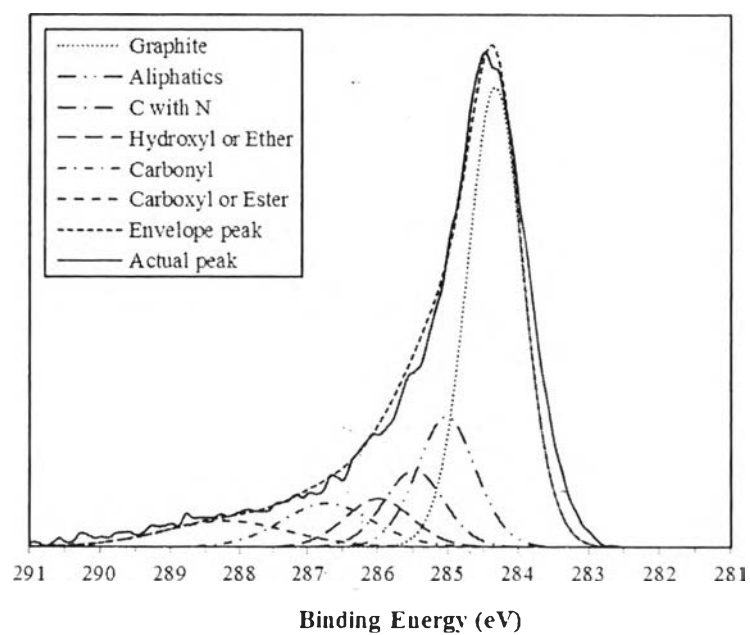
Figure G28 C1s XPS spectra of a 30 wt% DETA-derived PBZ carbon aerogel.
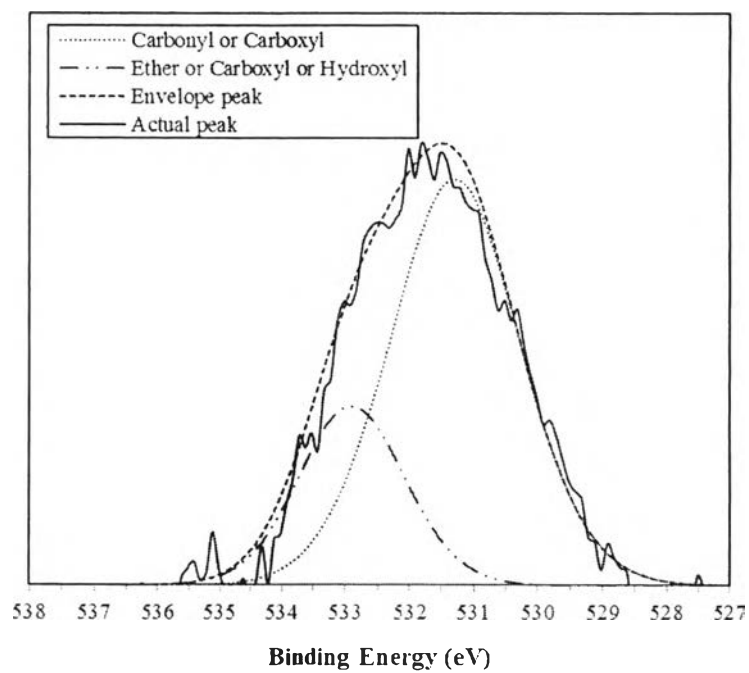
Figure G29 O1s XPS spectra of a 30 wt% DETA-derived PBZ carbon aerogel.
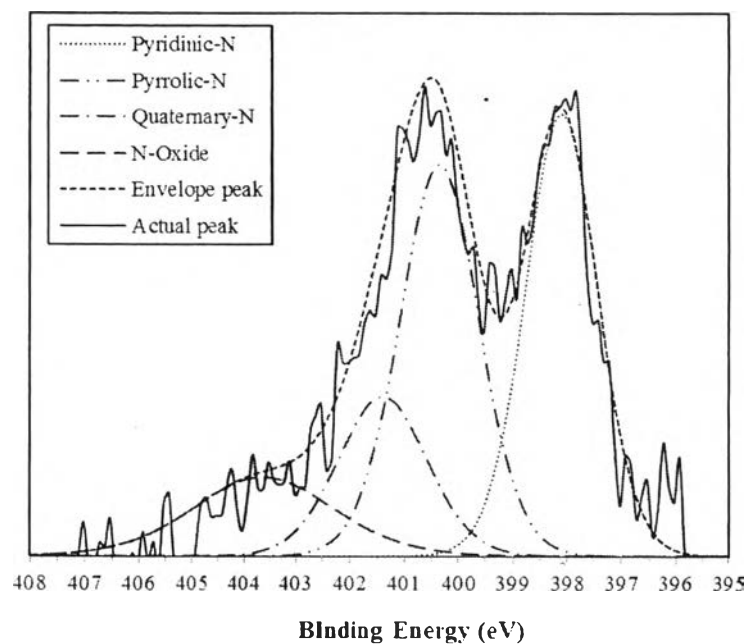
Figure G30 N1s XPS spectra of a 30 wt% DETA-derived PBZ carbon aerogel.
35 wt% DETA-derived PBZ carbon aerogel
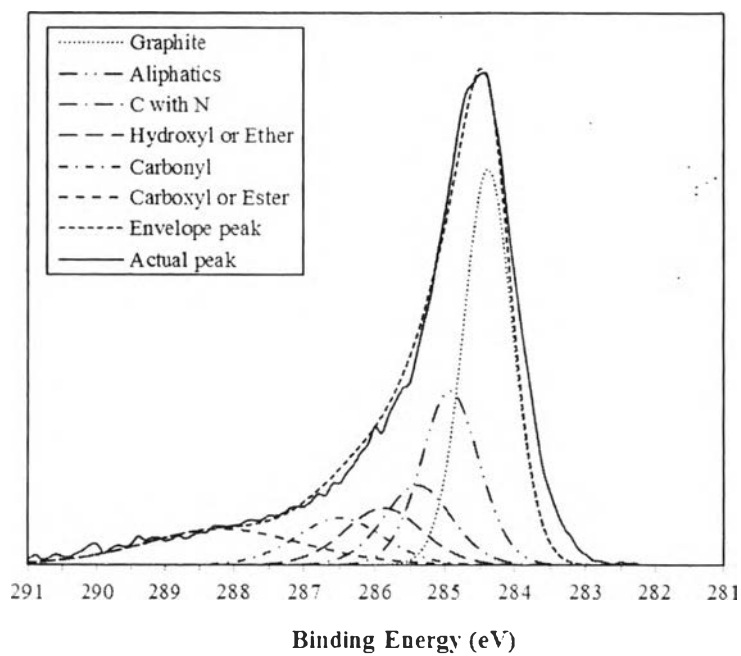
Figure G31 C1s XPS spectra of a 35 wt% DETA-derived PBZ carbon aerogel.
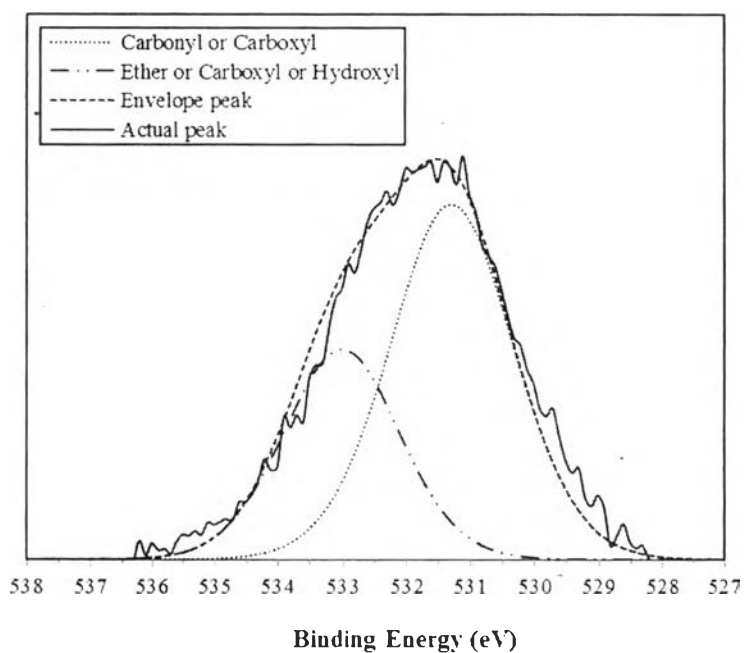
Figure G32 O1s XPS spectra of a 35 wt% DETA-derived PBZ carbon aerogel.
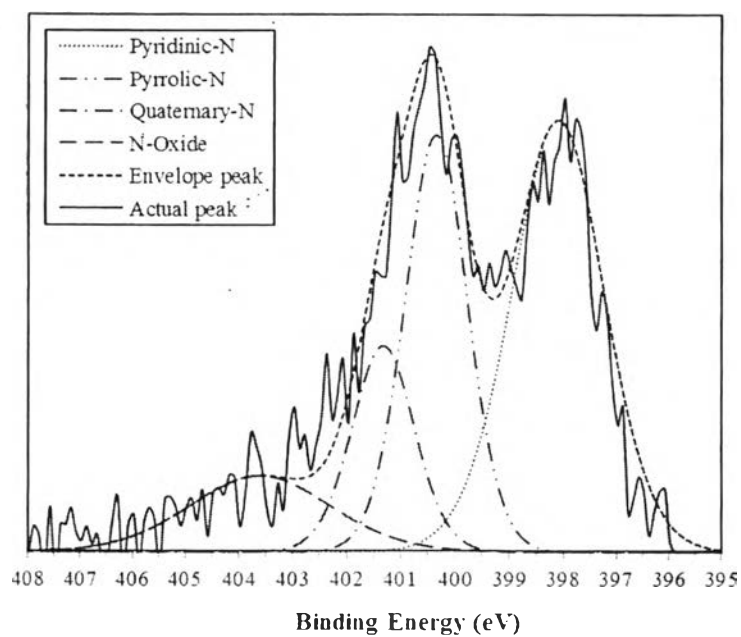
Figure G33 N1s XPS spectra of a 35 wt% DETA-derived PBZ carbon aerogel.

40 wt% DETA-derived PBZ carbon aerogel
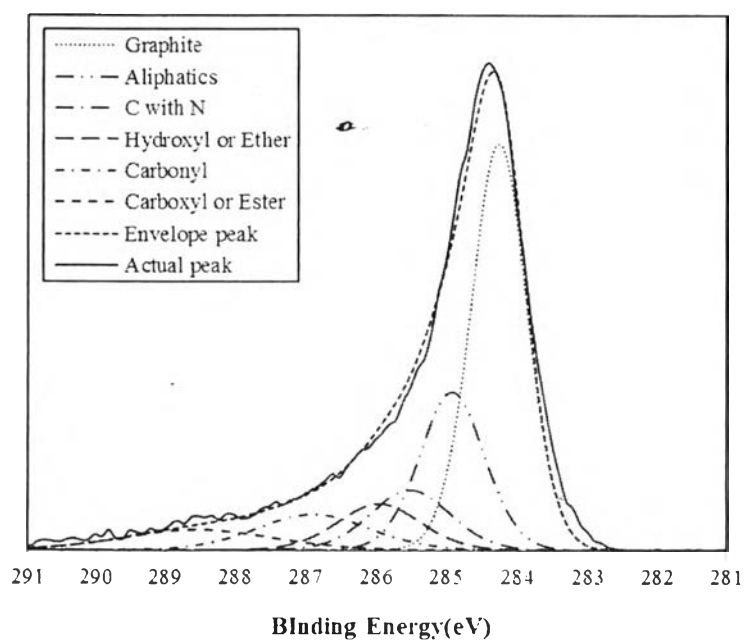
Figure G34 C1s XPS spectra of a 40 wt% DETA-derived PBZ carbon aerogel.
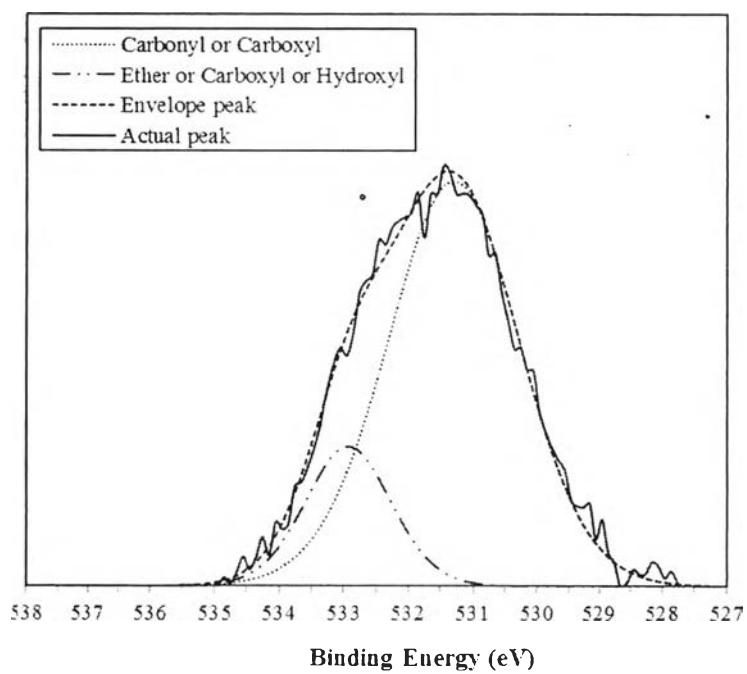
Figure G35 O1s XPS spectra of a 40 wt% DETA-derived PBZ carbon aerogel.
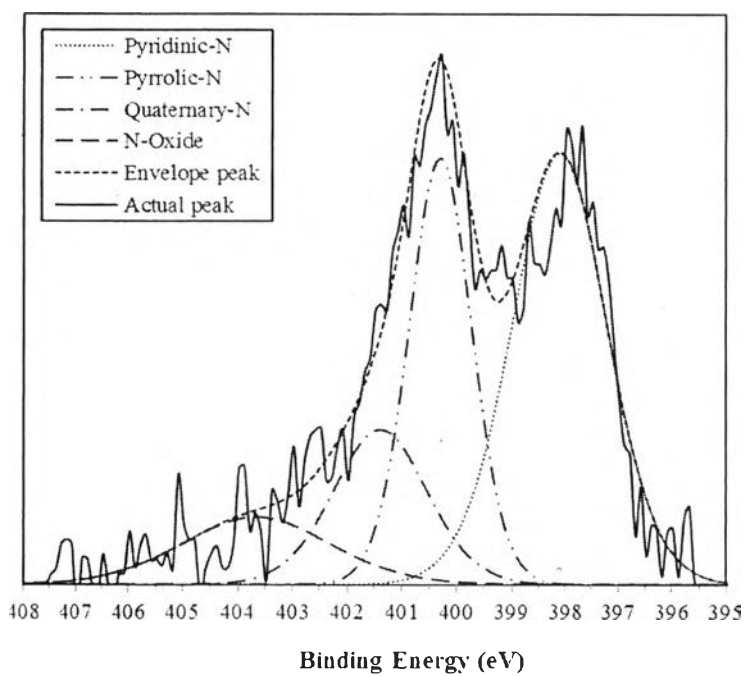
Figure G36 N1s XPS spectra of a 40 wt% DETA-derived PBZ carbon aerogel.

Activated carbon from PEHA-derived PBZ
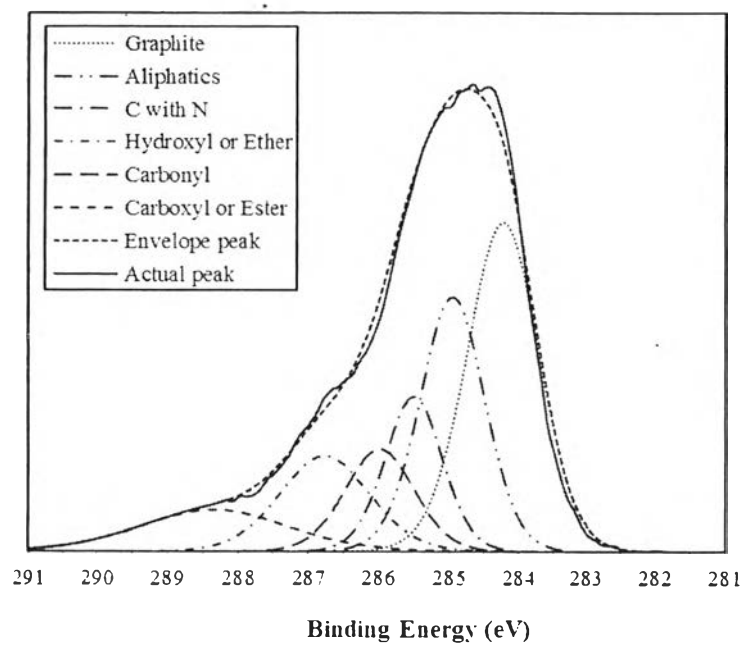
Figure G37 C1s XPS spectra of activated carbon from PEHA-derived PBZ.
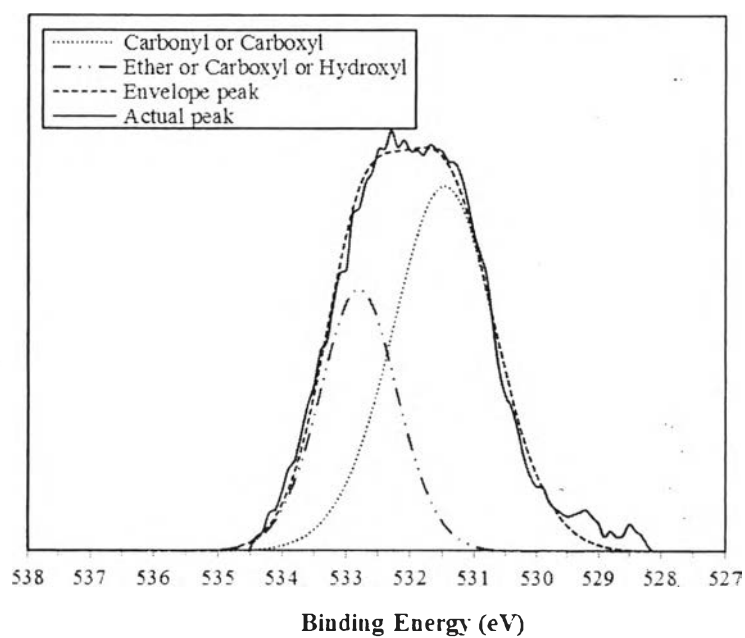
Figure G38 O1s XPS spectra of activated carbon from PEHA-derived PBZ.
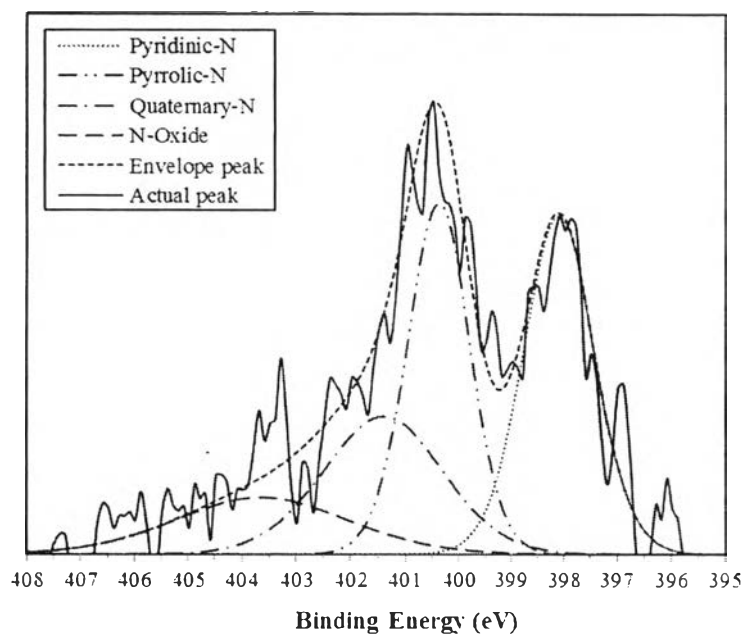
Figure G39 N1s XPS spectra of activated carbon from PEHA-derived PBZ.

30 wt% PEHA-derived PBZ carbon aerogel
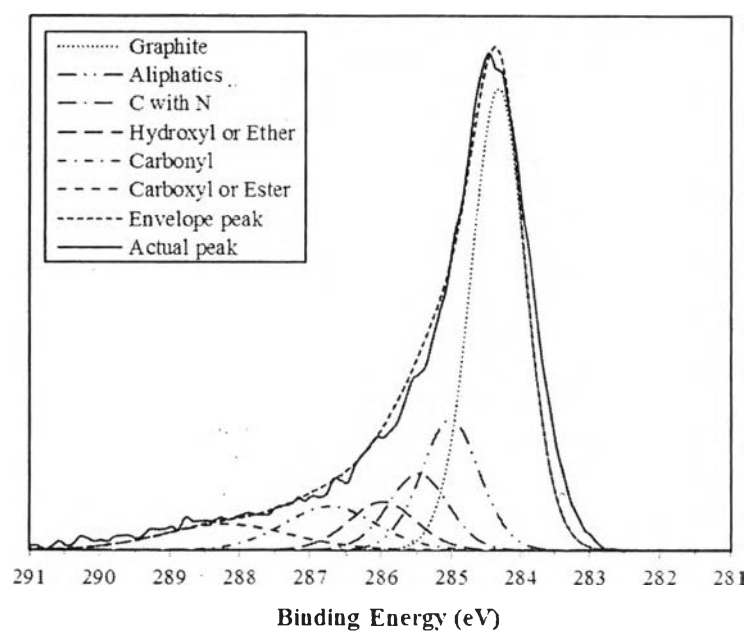
Figure G40 C1s XPS spectra of a 30 wt% PEHA-derived PBZ carbon aerogel.
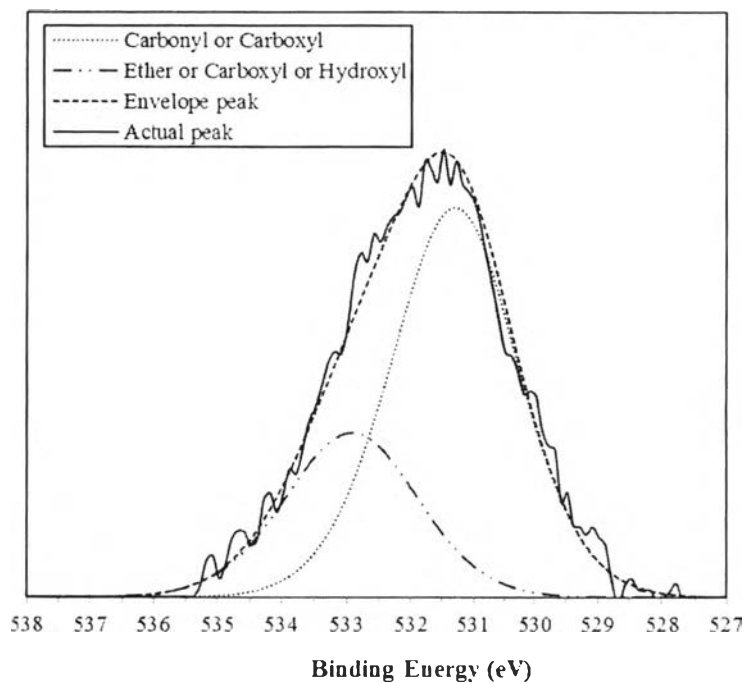
Figure G41 O1s XPS spectra of a 30 wt% PEHA-derived PBZ carbon aerogel.
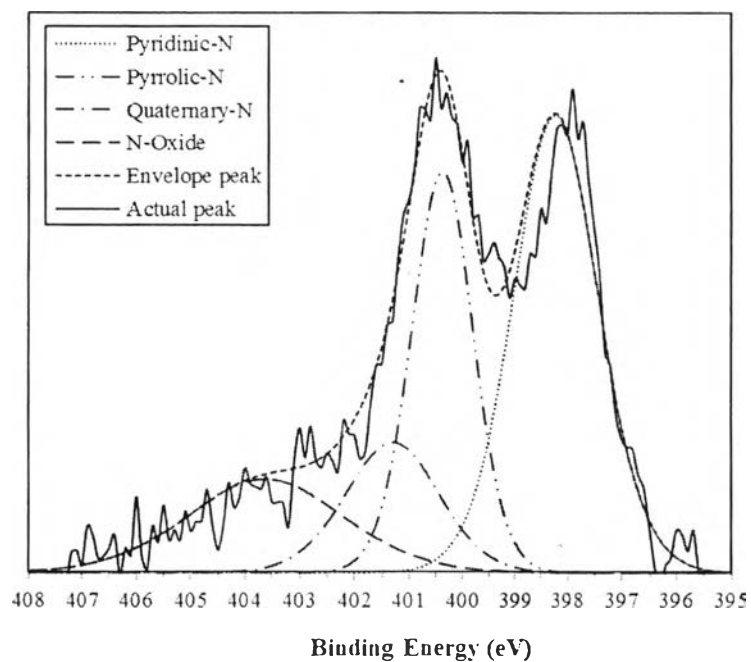
Figure G42 N1s XPS spectra of a 30 wt% PEHA-derived PBZ carbon aerogel.

35 wt% PEHA-derived PBZ carbon aerogel
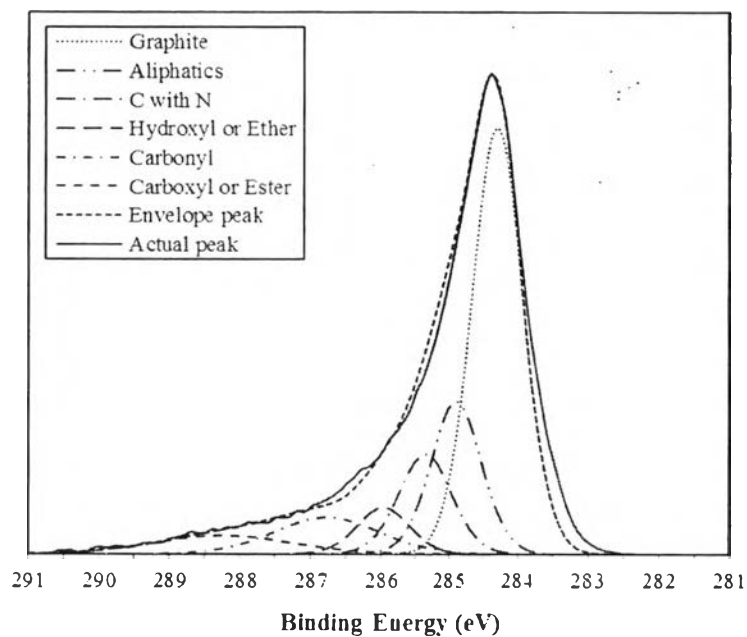
Figure G43 C1s XPS spectra of a 35 wt% PEHA-derived PBZ carbon aerogel.
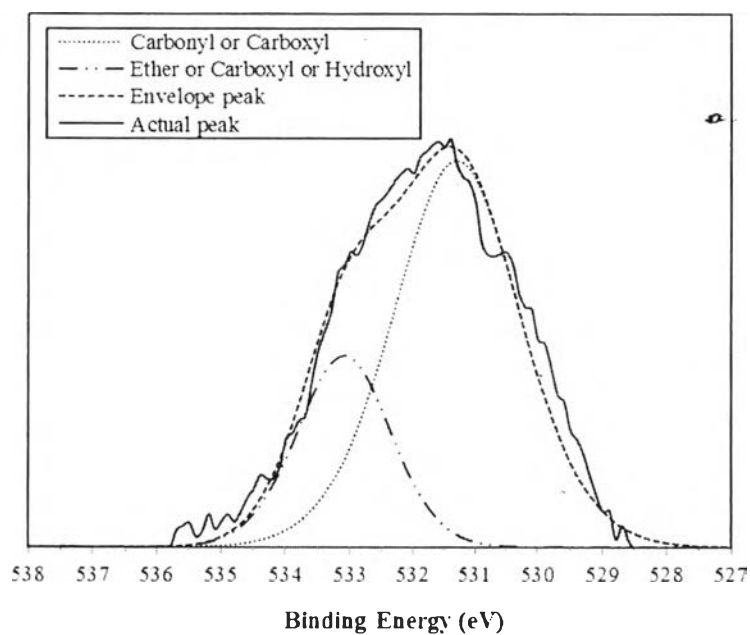
Figure G44 O1s XPS spectra of a 35 wt% PEHA-derived PBZ carbon aerogel.
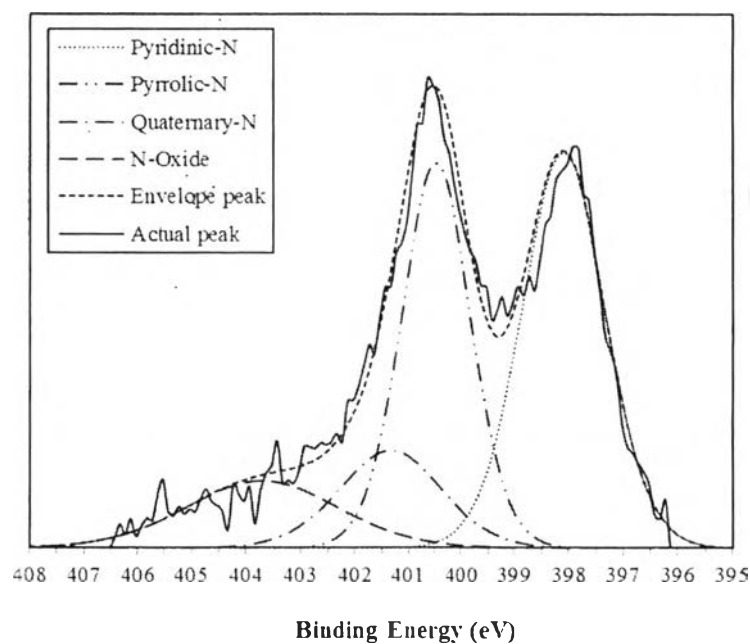
Figure G45 N1s XPS spectra of a 35 wt% PEHA-derived PBZ carbon aerogel.

40 wt% PEHA-derived PBZ carbon aerogel
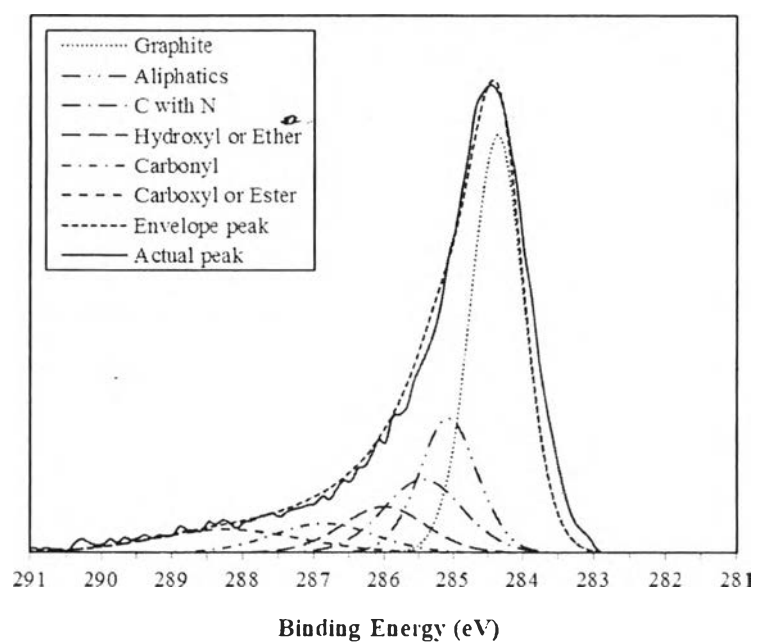
Figure G46 C1s XPS spectra of a 40 wt% PEHA-derived PBZ carbon aerogel.

Carbonyl or Carboxyl
Ether or Carboxyl or Hydroxyl
Envelope peak
Actual peak

538 537 536 535 534 533 532 531 530 529 528 527

Binding Energy (eV)
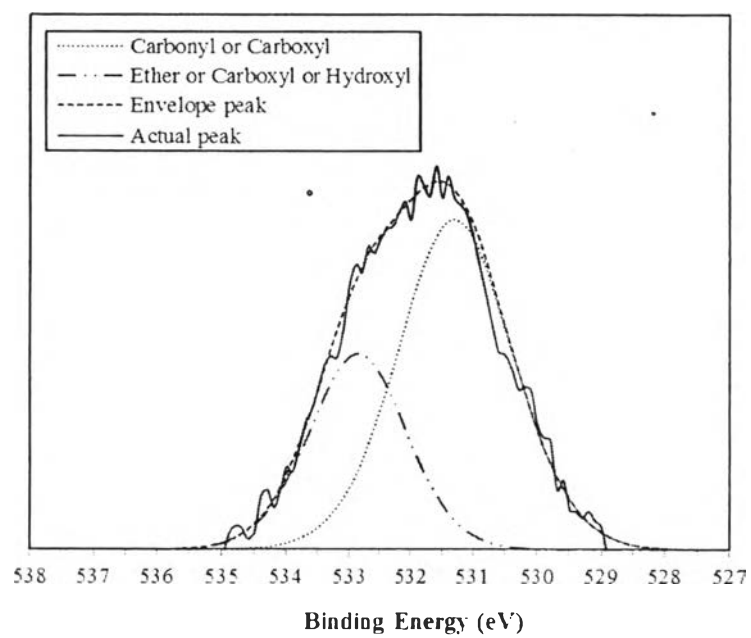
Figure G47 O1s XPS spectra of a 40 wt% PEHA-derived PBZ carbon aerogel.

Pyridinic-N
Pyrrolic-N
Quaternary-N
N-Oxide
Envelope peak
Actual peak

408 407 406 405 404 403 402 401 400 399 398 397 396 395

Binding Energy (eV)
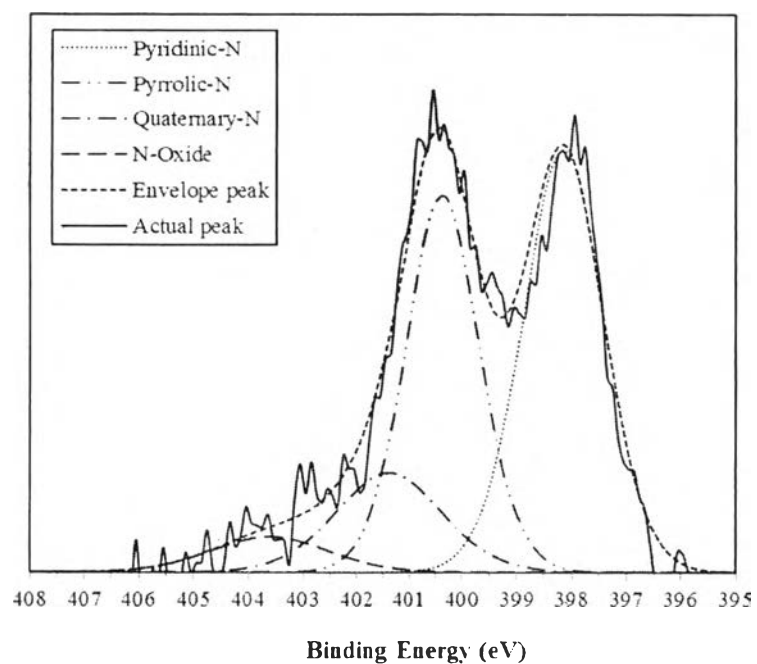
Figure G48 N1s XPS spectra of a 40 wt% PEHA-derived PBZ carbon aerogel.

Activated carbon from DETA-derived PBZ at activation temperature of 900 °C
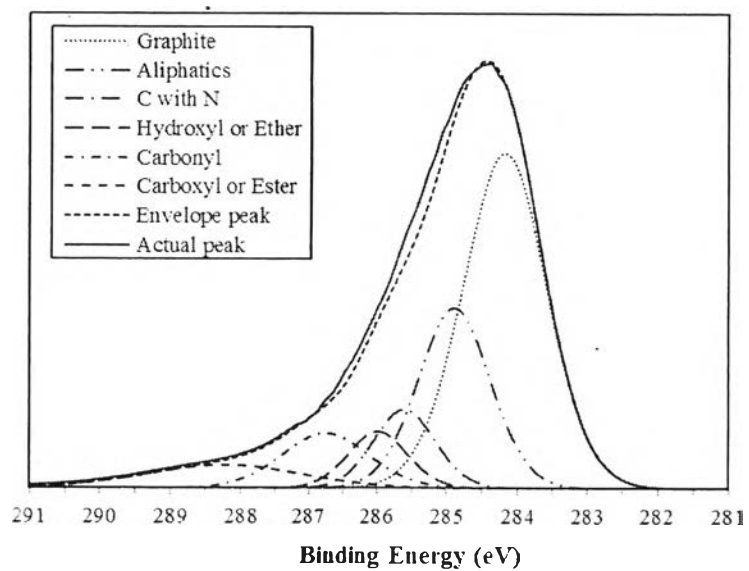
Figure G49 C1s XPS spectra of activated carbon from DETA-derived PBZ at activation temperature of 900 °C.
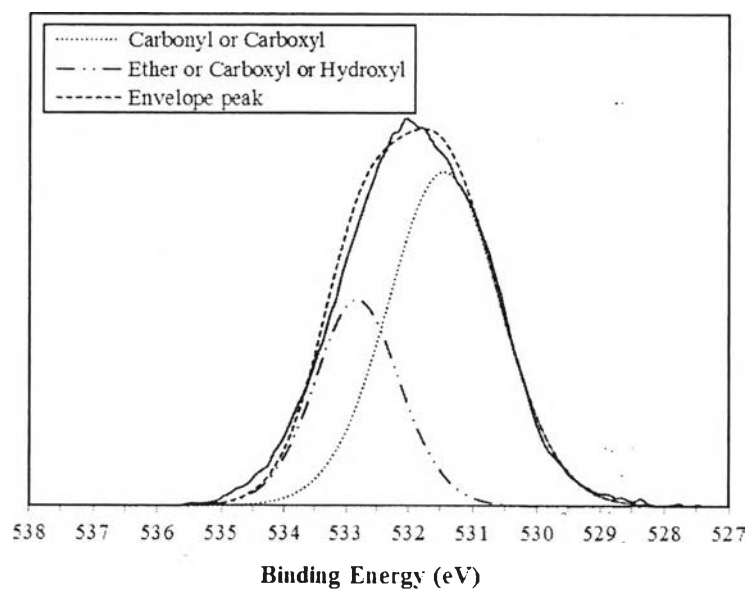
Figure G50 O1s XPS spectra of activated carbon from DETA-derived PBZ at activation temperature of 900 °C.
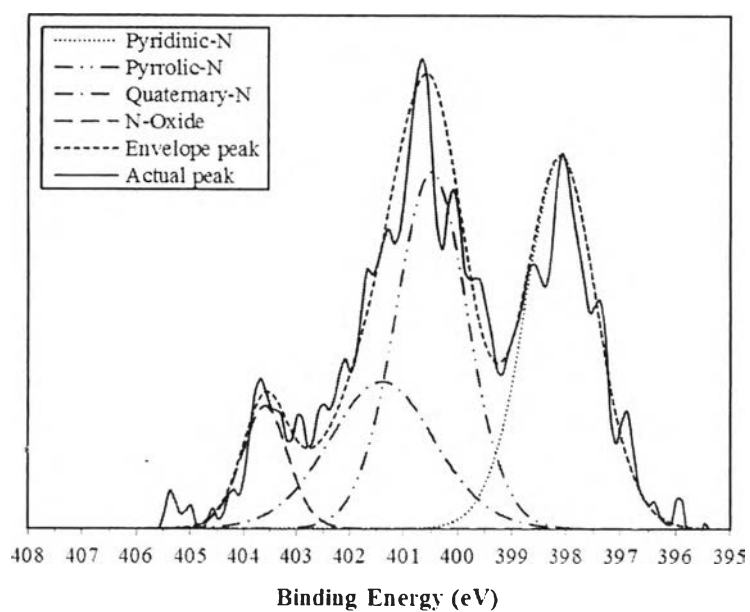
Figure G51 N1s XPS spectra of activated carbon from DETA-derived PBZ at activation temperature of 900 °C.

30 wt% DETA-derived PBZ carbon aerogel at activation temperature of 900 °C
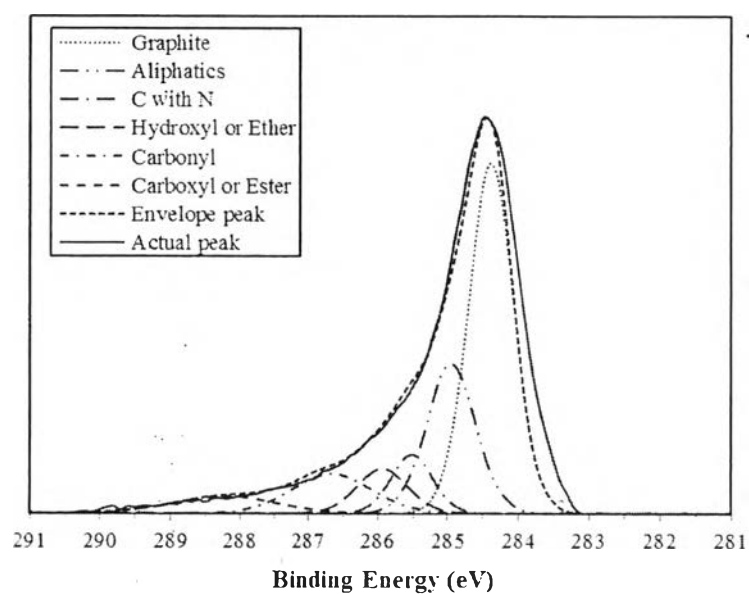
Figure G52 C1s XPS spectra of a 30 wt% DETA-derived PBZ carbon aerogel at activation temperature of 900 °C.
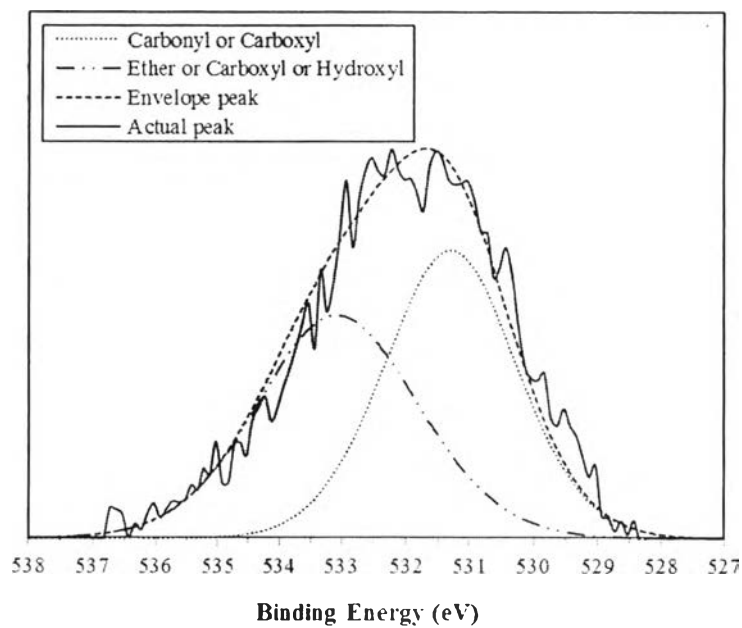
Figure G53 O1s XPS spectra of a 30 wt% DETA-derived PBZ carbon aerogel at activation temperature of 900 °C.
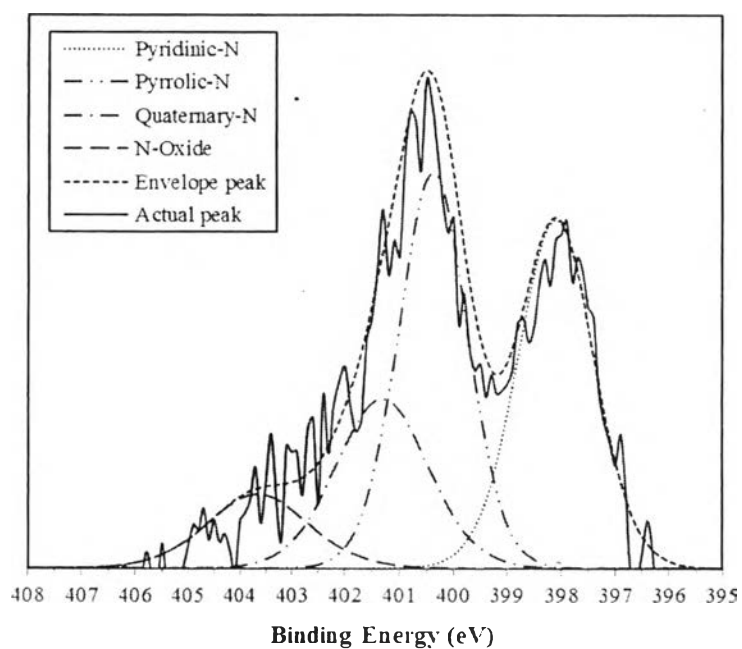
Figure G54 N1s XPS spectra of a 30 wt% DETA-derived PBZ carbon aerogel at activation temperature of 900 °C.

30 wt% DETA-derived PBZ carbon aerogel loading with non-ionic surfactant at activation temperature of 900 °C
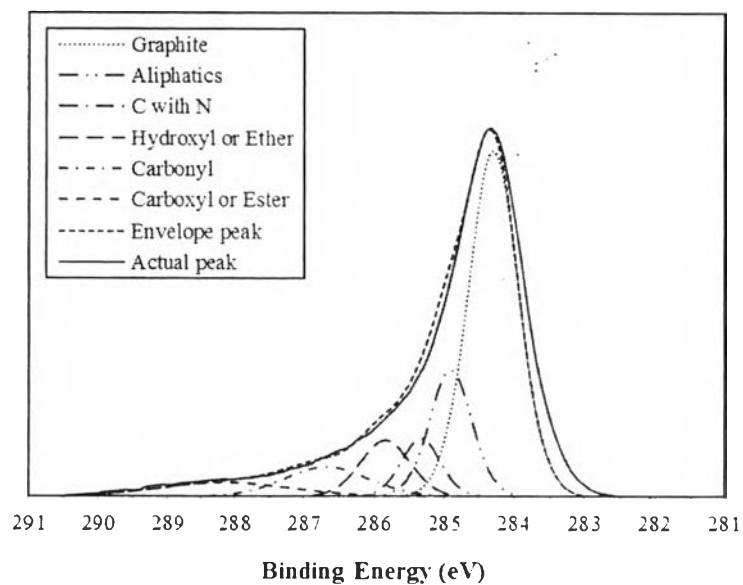
Figure G55 C1s XPS spectra of a 30 wt% DETA-derived PBZ carbon aerogel loading with non-ionic surfactant at ac-tivation temperature of 900 °C.
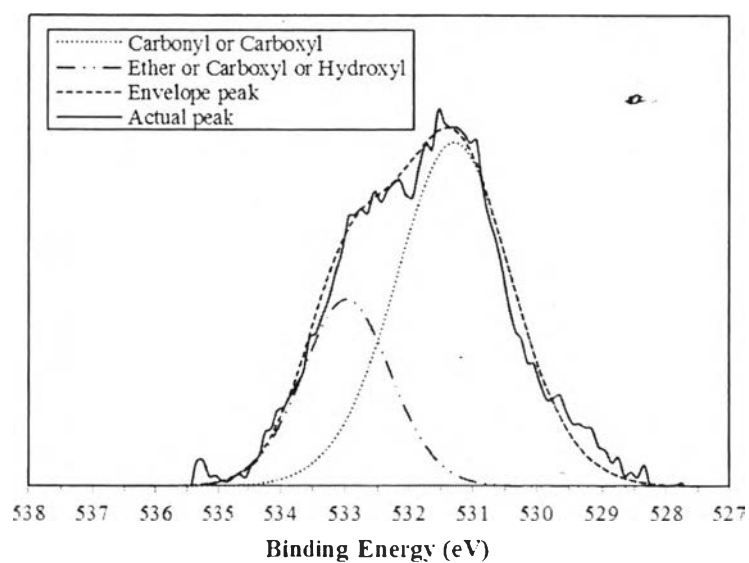
Figure G56 O1s XPS spectra of a 30 wt% DETA-derived PBZ carbon aerogel loading with non-ionic surfactant at ac-tivation temperature of 900 °C.
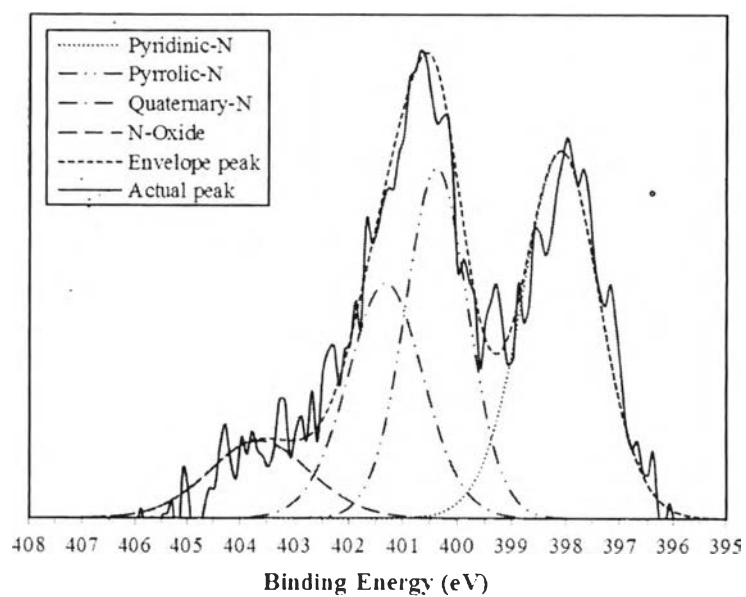
Figure G57 N1s XPS spectra of a 30 wt% DETA-derived PBZ carbon aerogel loading with non-ionic surfactant at activation temperature of 900 °C.

Activated carbon from PEHA-derived PBZ at activation temperature of 900 °C
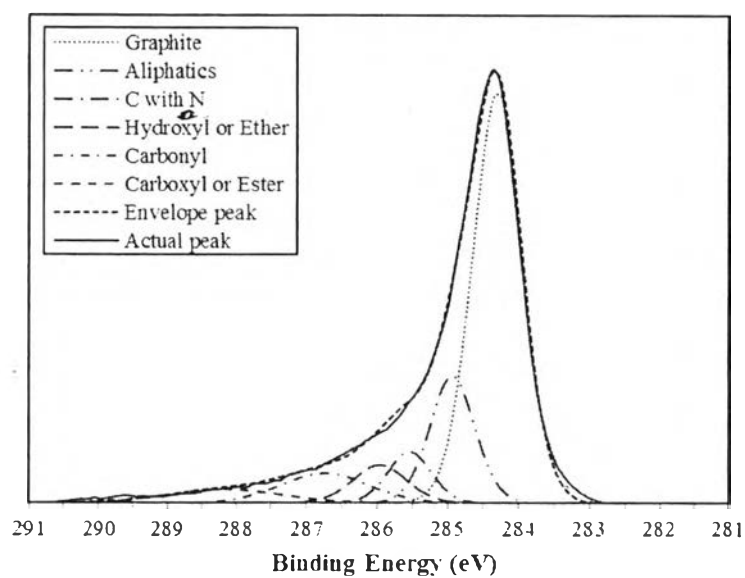
Figure G58 C1s XPS spectra of activated carbon from PEHA-derived PBZ at activation temperature of 900 °C.
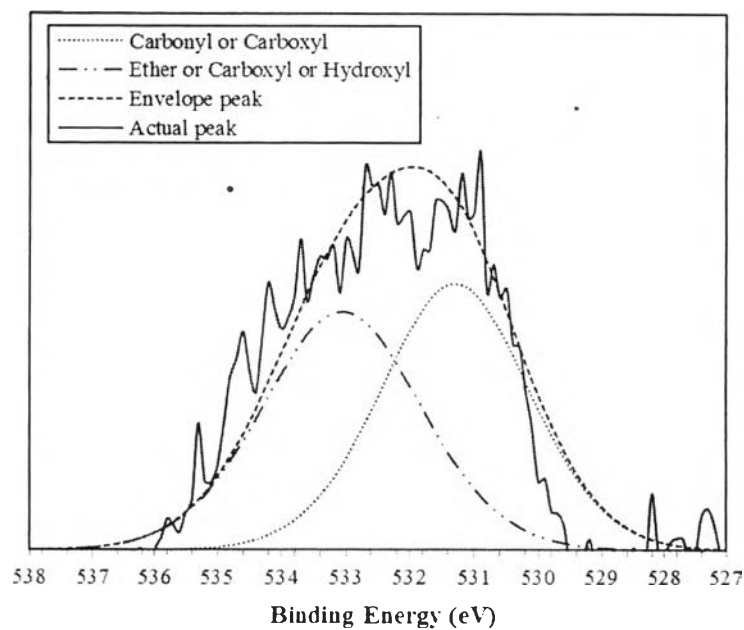
Figure G59 O1s XPS spectra of activated carbon from PEHA-derived PBZ at activation temperature of 900 °C.
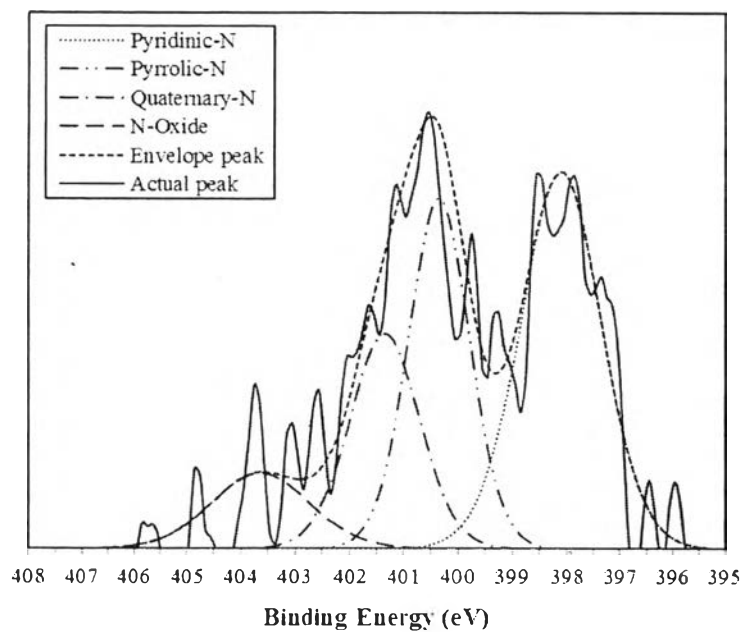
Figure G60 N1s XPS spectra of activated carbon from PEHA-derived PBZ at activation temperature of 900 °C.

30 wt% PEHA-derived PBZ carbon aerogel at activation temperature of 900 °C
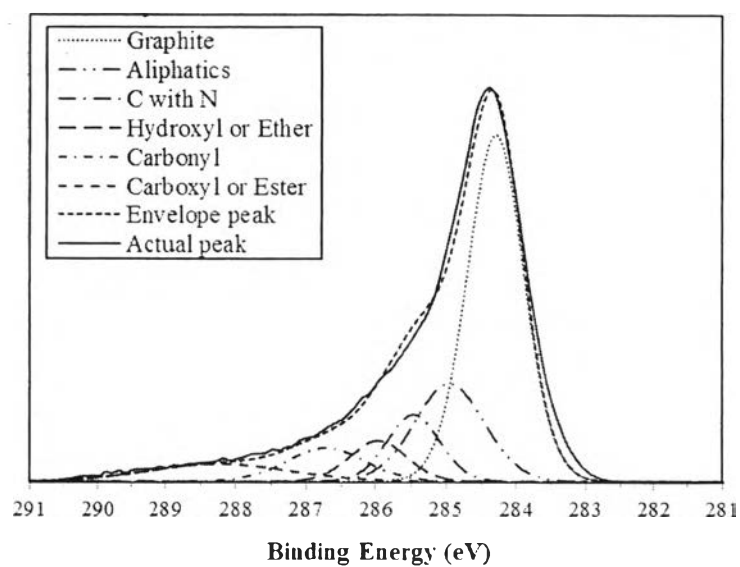
Figure G61 C1s XPS spectra of a 30 wt% PEHA-derived PBZ carbon aerogel at activation temperature of 900 °C.
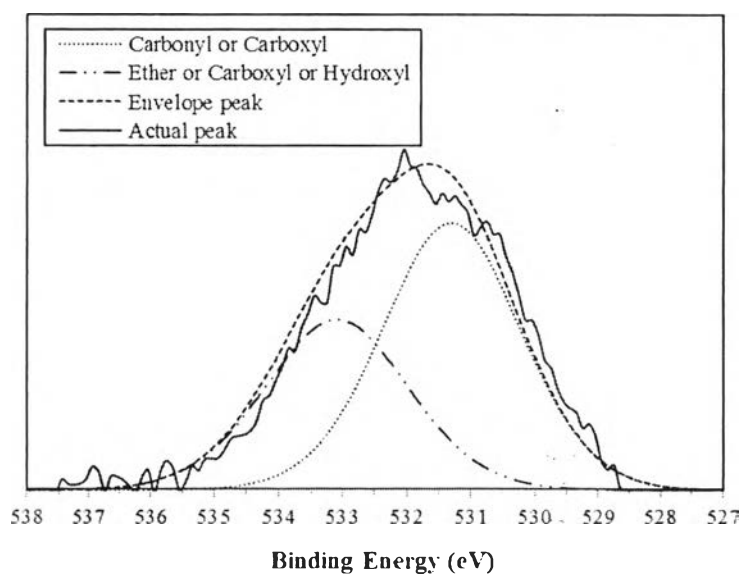
Figure G62 O1s XPS spectra of a 30 wt% PEHA-derived PBZ carbon aerogel at activation temperature of 900 °C.
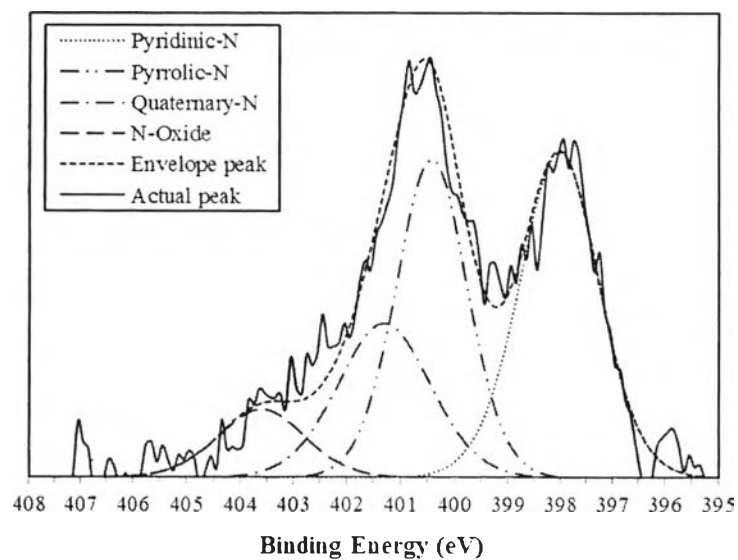
Figure G63 N1s XPS spectra of a 30 wt% PEHA-derived PBZ carbon aerogel at activation temperature of 900 °C.

30 wt% PEHA-derived PBZ carbon aerogel loading with non-ionic surfactant at activation temperature of 900 °C
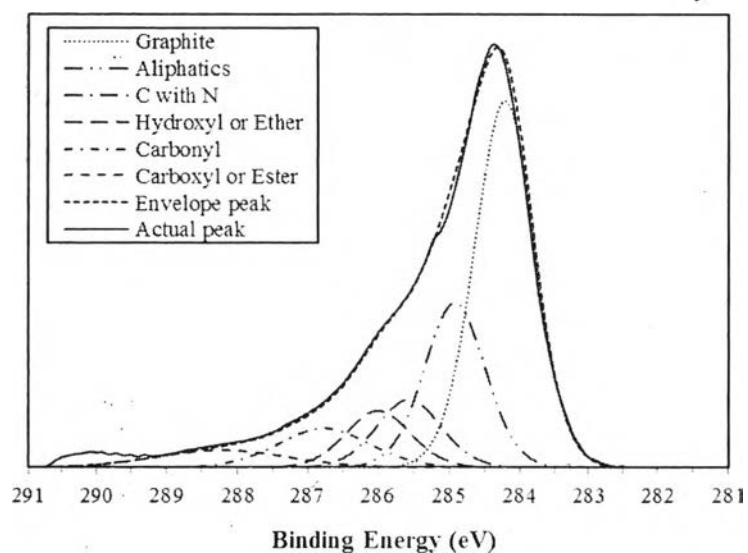
Figure G64 C1s XPS spectra of a 30 wt% PEHA-derived PBZ carbon aerogel loading with non-ionic surfactant at ac-tivation temperature of 900 °C.
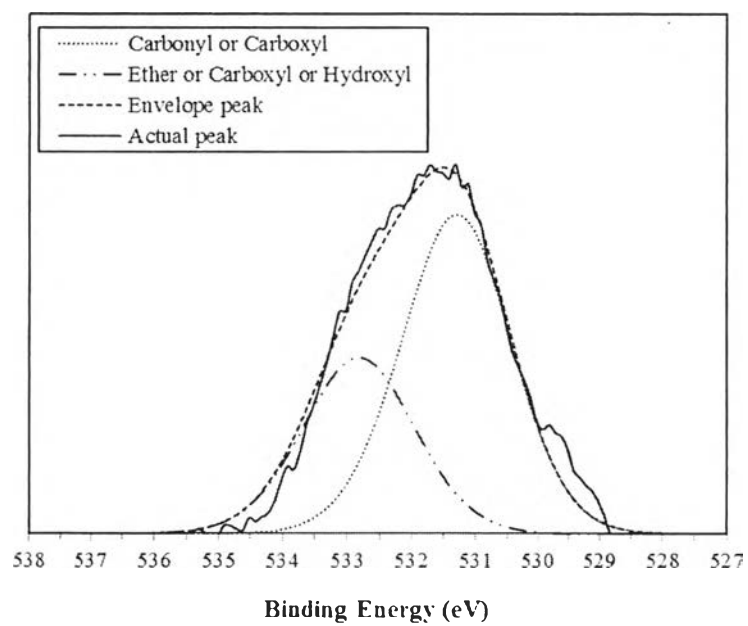
Figure G65 Ols XPS spectra of a 30 wt% PEHA-derived PBZ carbon aerogel loading with non-ionic surfactant at ac-tivation temperature of 900 °C.
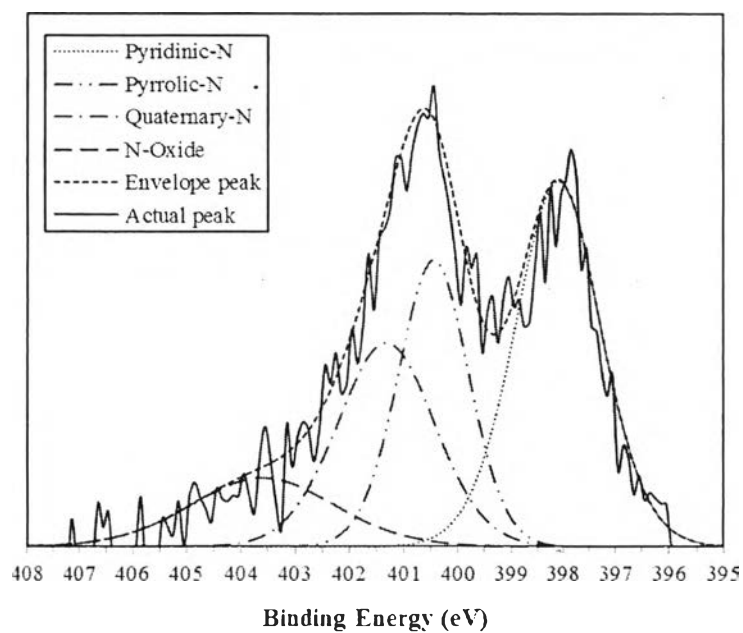
Figure G66 N1s XPS spectra of a 30 wt% PEHA-derived PBZ carbon aerogel loading with non-ionic surfactant at activation temperature of 900 °C.

Appendix H Isotherm, BJH Pore Size Distribution, and HK Pore Size Distribution of all Adsorbents

30 wt% DETA-derived PBZ organic aerogel
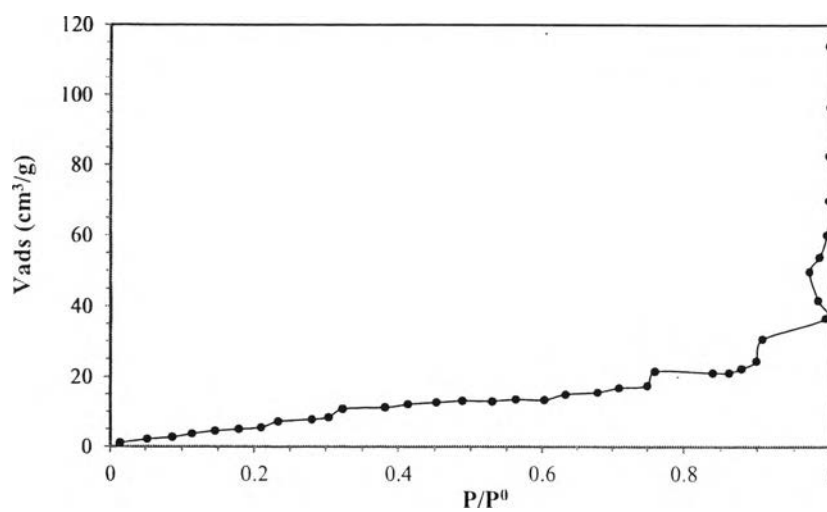
Figure H1 Isotherm of a 30 wt% DETA-derived PBZ organic aerogel.
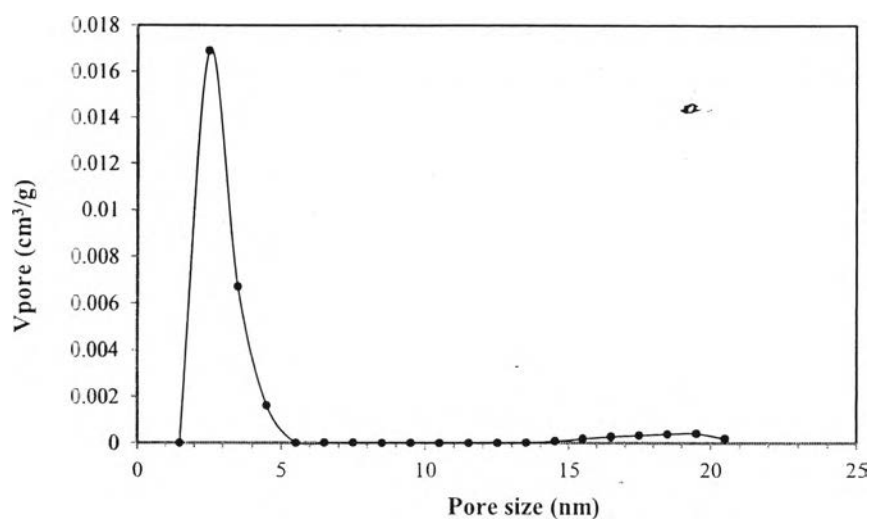
Figure H2 Barrett-Joyner-Halenda pore size distribution of a 30 wt% DETA-derived PBZ organic aerogel.
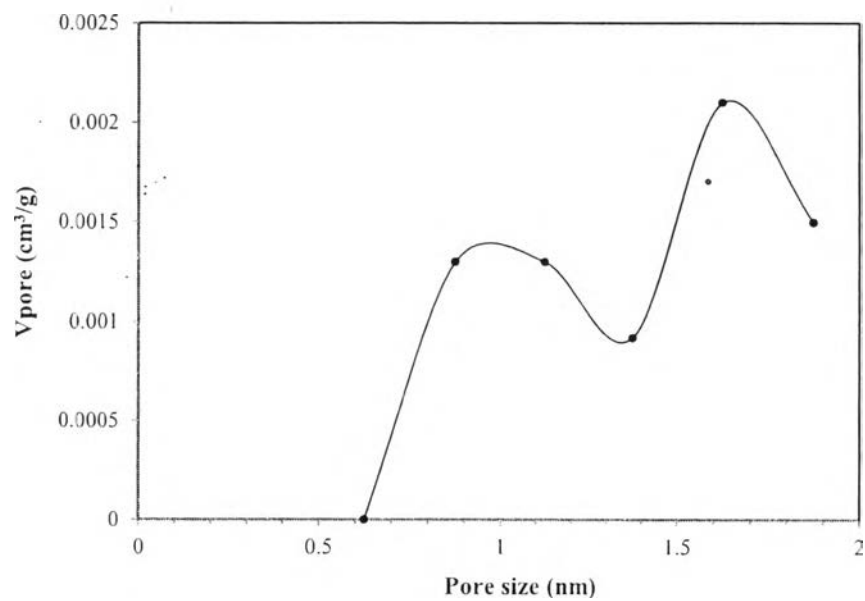
Figure H3 Horvath and Kawazoe pore size distribution of a 30 wt% DETA-derived PBZ organic aerogel.

35 wt% DETA-derived PBZ organic aerogel
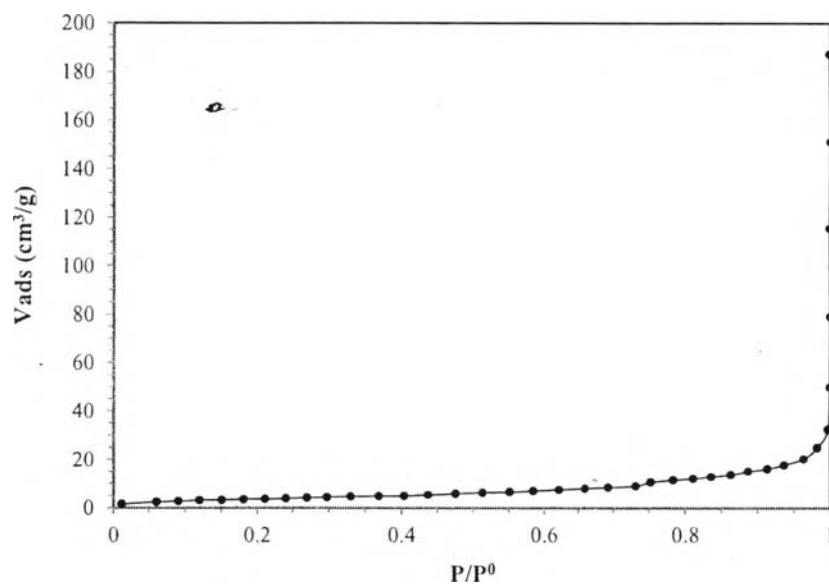
Figure H4 Isotherm of a 35 wt% DETA-derived PBZ organic aerogel.
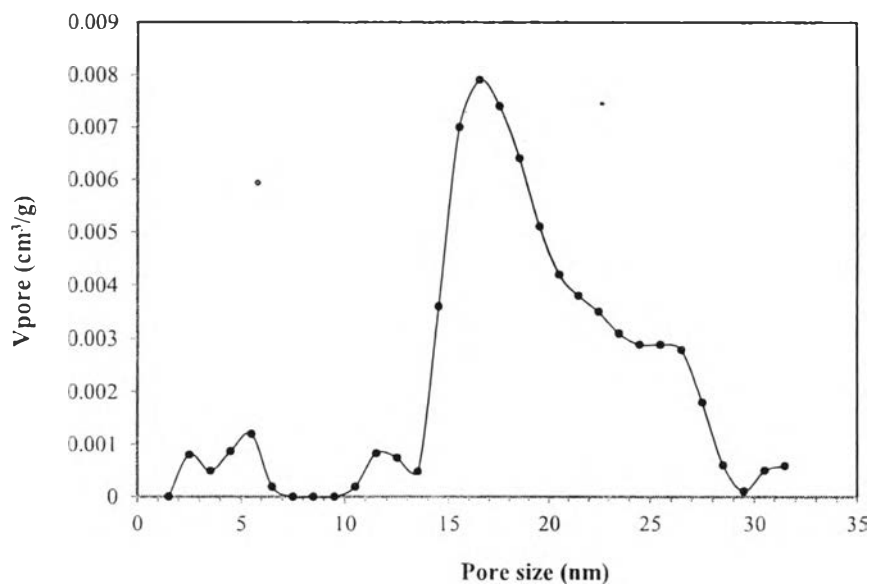
Figure H5 Barrett-Joyner-Halenda pore size distribution of a 35 wt% DETA-derived PBZ organic aerogel.
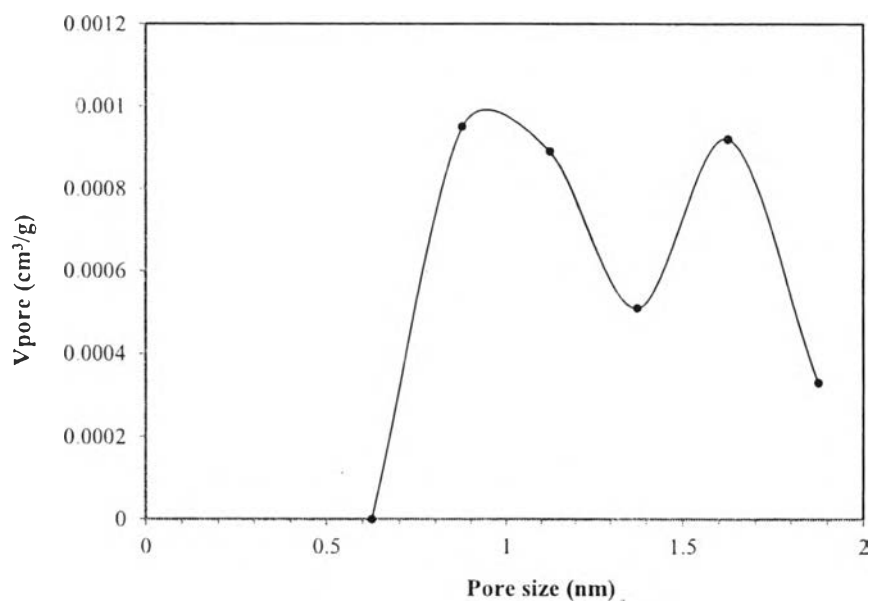
Figure C6 Horvath and Kawazoe pore size distribution of a 35 wt% DETA-derived PBZ organic aerogel.

40 wt% DETA-derived PBZ organic aerogel
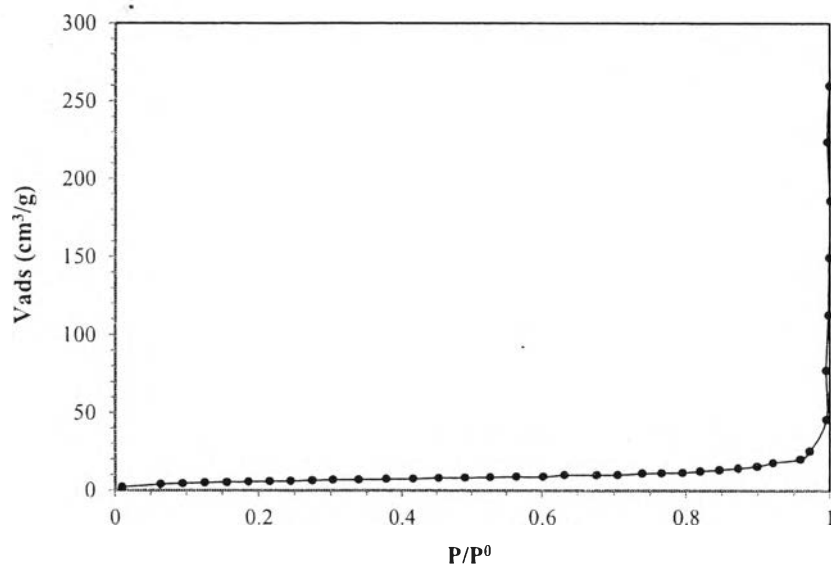
Figure H7 Isotherm of a 40 wt% DETA-derived PBZ organic aerogel.
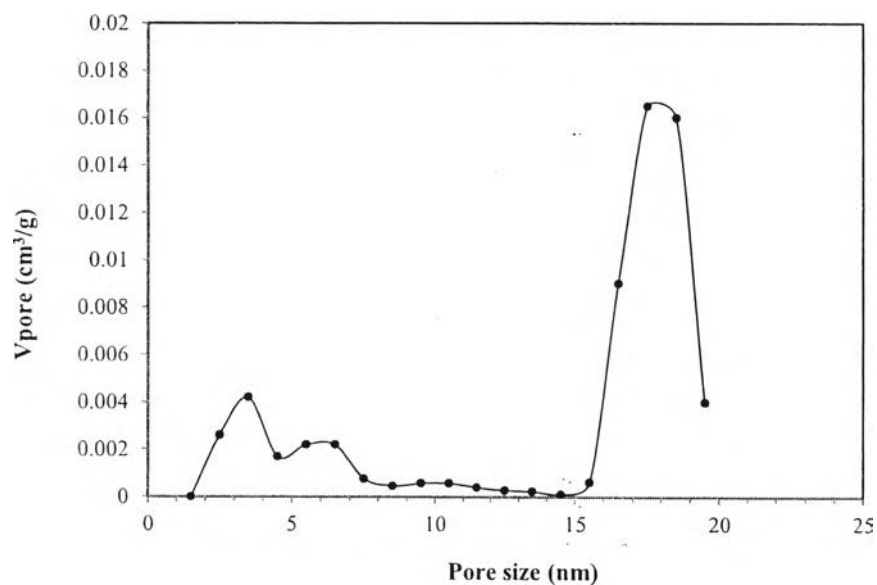
Figure H8 Barrett-Joyner-Halenda pore size distribution of a 40 wt% DETA-derived PBZ organic aerogel.
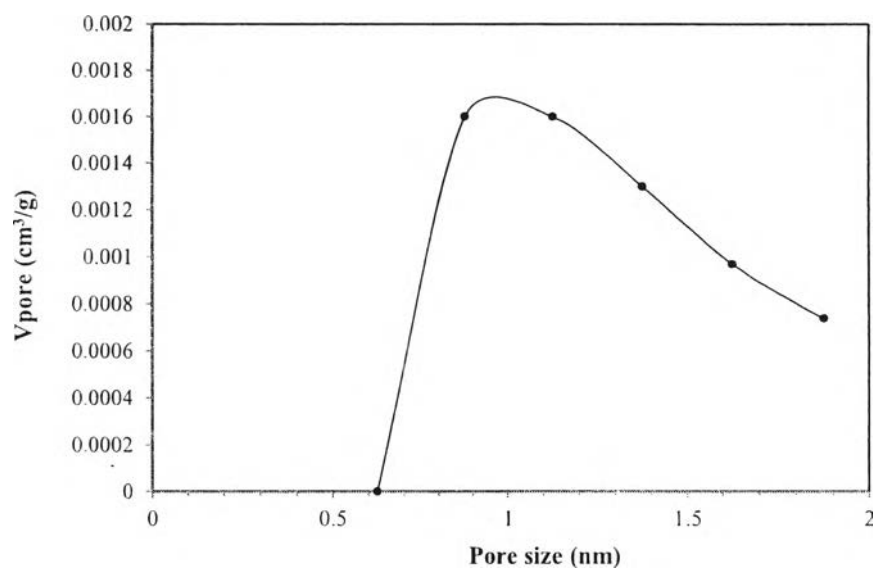
Figure H9 Horvath and Kawazoe pore size distribution of a 40 wt% DETA-derived PBZ organic aerogel.

30 wt% PEHA-derived PBZ organic aerogel
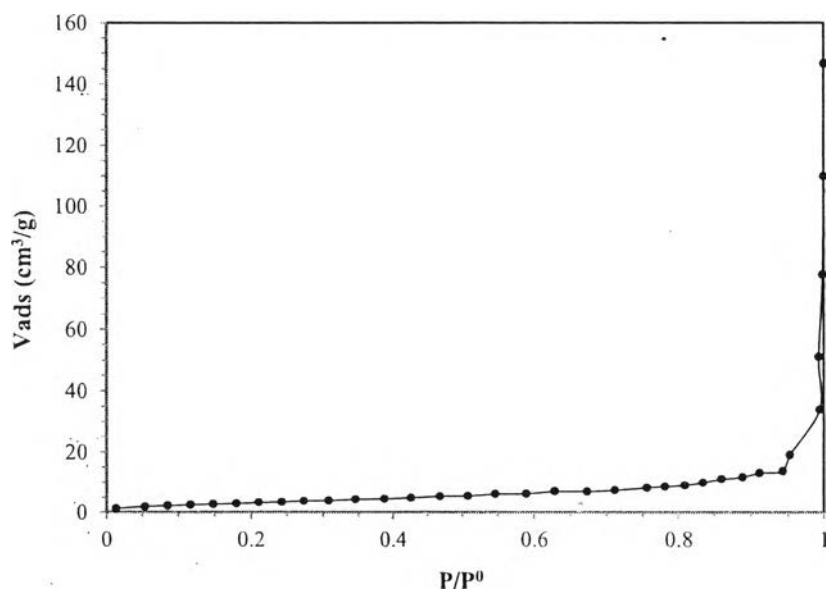
Figure H10 Isotherm of a 30 wt% PEHA-derived PBZ organic aerogel.
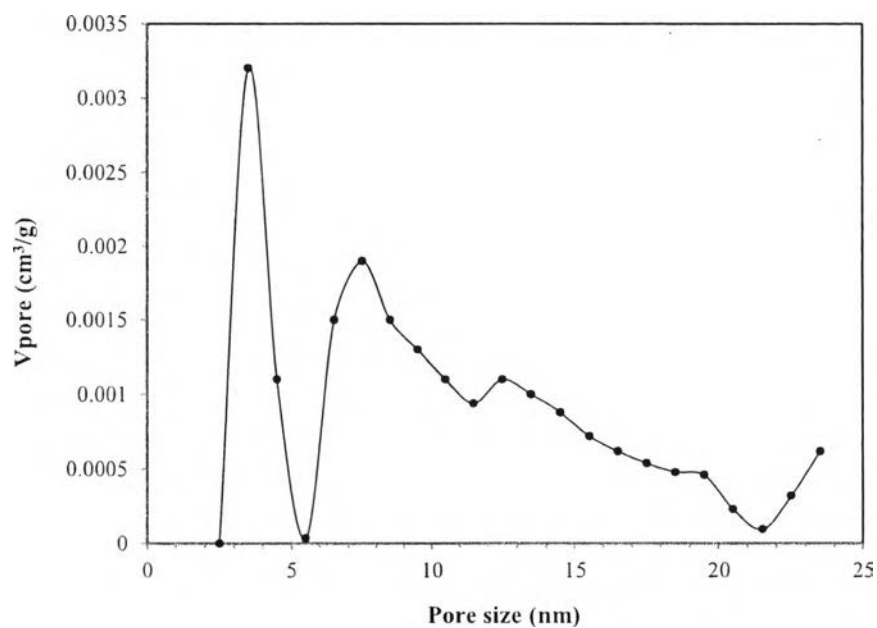
Figure H11 Barrett-Joyner-Halenda pore size distribution of a 30 wt% PEHA-derived PBZ organic aerogel.
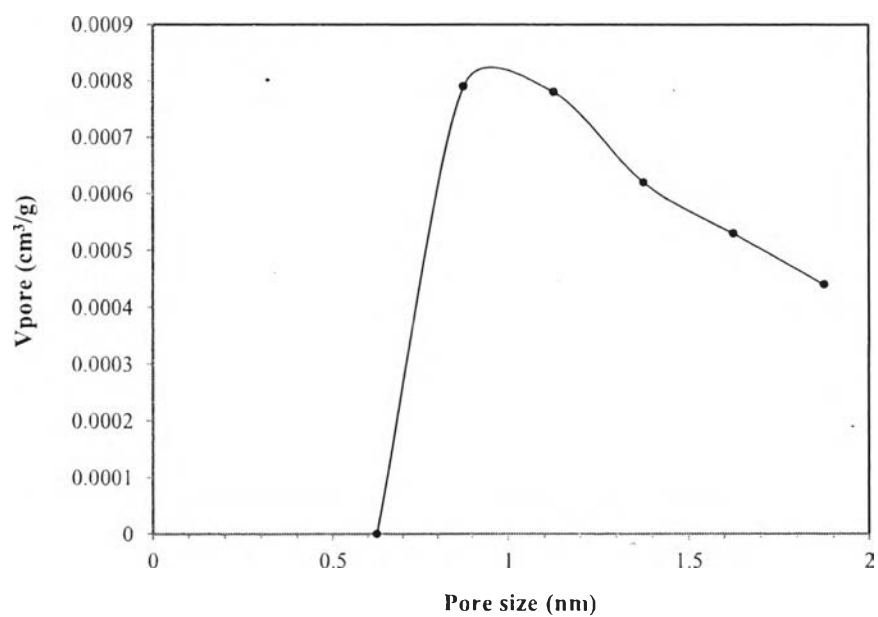
Figure H12 Horvath and Kawazoe pore size distribution of a 30 wt% PEHA-derived PBZ organic aerogel.

35 wt% PEHA-derived PBZ organic aerogel
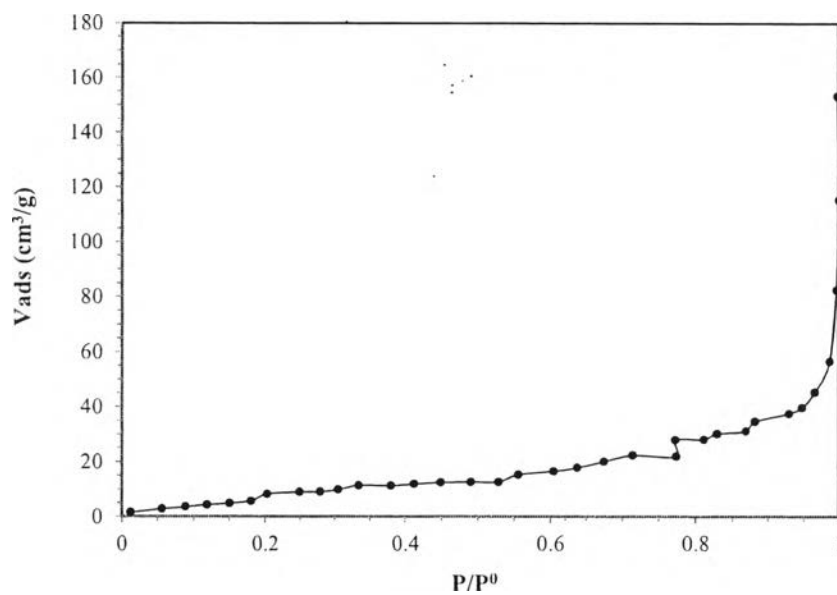
Figure H13 Isotherm of a 35 wt% PEHA-derived PBZ organic aerogel.
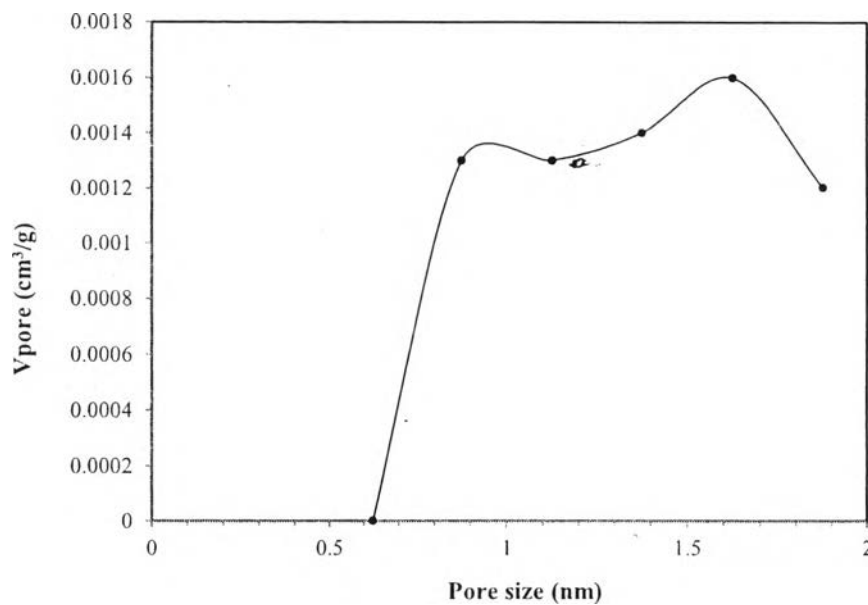
Figure H14 Horvath and Kawazoe pore size distribution of a 35 wt% PEHA-derived PBZ organic aerogel.

40 wt% PEHA-derived PBZ organic aerogel
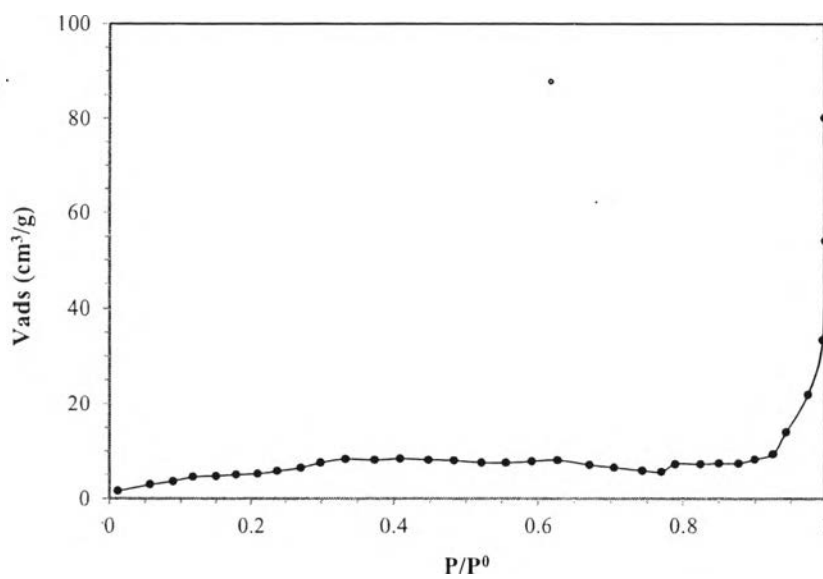
Figure H15 Isotherm of a 40 wt% PEHA-derived PBZ organic aerogel.
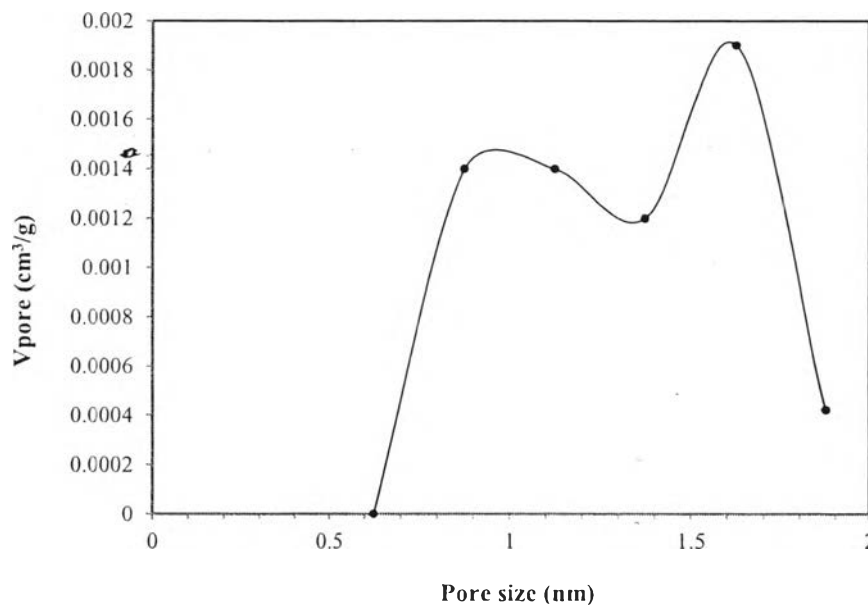
Figure H16 Horvath and Kawazoe pore size distribution of a 40 wt% PEHA-derived PBZ organic aerogel.

Activated carbon from DETA-derived PBZ
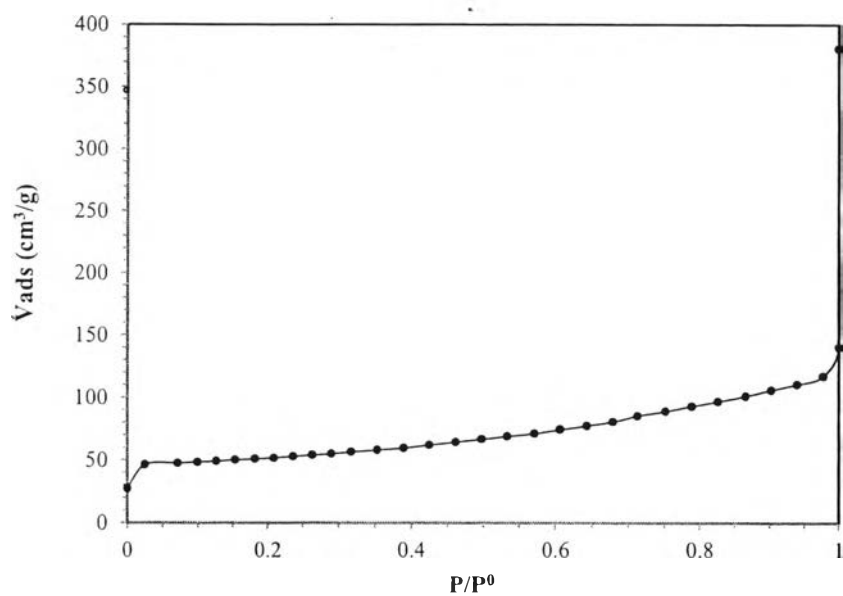
Figure H17 Isotherm of activated carbon from DETA-derived PBZ.
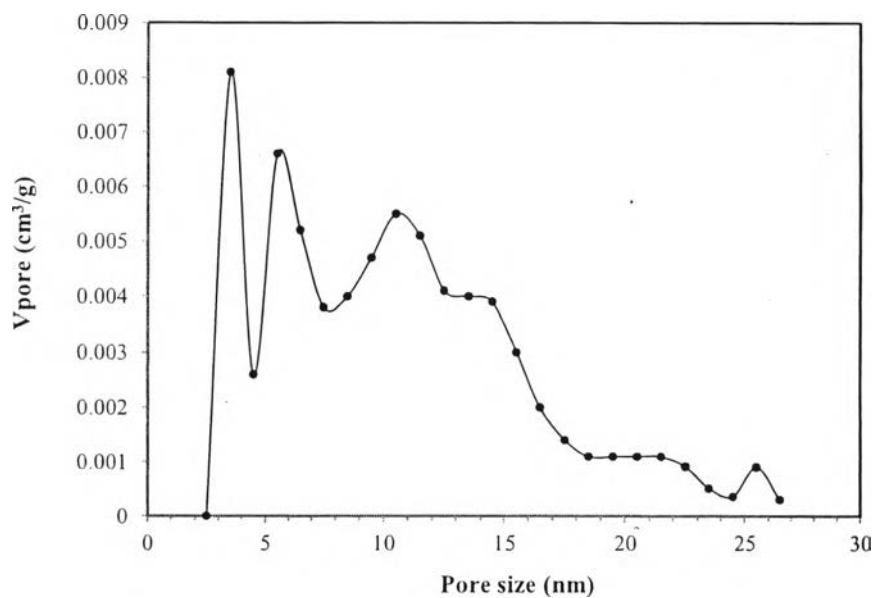
Figure H18 Barrett-Joyner-Halenda pore size distribution of activated carbon from DETA-derived PBZ.
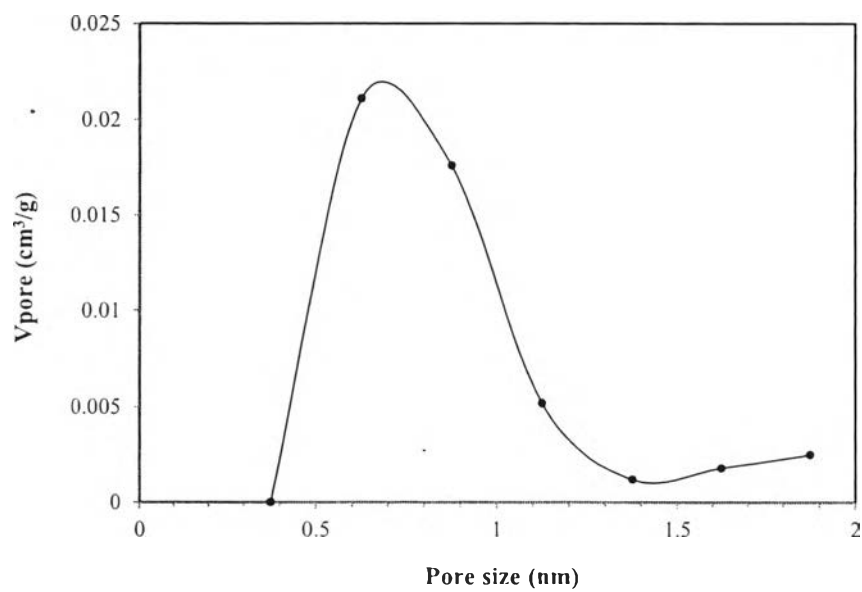
Figure H19 Horvath and Kawazoe pore size distribution of activated carbon from DETA-derived PBZ.

30 wt% DETA-derived PBZ carbon aerogel
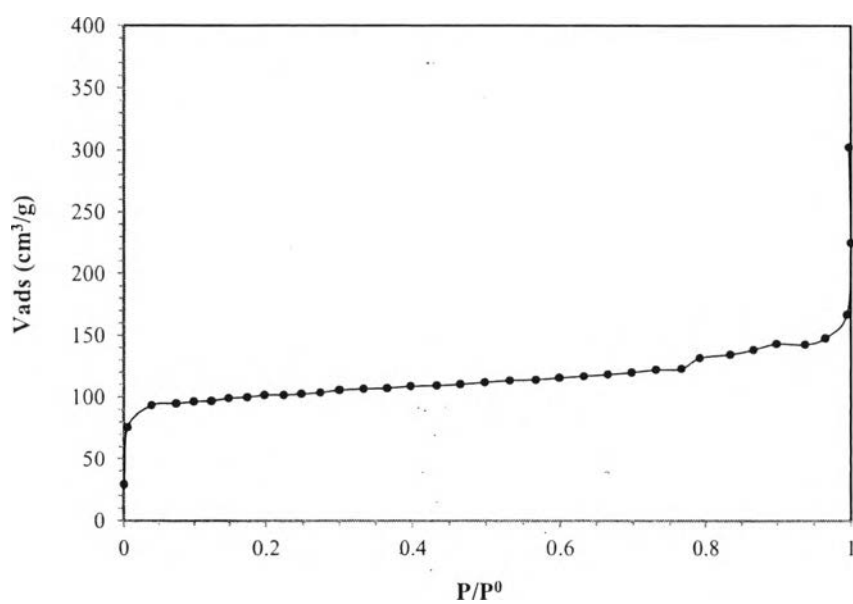
Figure H20 Isotherm of a 30 wt% DETA-derived PBZ carbon aerogel.
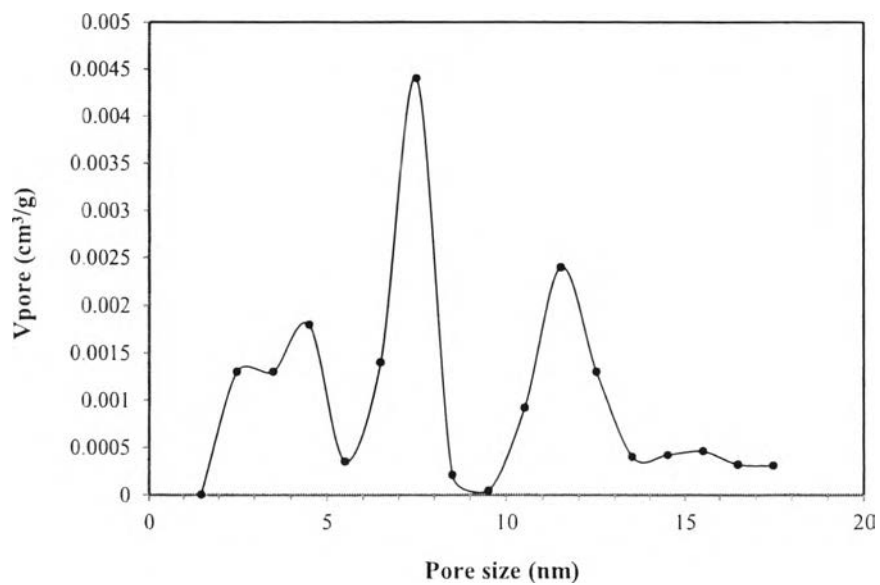
Figure H21 Barrett-Joyner-Halenda pore size distribution of a 30 wt% DETA-derived PBZ carbon aerogel.
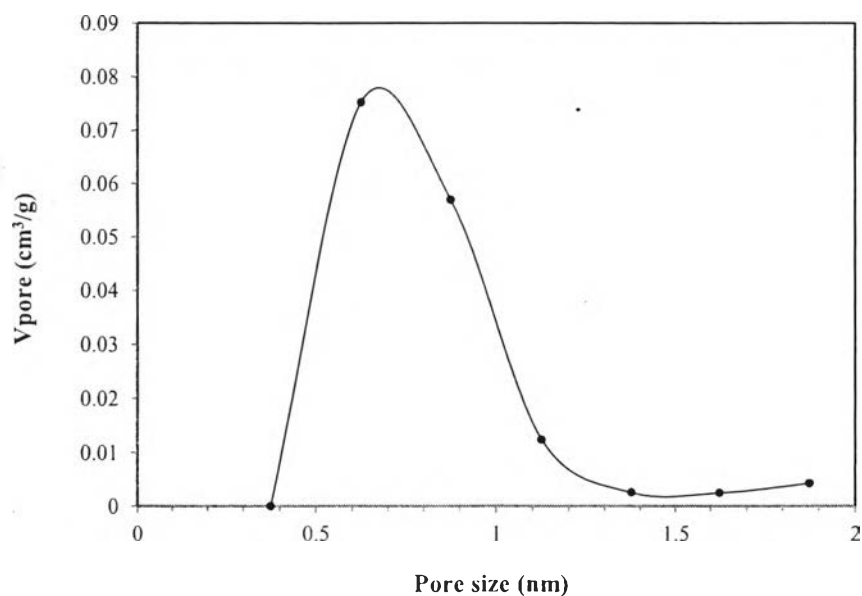
Figure H22 Horvath and Kawazoe pore size distribution of a 30 wt% DETA-derived PBZ carbon aerogel.

35 wt% DETA-derived PBZ carbon aerogel
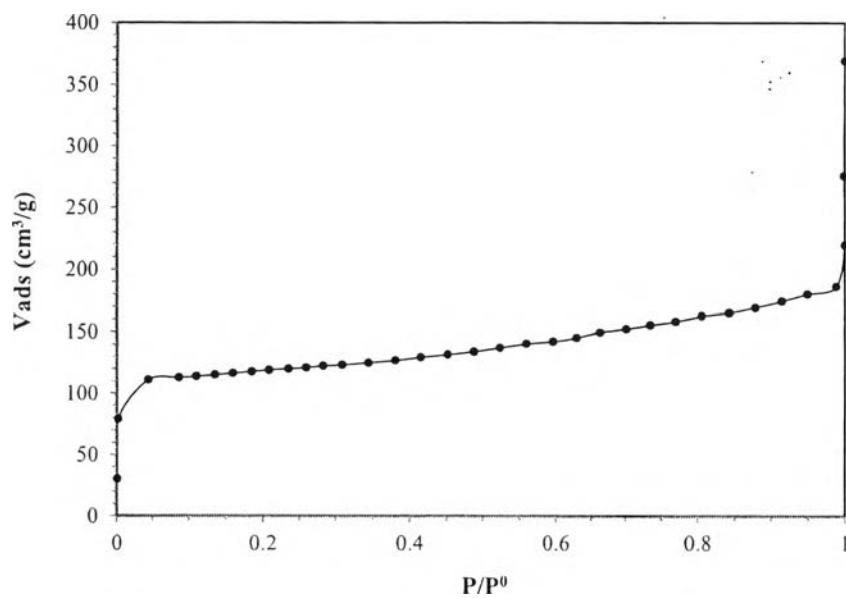
Figure H23 Isotherm of a 35 wt% DETA-derived PBZ carbon aerogel.
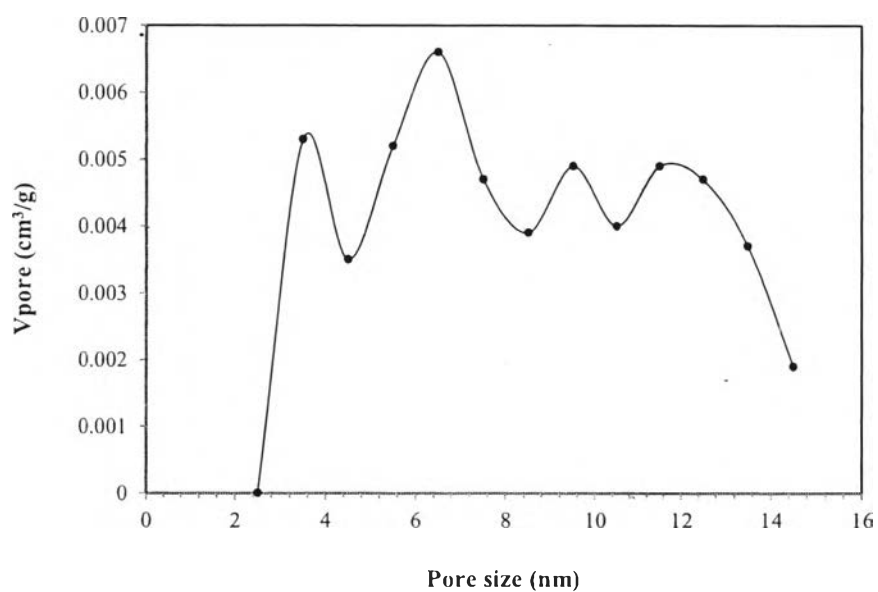
Figure H24 Barrett-Joyner-Halenda pore size distribution of a 35 wt% DETA-derived PBZ carbon aerogel.
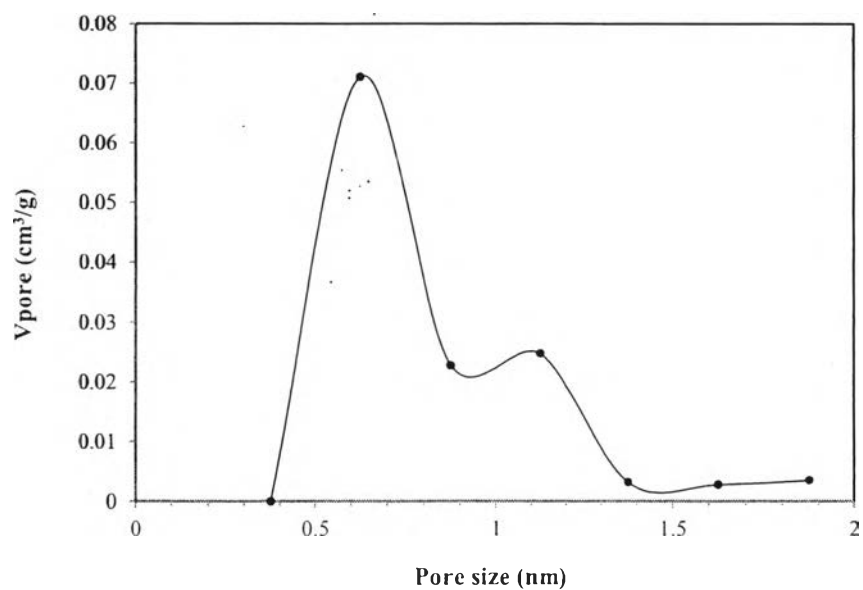
Figure H25 Horvath and Kawazoe pore size distribution of a 35 wt% DETA-derived PBZ carbon aerogel.

40 wt% DETA-derived PBZ carbon aerogel
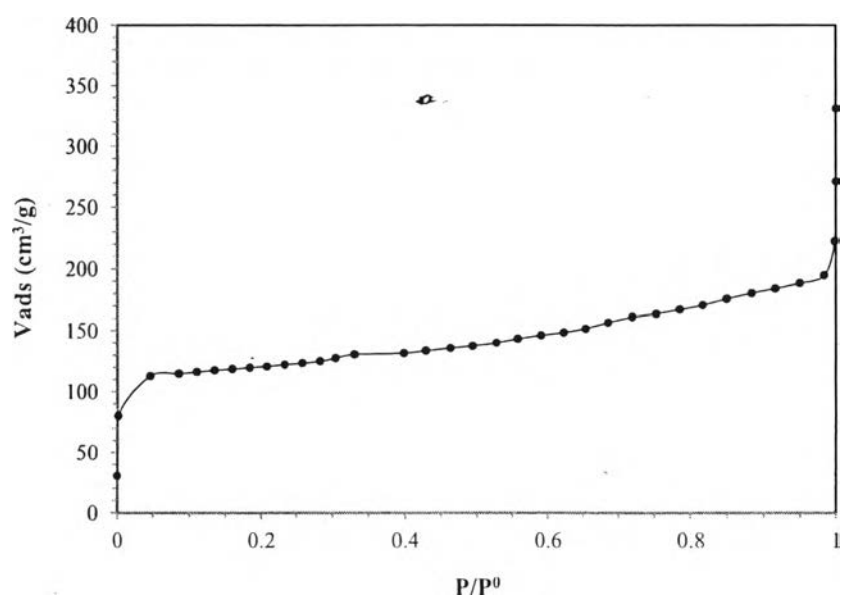
Figure H26 Isotherm of a 40 wt% DETA-derived PBZ carbon aerogel.
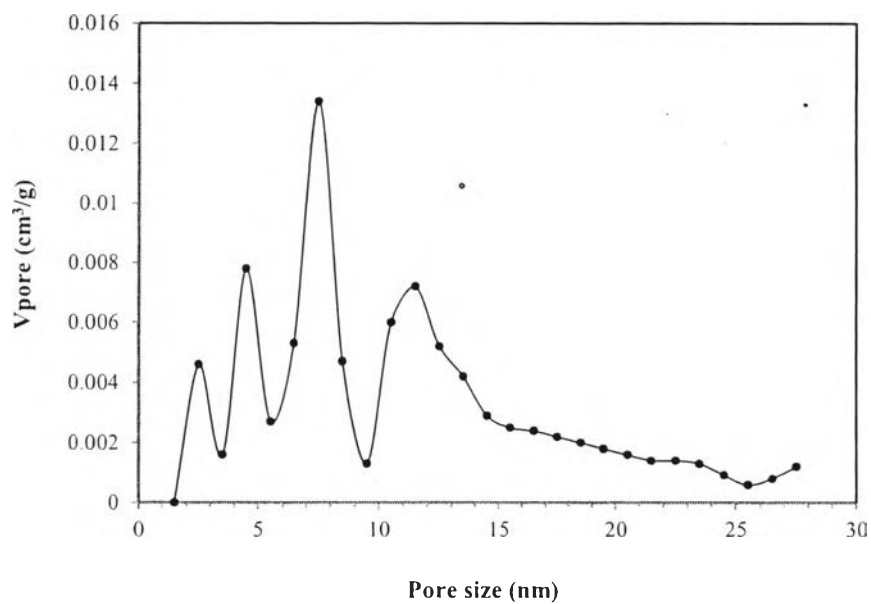
Figure H27   Barrett-Joyner-Halenda pore size distribution of a 40 wt% DETA-derived PBZ carbon aerogel.
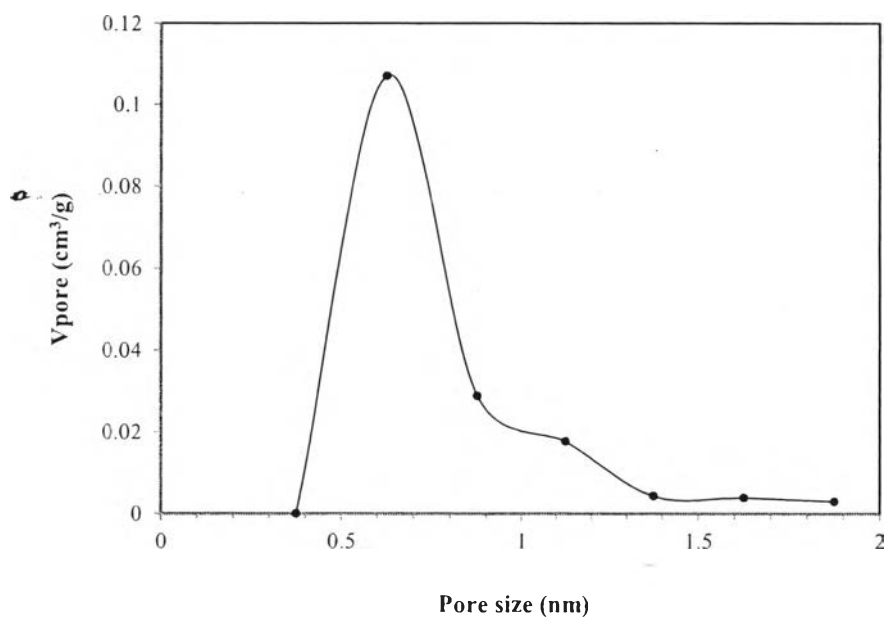
Figure H28   Horvath and Kawazoe pore size distribution of a 40 wt% DETA-derived PBZ carbon aerogel.

Activated carbon from PEHA-derived PBZ
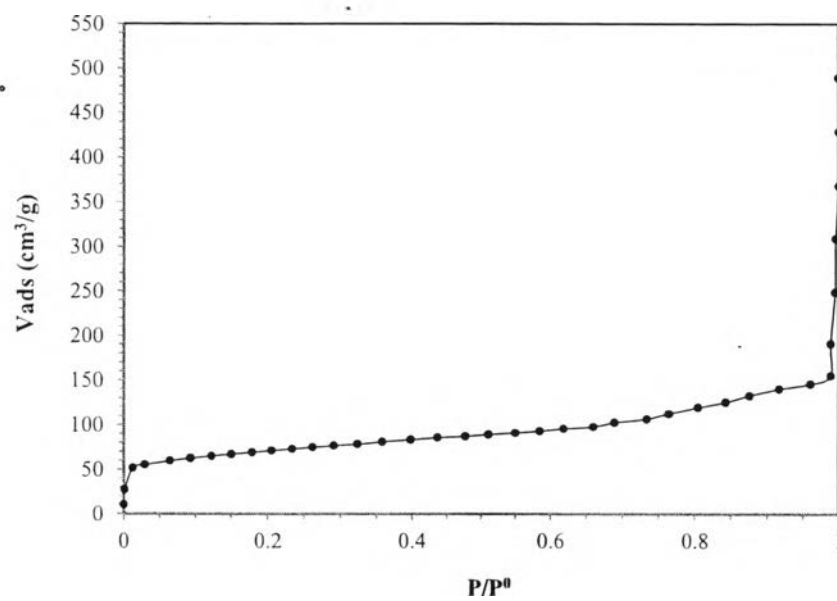
Figure H29 Isotherm of activated carbon from PEHA-derived PBZ.
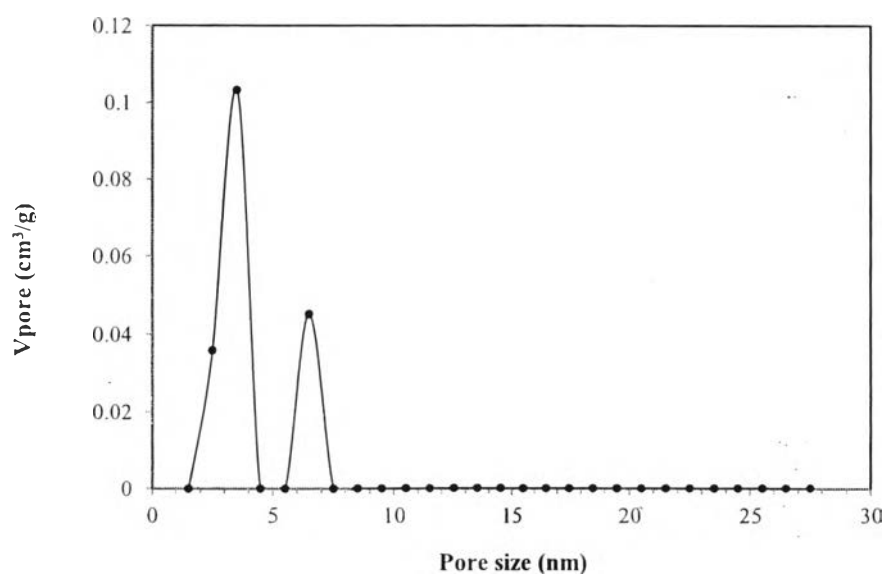
Figure H30 Barrett-Joyner-Halenda pore size distribution of activated carbon from PEHA-derived PBZ.
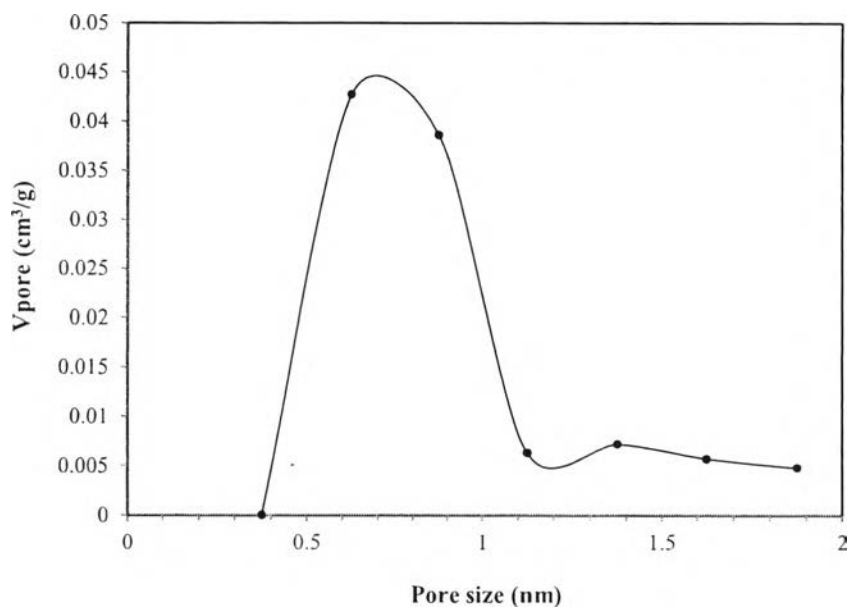
Figure H31 Horvath and Kawazoe pore size distribution of activated carbon from PEHA-derived PBZ.

30 wt% PEHA-derived PBZ carbon aerogel
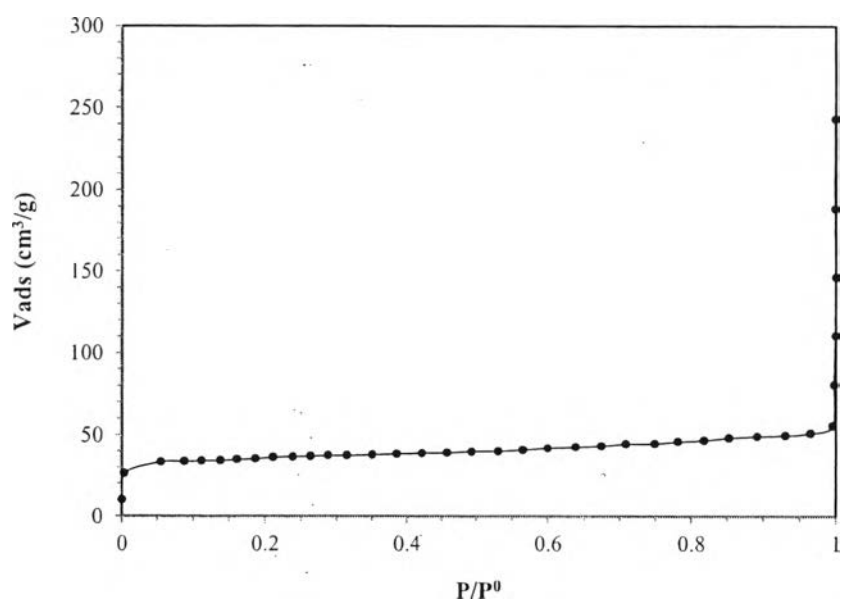
Figure H32 Isotherm of a 30 wt% PEHA-derived PBZ carbon aerogel.
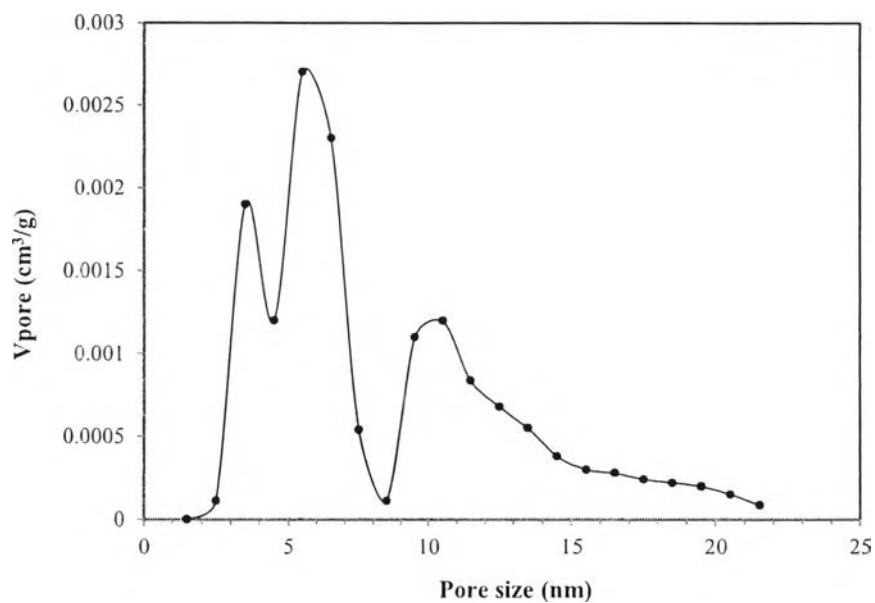
Figure H33 Barrett-Joyner-Halenda pore size distribution of a 30 wt% PEHA-derived PBZ carbon aerogel.
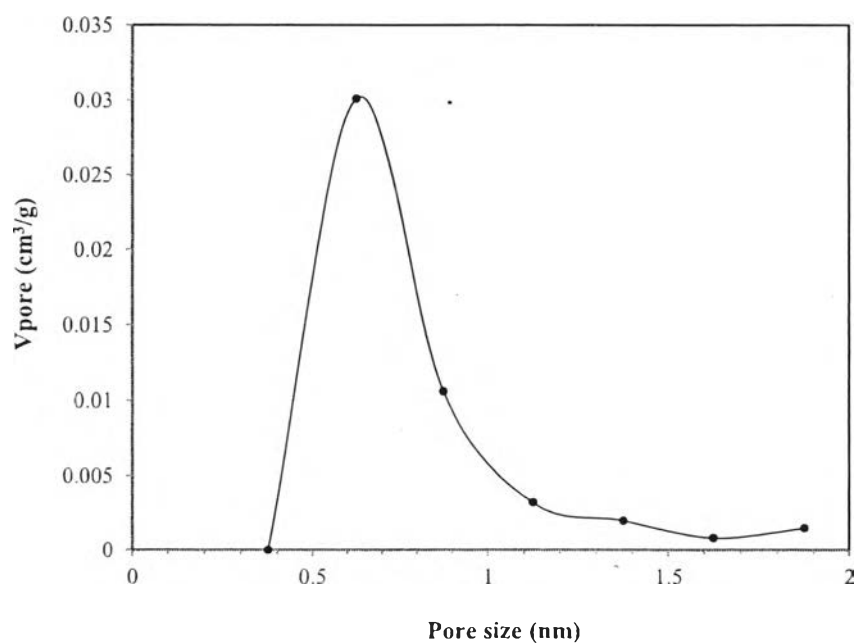
Figure H34 Horvath and Kawazoe pore size distribution of a 30 wt% PEHA-derived PBZ carbon aerogel.

35 wt% PEHA-derived PBZ carbon aerogel
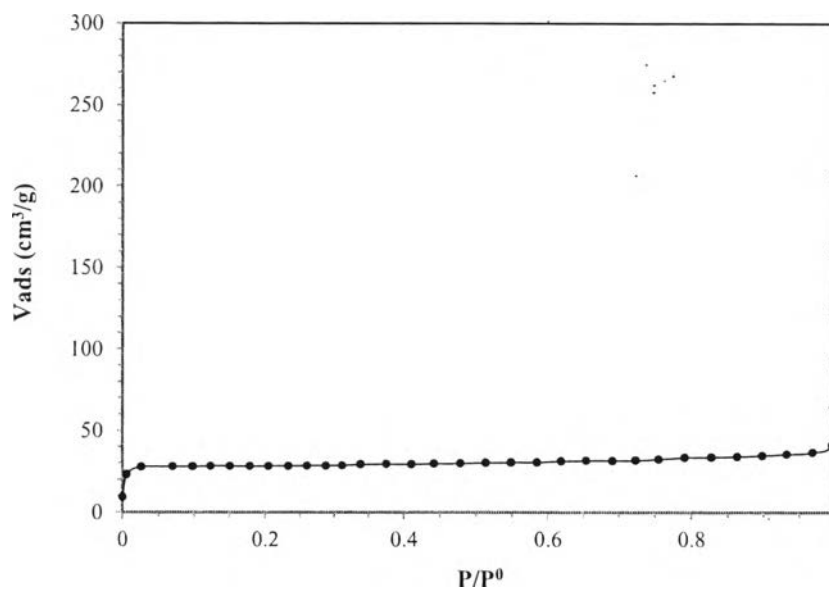
Figure H35 Isotherm of a 35 wt% PEHA-derived PBZ carbon aerogel.
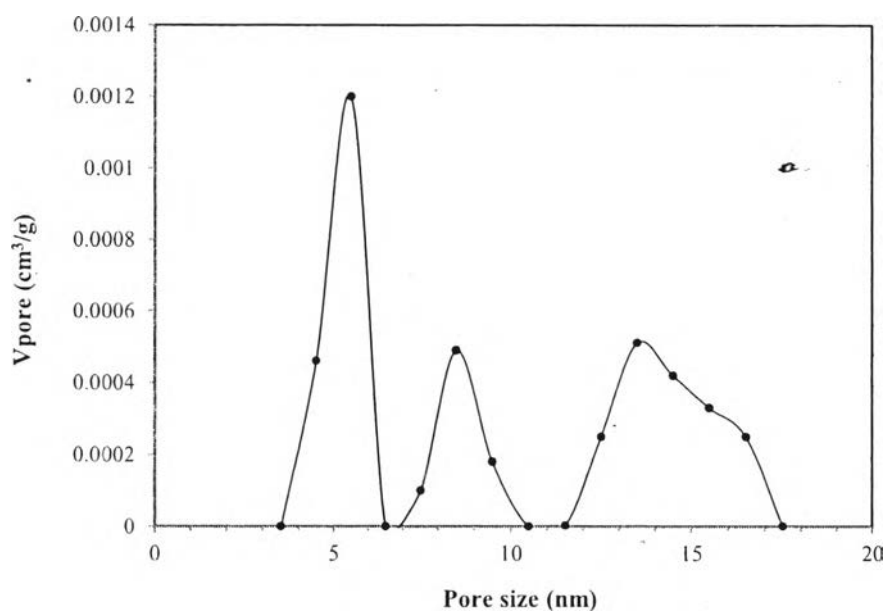
Figure H36   Barrett-Joyner-Halenda pore size distribution of a 35 wt% PEHA-derived PBZ carbon aerogel.
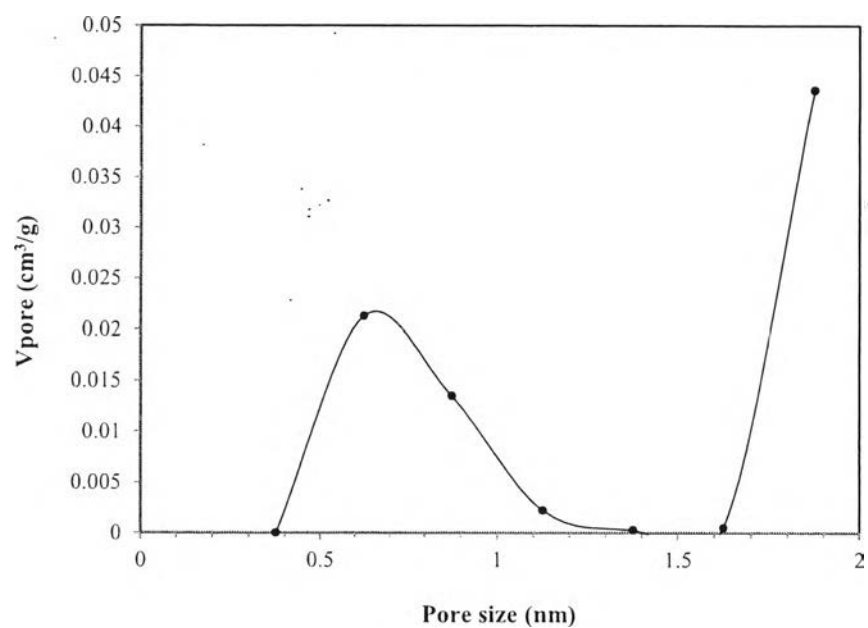
Figure H37 Horvath and Kawazoe pore size distribution of a 35 wt% PEHA-derived PBZ carbon aerogel.

40 wt% PEHA-derived PBZ carbon aerogel
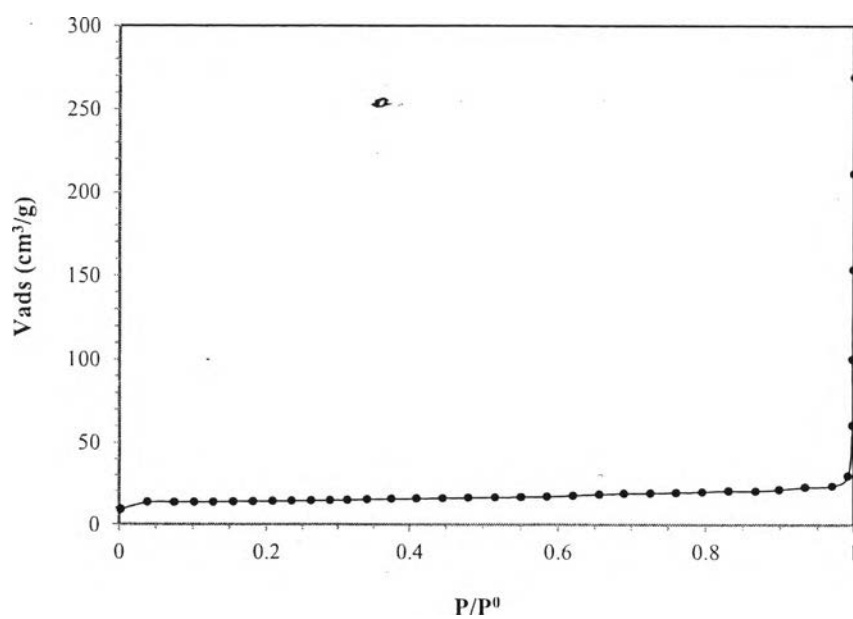
Figure H38 Isotherm of a 40 wt% PEHA-derived PBZ carbon aerogel.
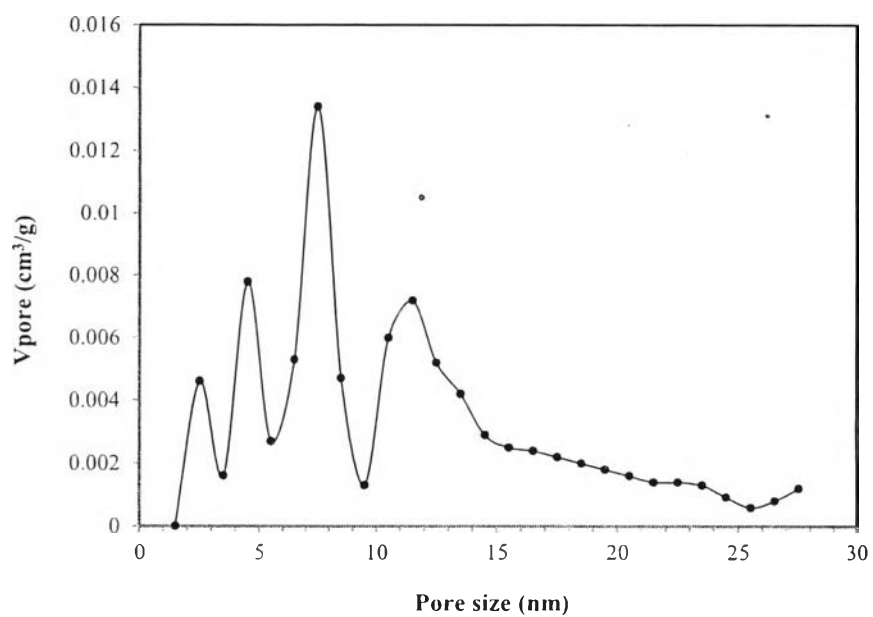
Figure H39   Barrett-Joyner-Halenda pore size distribution of a 40 wt% PEHA-derived PBZ carbon aerogel.
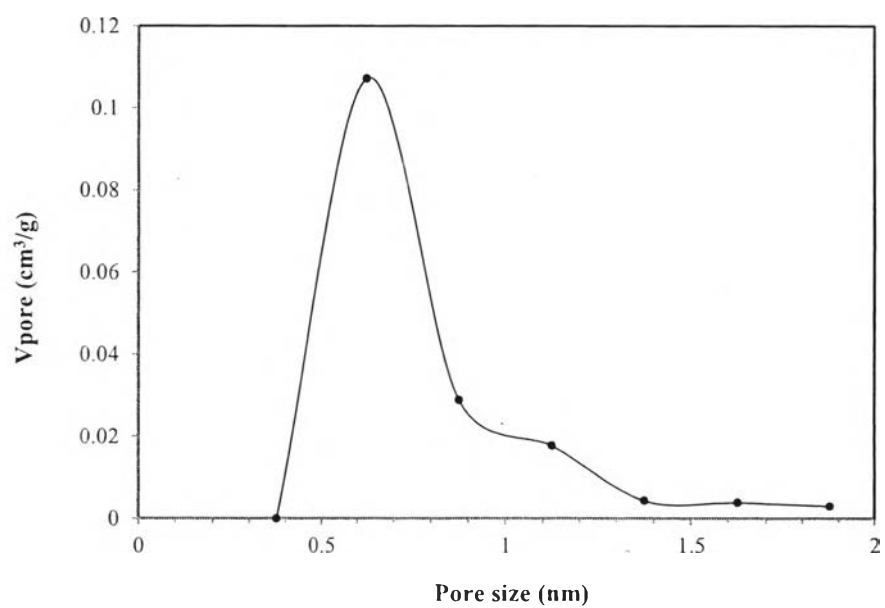
Figure H40   Horvath and Kawazoe pore size distribution of a 40 wt% PEHA-derived PBZ carbon aerogel.

Activated carbon from DETA-derived PBZ at activation temperature of **900** °C
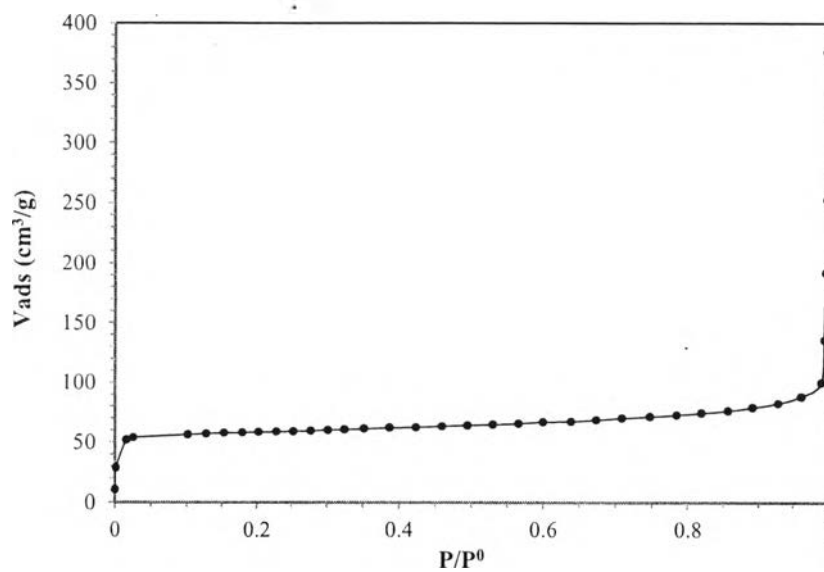
Figure H41 Isotherm of activated carbon from DETA-derived PBZ at activation temperature of 900 °C.
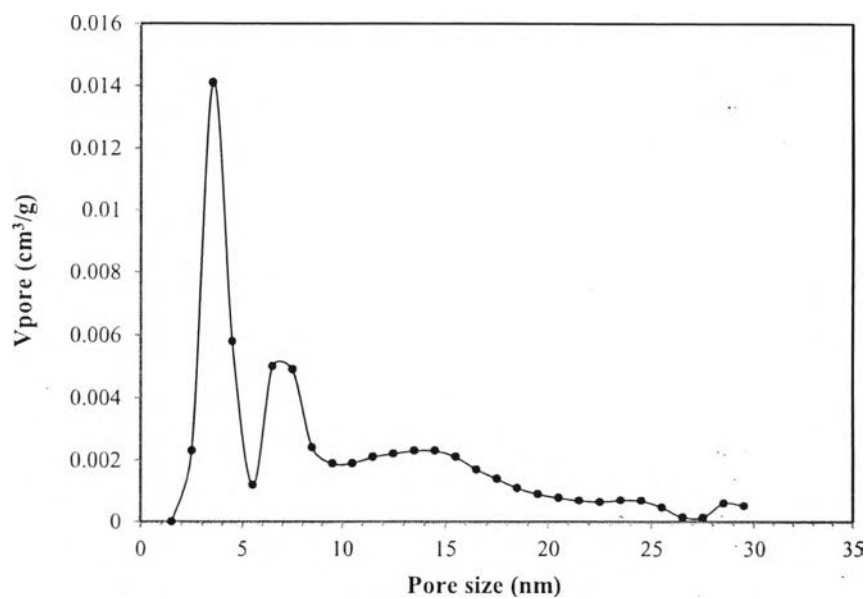
Figure H42 Barrett-Joyner-Halenda pore size distribution of activated carbon from DETA-derived PBZ at activation temperature of 900 °C.
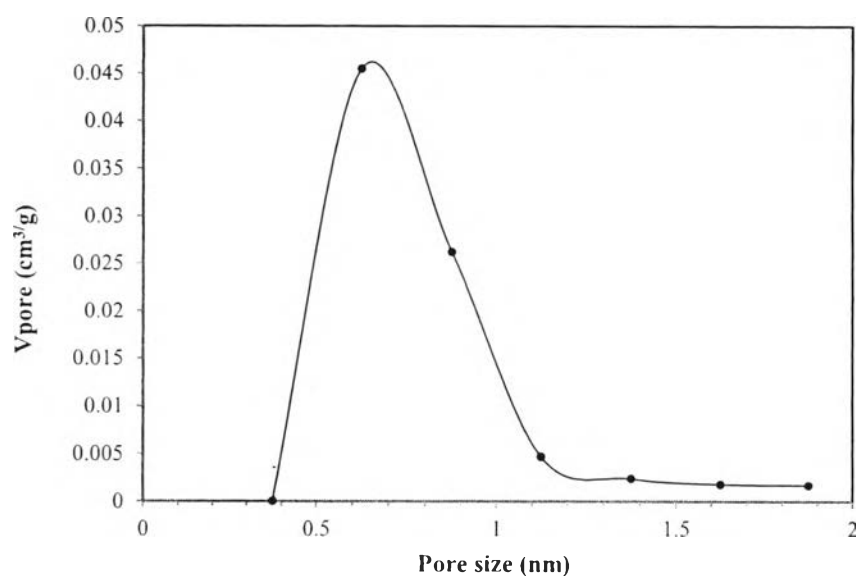
Figure H43 Horvath and Kawazoe pore size distribution of activated carbon from DETA-derived PBZ at activation temperature of 900 °C.

30 wt% DETA-derived PBZ carbon aerogel at activation temperature of 900 °C
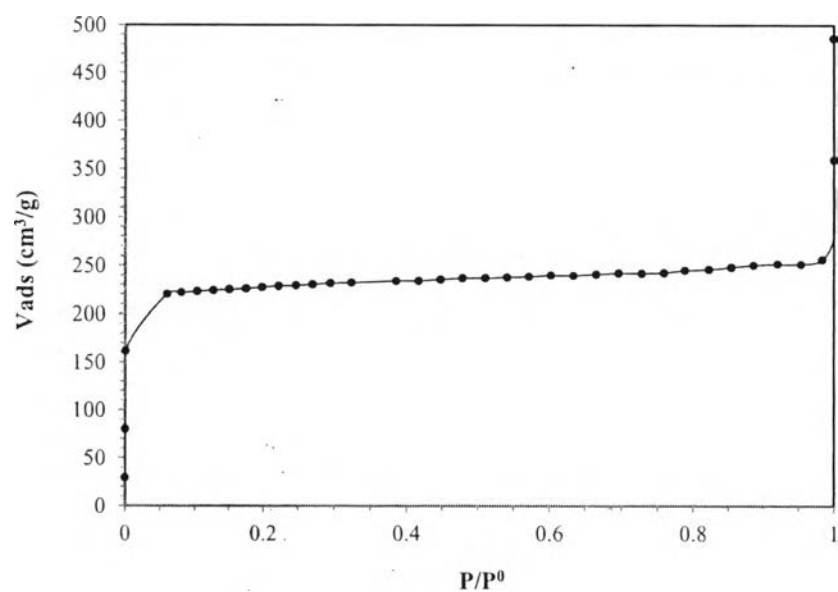
Figure H44 Isotherm of a 30 wt% DETA-derived PBZ carbon aerogel at activation temperature of 900 °C.
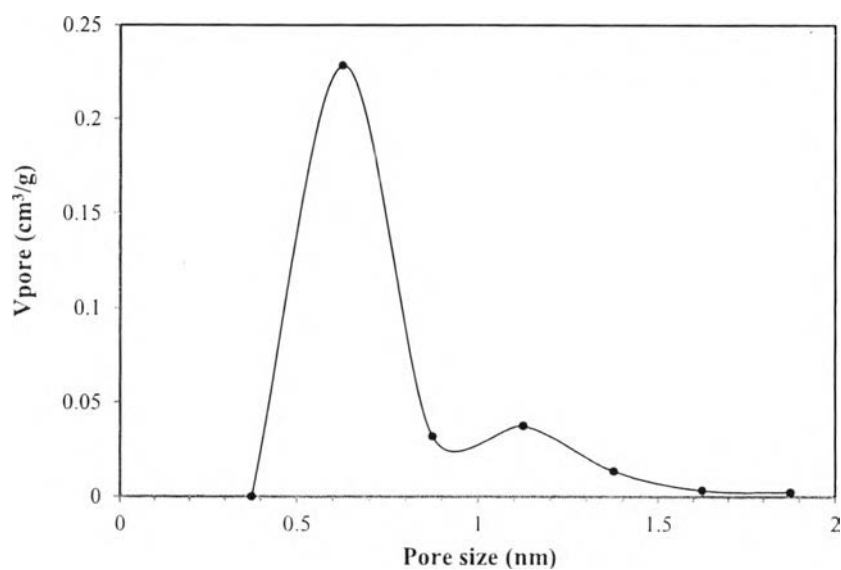
Figure H45 Horvath and Kawazoe pore size distribution of a 30 wt% DETA-derived PBZ carbon aerogel at activation temperature of 900 °C.

30 wt% DETA-derived PBZ carbon aerogel loading with non-ionic surfactant at activation temperature of 900 °C
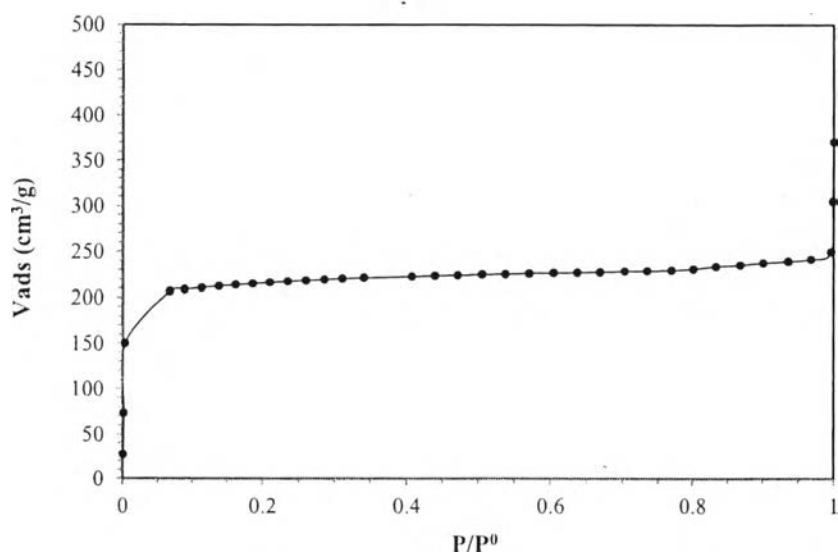
Figure H46 Isotherm of a 30 wt% DETA-derived PBZ carbon aerogel loading with non-ionic surfactant at activation temperature of 900 °C.
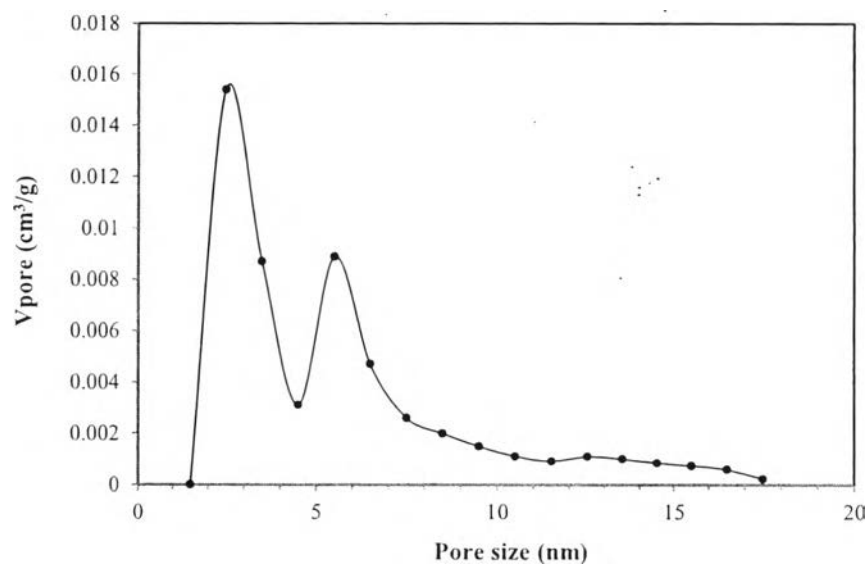
Figure H47 Barrett-Joyner-Halenda pore size distribution of a 30 wt% DETA-derived PBZ carbon aerogel loading with non-ionic surfactant at activation temperature of 900 °C.
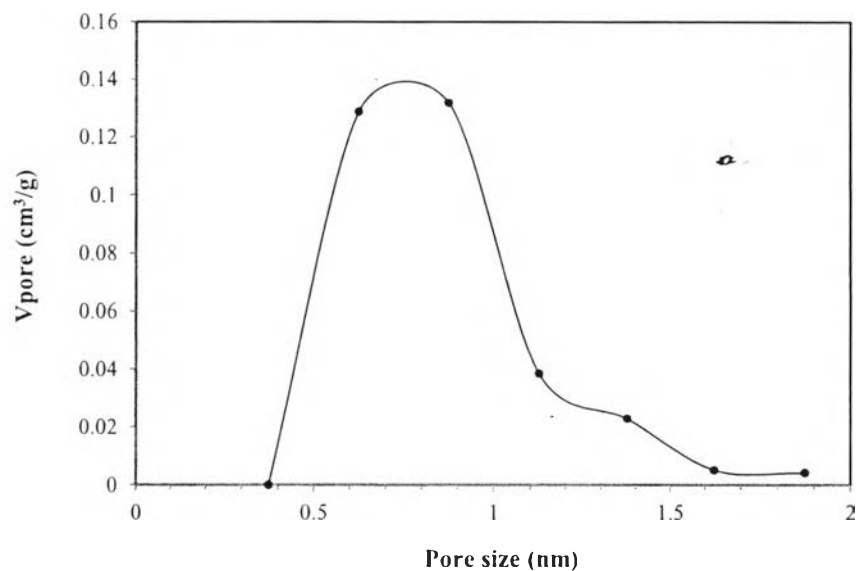
Figure H48 Horvath and Kawazoe pore size distribution of a 30 wt% DETA-derived PBZ carbon aerogel loading with non-ionic surfactant at ac-tivation temperature of 900 °C.

Activated carbon from PEHA-derived PBZ at activation temperature of 900 °C
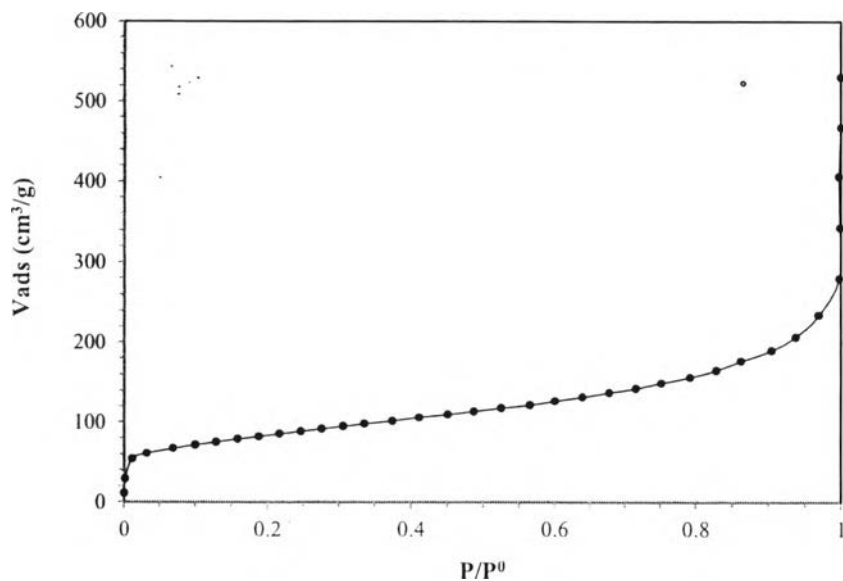
Figure H49 Isotherm of activated carbon from PEHA-derived PBZ at activation temperature of 900 °C.
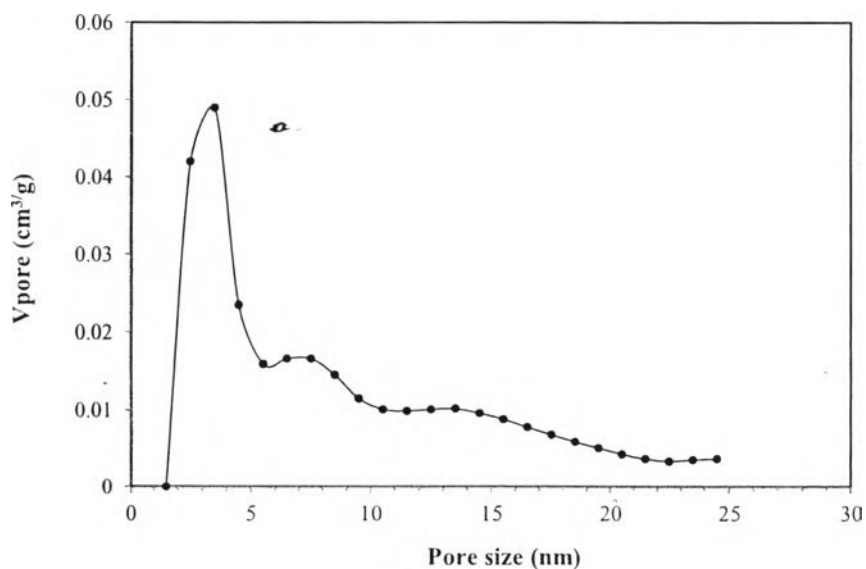
Figure H50 Barrett-Joyner-Halenda pore size distribution of activated carbon from PEHA-derived PBZ at activation temperature of 900 °C.
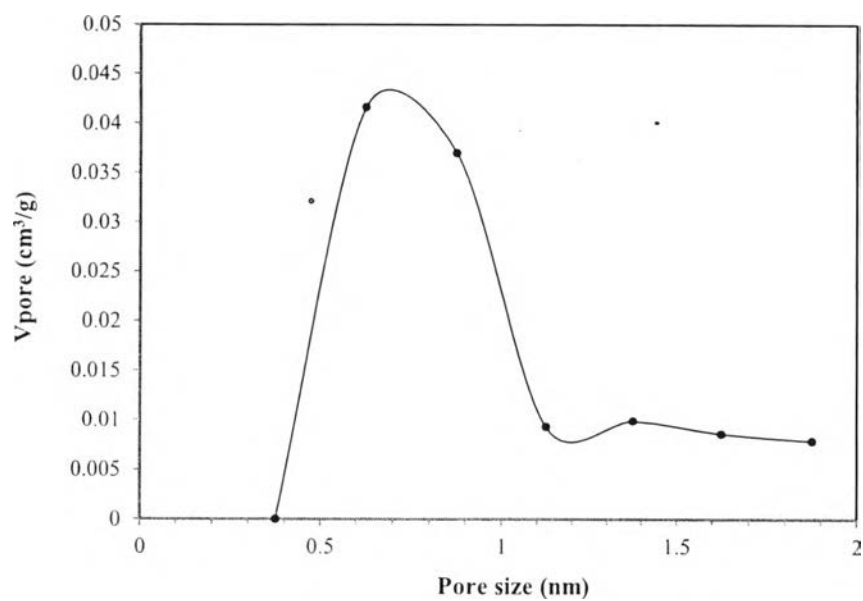
Figure H51 Horvath and Kawazoe pore size distribution of activated carbon from PEHA-derived PBZ at activation temperature of 900 °C.

30 wt% PEHA-derived PBZ carbon aerogel at activation temperature of 900 °C
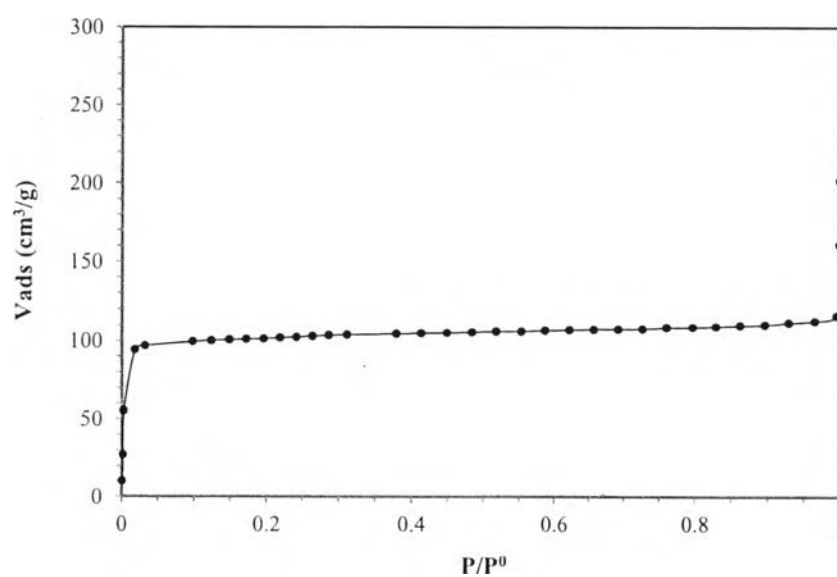
Figure H52 Isotherm of a 30 wt% PEHA-derived PBZ carbon aerogel at activation temperature of 900 °C.
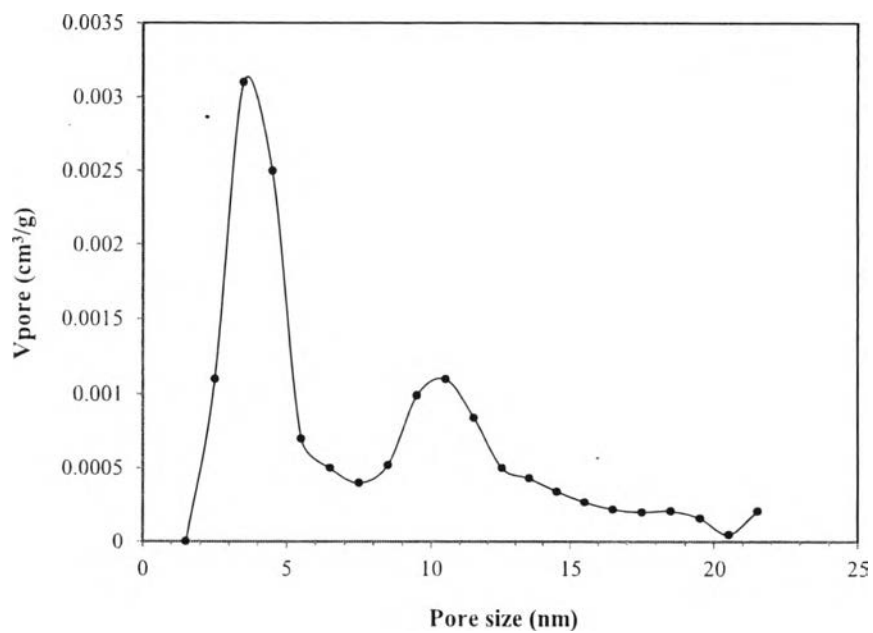
Figure H53 Barrett-Joyner-Halenda pore size distribution of a 30 wt% PEHA-derived PBZ carbon aerogel at activation temperature of 900 °C.
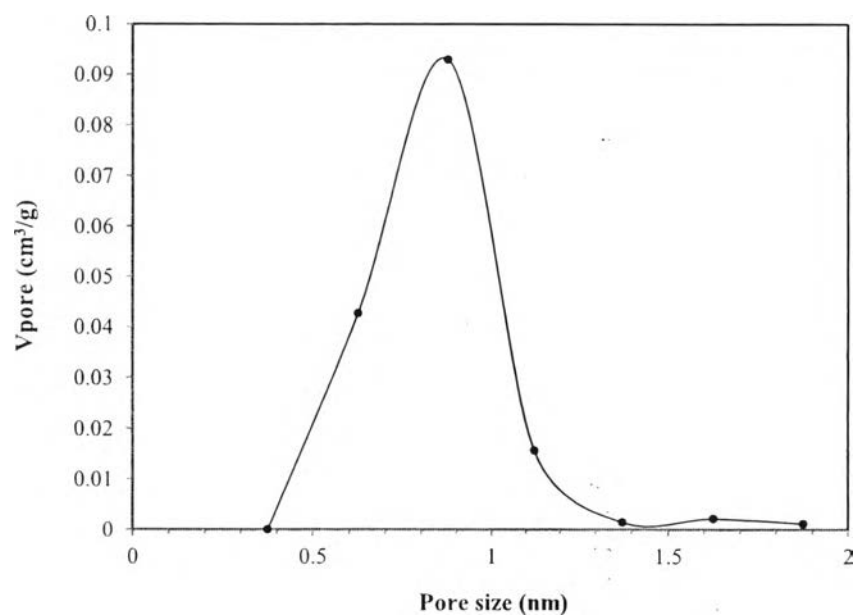
Figure H54 Horvath and Kawazoe pore size distribution of a 30 wt% PEHA-derived PBZ carbon aerogel at activation temperature of 900 °C.

30 wt% PEHA-derived PBZ carbon aerogel loading with non-ionic surfactant at activation temperature of 900 °C
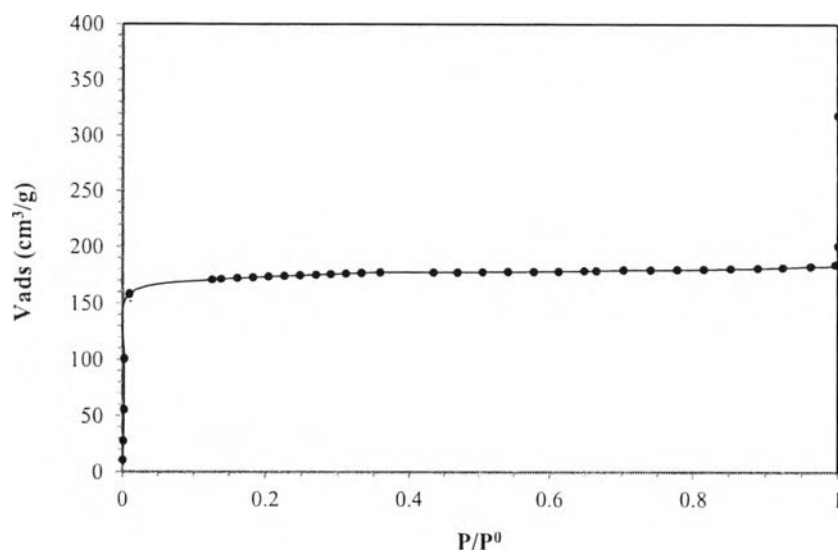
Figure H55 Isotherm of a 30 wt% PEHA-derived PBZ carbon aerogel loading with non-ionic surfactant at activation temperature of 900 °C.
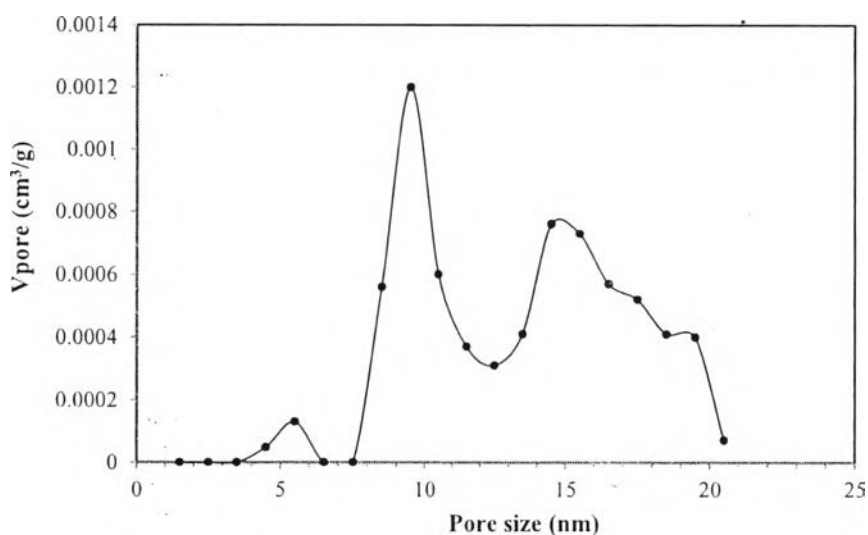
Figure H56 Barrett-Joyner-Halenda pore size distribution of a 30 wt% PEHA-derived PBZ carbon aerogel loading with non-ionic surfactant at activation temperature of 900 °C.
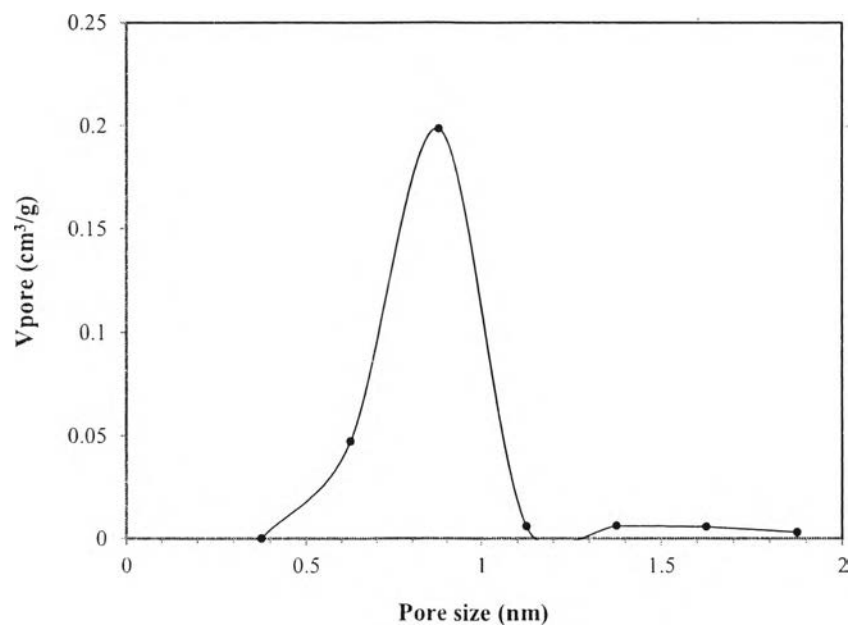
Figure H57 Horvath and Kawazoe pore size distribution of a 30 wt% PEHA-derived PBZ carbon aerogel loading with non-ionic surfactant at ac-tivation temperature of 900 °C.

Appendix I Adsorption/Desorption Isotherms of all Materials
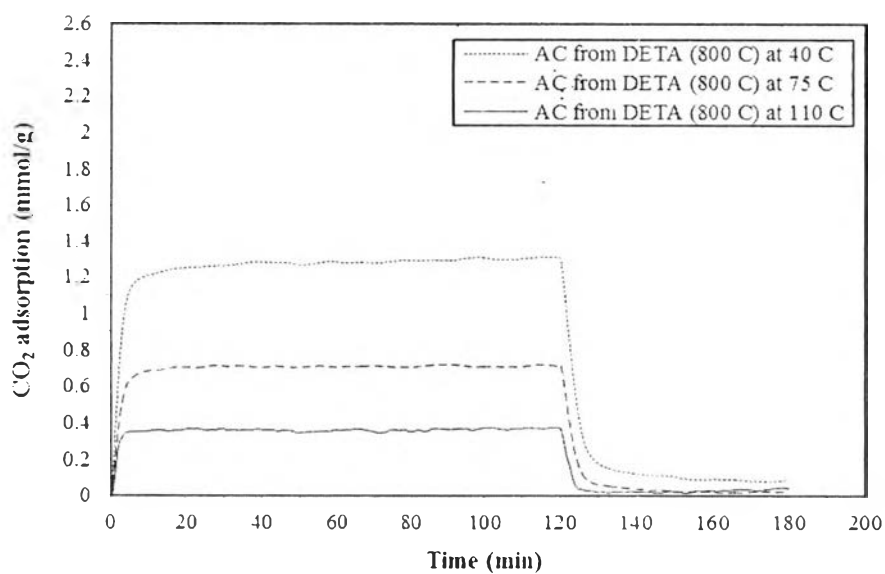
Figure I1 Adsorption/desorption isotherms of DETA-derived activated carbons at activating temperature of 800 °C (at 40, 75, 110 °C and 1 bar).
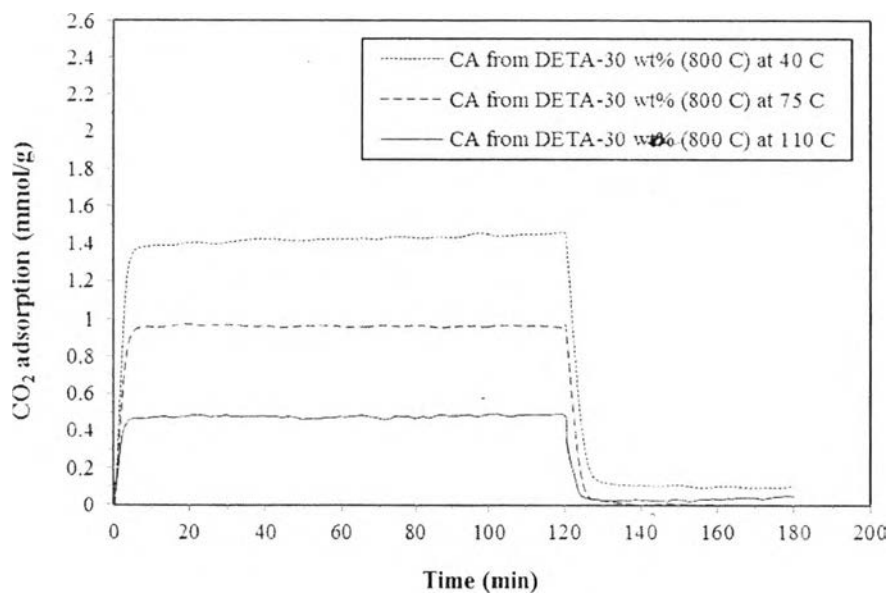
Figure I2 Adsorption/desorption isotherms of carbon aerogels from 30 wt% DETA-derived PBZ at activating temperature of 800 °C (at 40, 75, 110 °C and 1 bar).
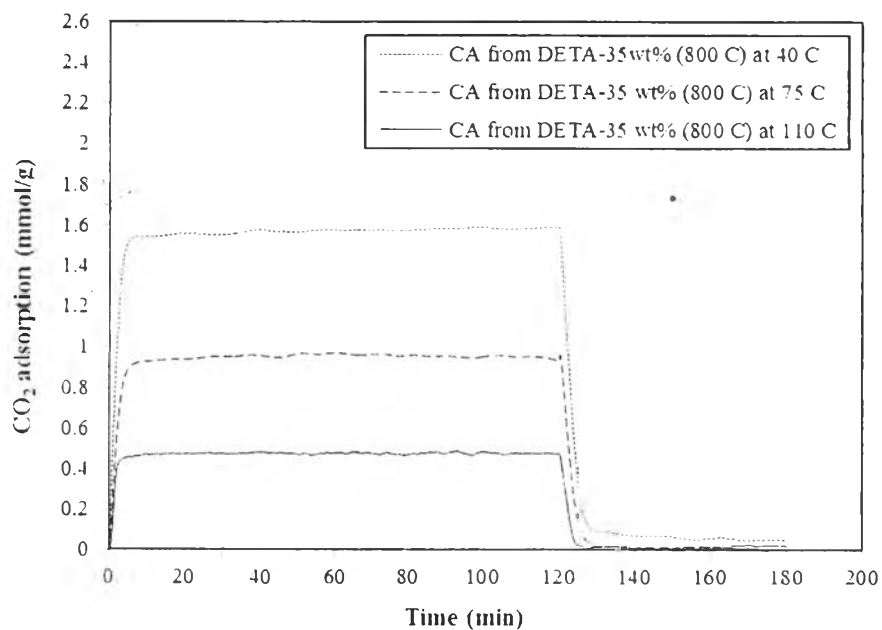
Figure I3 Adsorption/desorption isotherms of carbon aerogels from 35 wt% DETA-derived PBZ at activating temperature of 800 °C (at 40, 75, 110 °C and 1 bar).
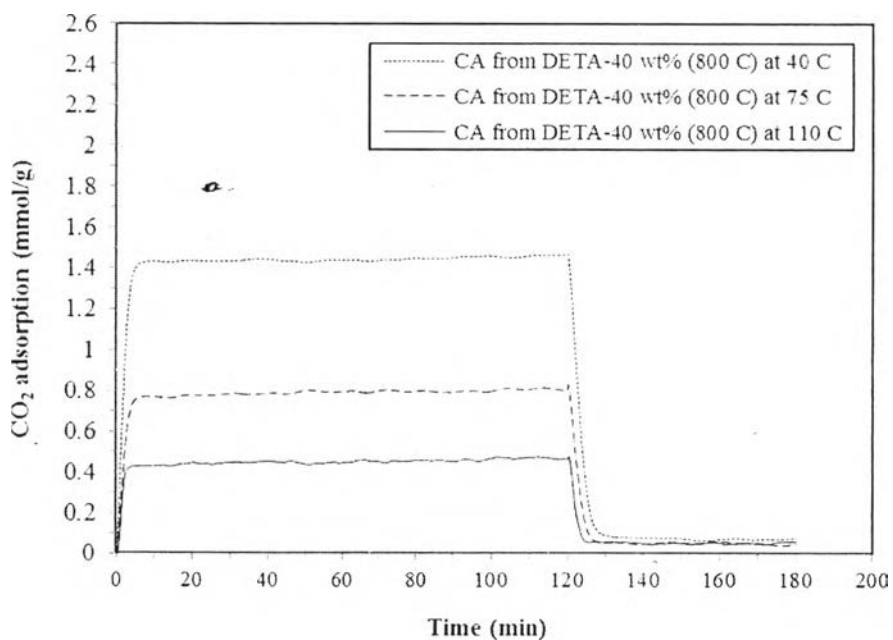
Figure I4 Adsorption/desorption isotherms of carbon aerogels from 40 wt% DETA-derived PBZ at activating temperature of 800 °C (at 40, 75, 110 °C and 1 bar).
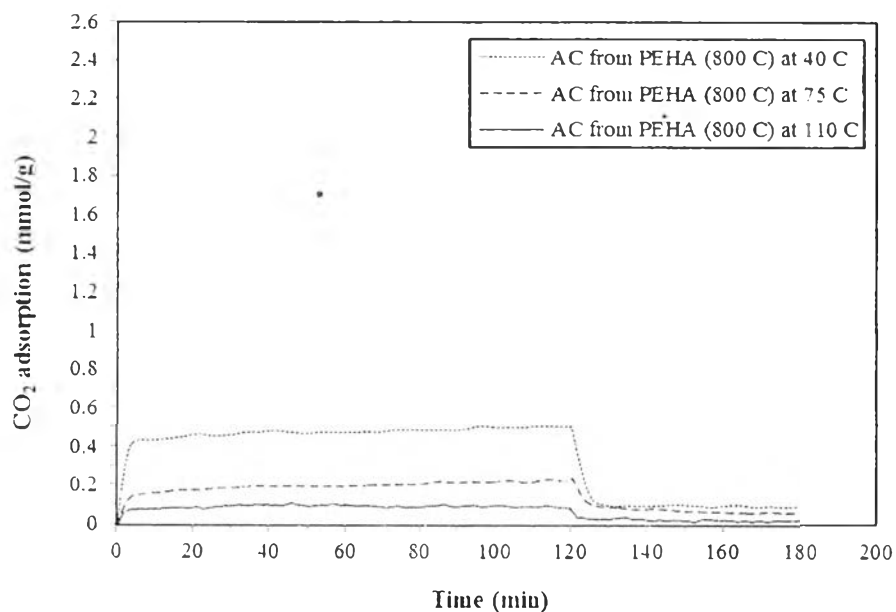
Figure I5 Adsorption/desorption isotherms of PEHA-derived activated carbons at activating temperature of 800 °C (at 40, 75, 110 °C and 1 bar).
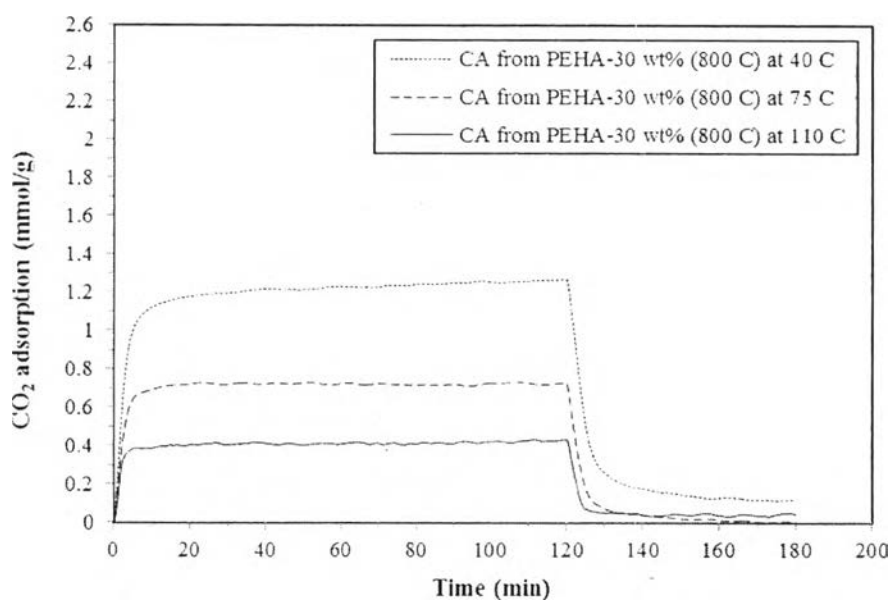
Figure I6 Adsorption/desorption isotherms of carbon aerogels from 30 wt% PEHA-derived PBZ at activating temperature of 800 °C (at 40, 75, 110 °C and 1 bar).
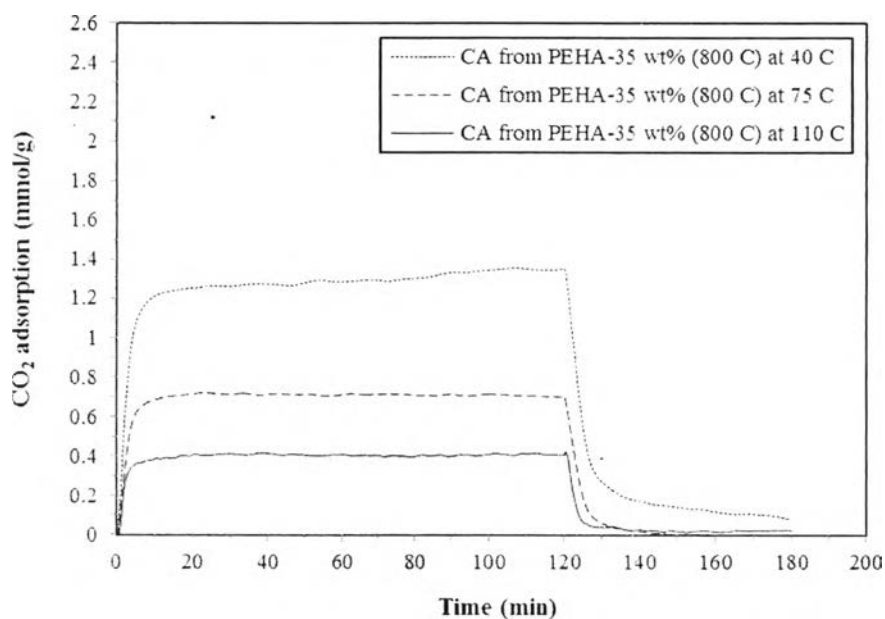
Figure I7 Adsorption/desorption isotherms of carbon aerogels from 35 wt% PEHA-derived PBZ at activating temperature of 800 °C (at 40, 75, 110 °C and 1 bar).
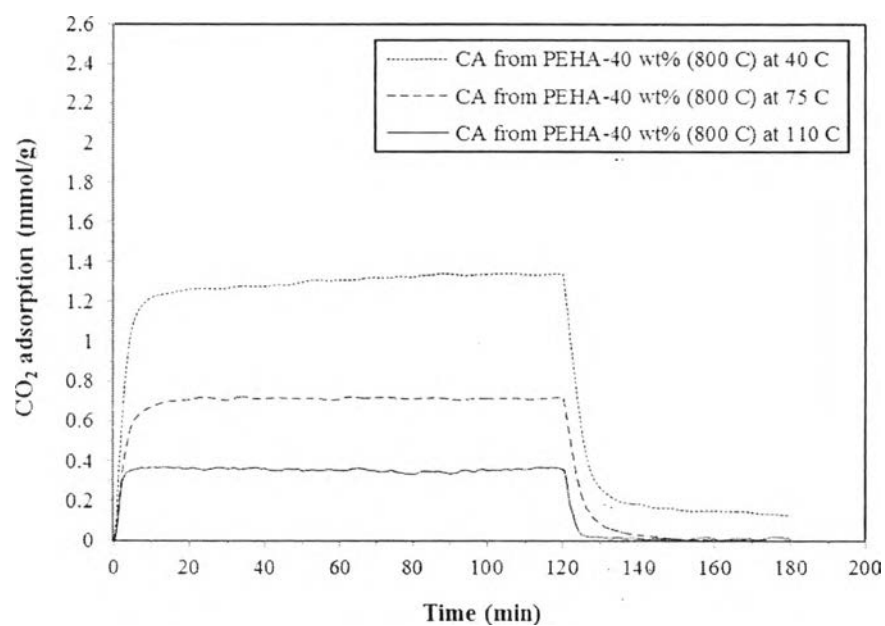
Figure I8 Adsorption/desorption isotherms of carbon aerogels from 40 wt% PEHA-derived PBZ at activating temperature of 800 °C (at 40, 75, 110 °C and 1 bar).
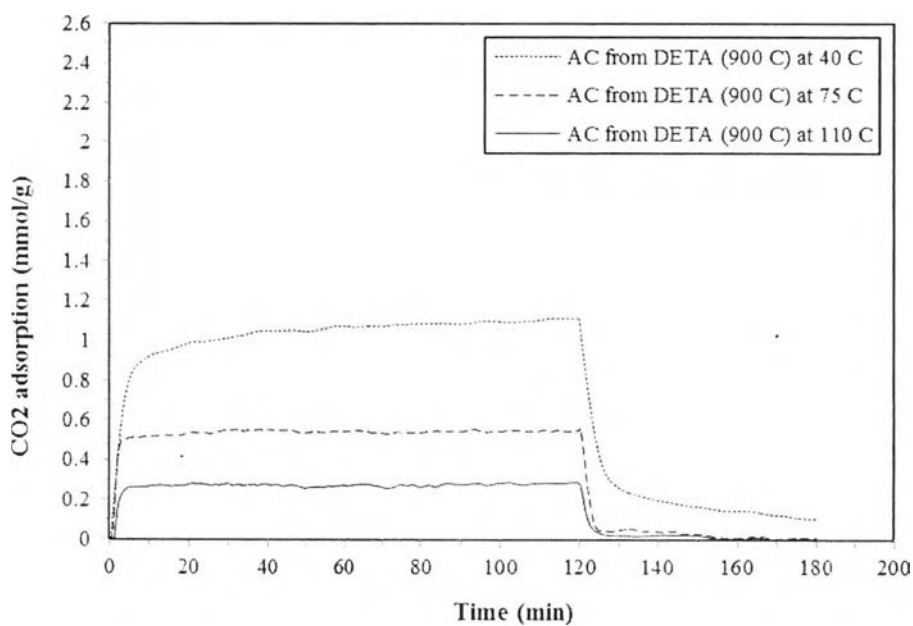
Figure 19 Adsorption/desorption isotherms of DETA-derived activated carbons at activating temperature of 900 °C (at 40, 75, 110 °C and 1 bar).
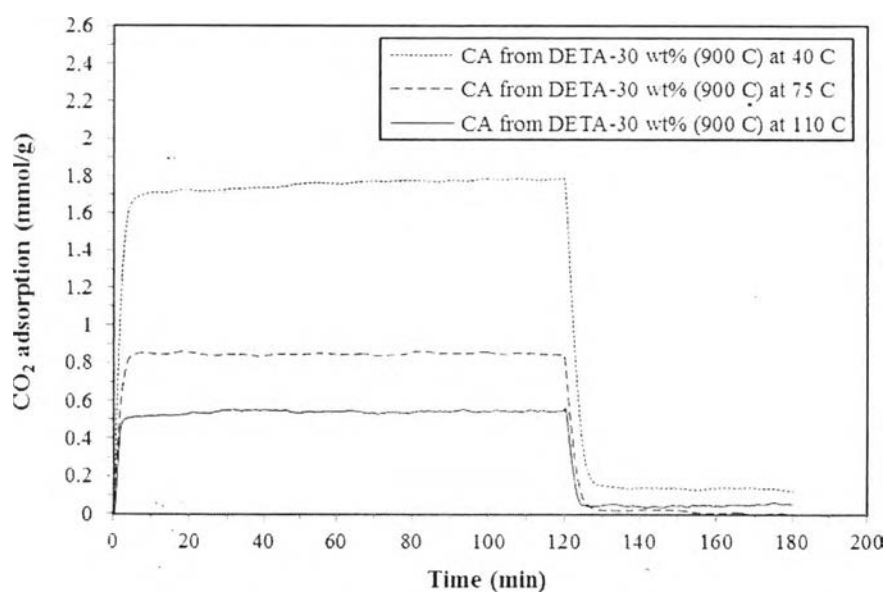
Figure 110 Adsorption/desorption isotherms of carbon aerogels from 30 wt% DETA-derived PBZ at activating temperature of 900 °C (at 40, 75, 110 °C and 1 bar).
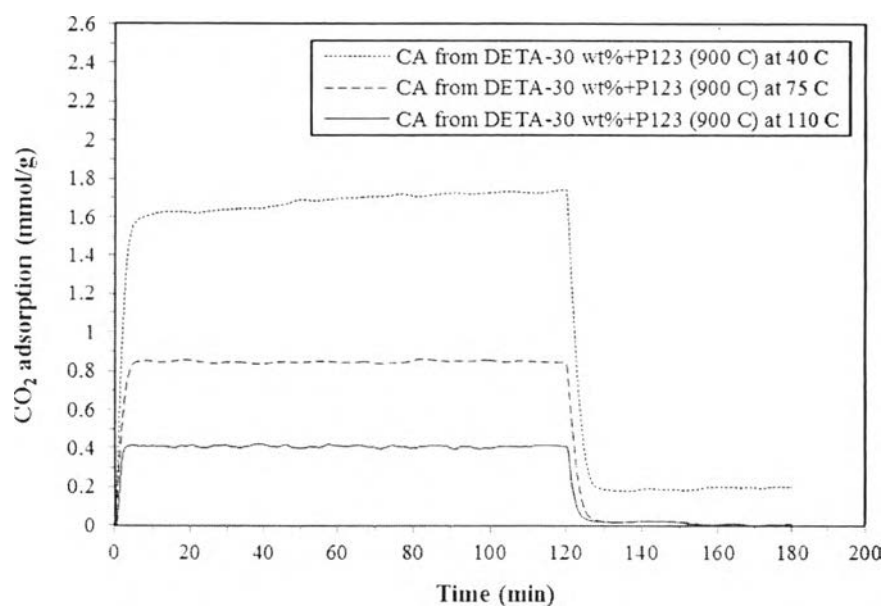
Figure I11 Adsorption/desorption isotherms of carbon aerogels from 30 wt% DETA-derived PBZ loading non-ionic surfactant at activating temperature of 900 °C (at 40, 75, 110 °C and 1 bar).
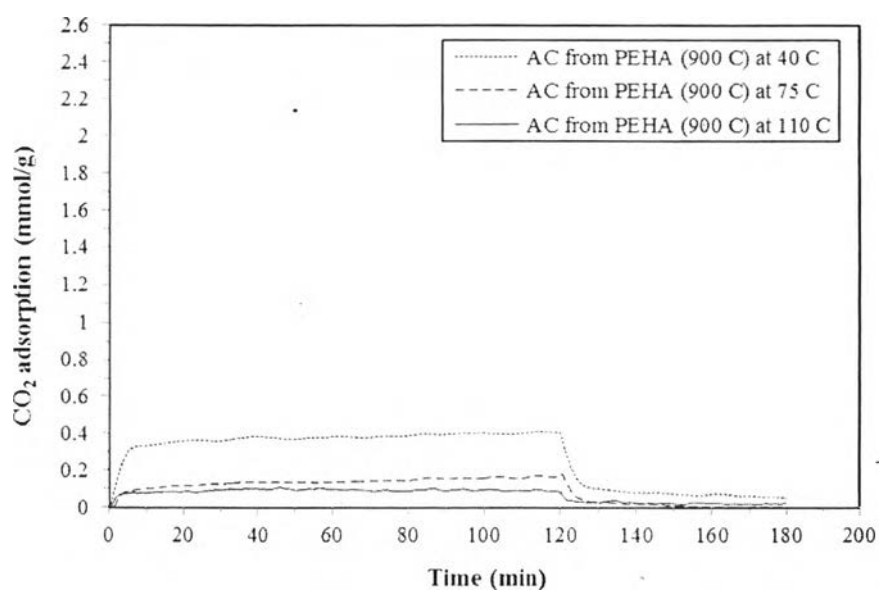
Figure I12 Adsorption/desorption isotherms of PEHA-derived activated carbons at activating temperature of 900 °C (at 40, 75, 110 °C and 1 bar).
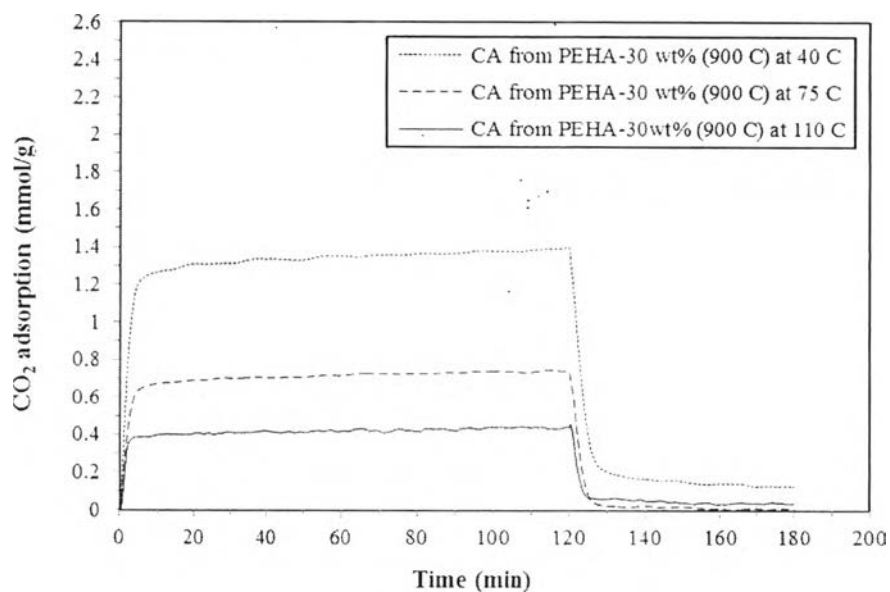
Figure I13 Adsorption/desorption isotherms of carbon aerogels from 30 wt% PEHA-derived PBZ at activating temperature of 900 °C (at 40, 75, 110 °C and 1 bar).
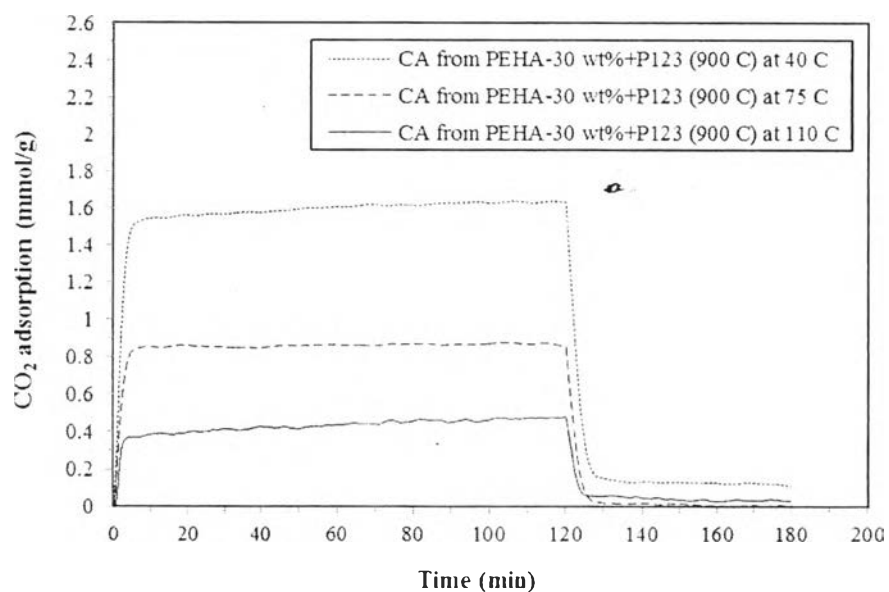
Figure I14 Adsorption/desorption isotherms of carbon aerogels from 30 wt% PEHA-derived PBZ loading non-ionic surfactant at activating temperature of 900 °C (at 40, 75, 110 °C and 1 bar).

Appendix J SEM Images of all Materials
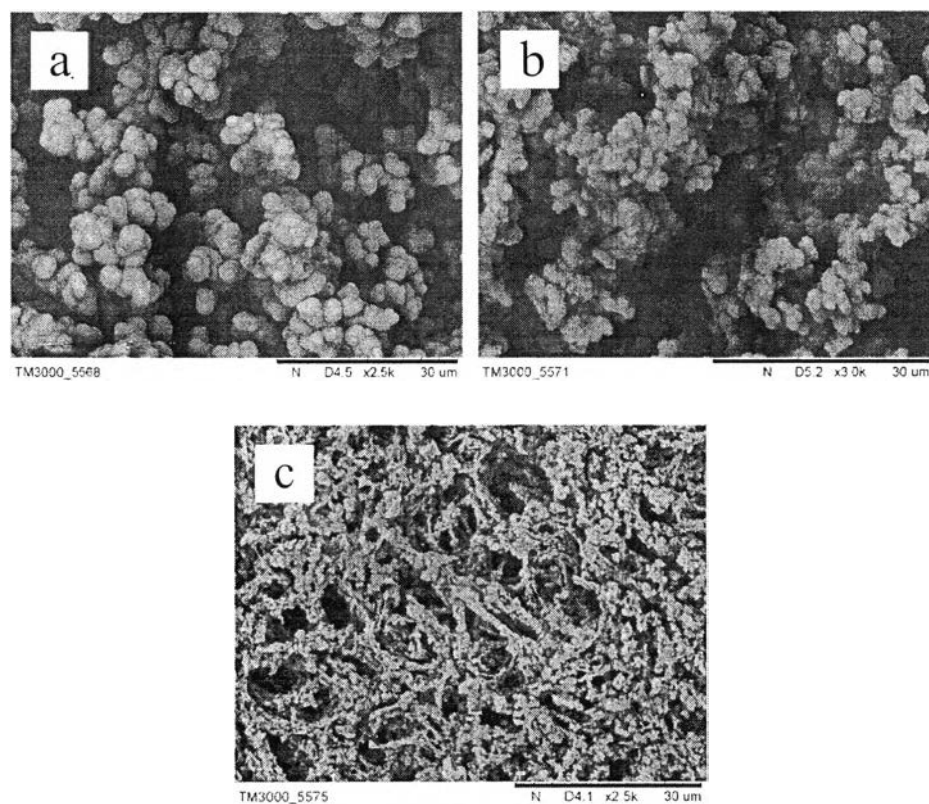
Figure J1 SEM images of (a) fully cured DETA-derived PBZ aerogel at 20 wt%, (b) 25 wt%, and (c) 30 wt% of monomer solutions.
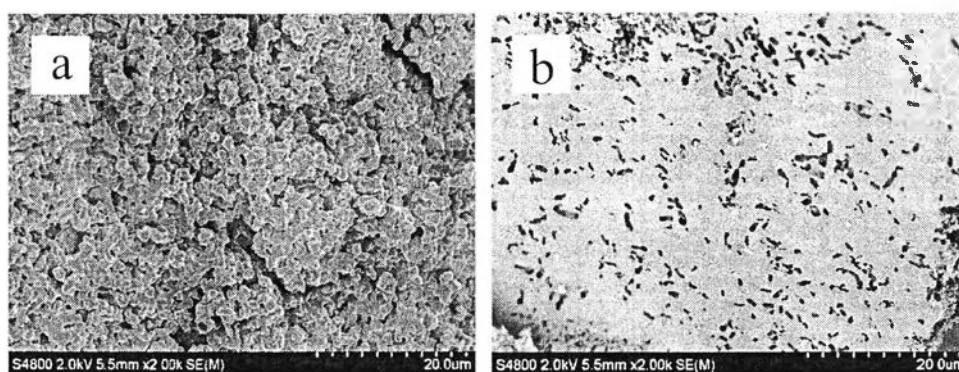
Figure J2 SEM images of (a) activated carbon from DETA-derived PBZ and (b) activated carbon from PEHA-derived PBZ at activating temperature of 800 °C.
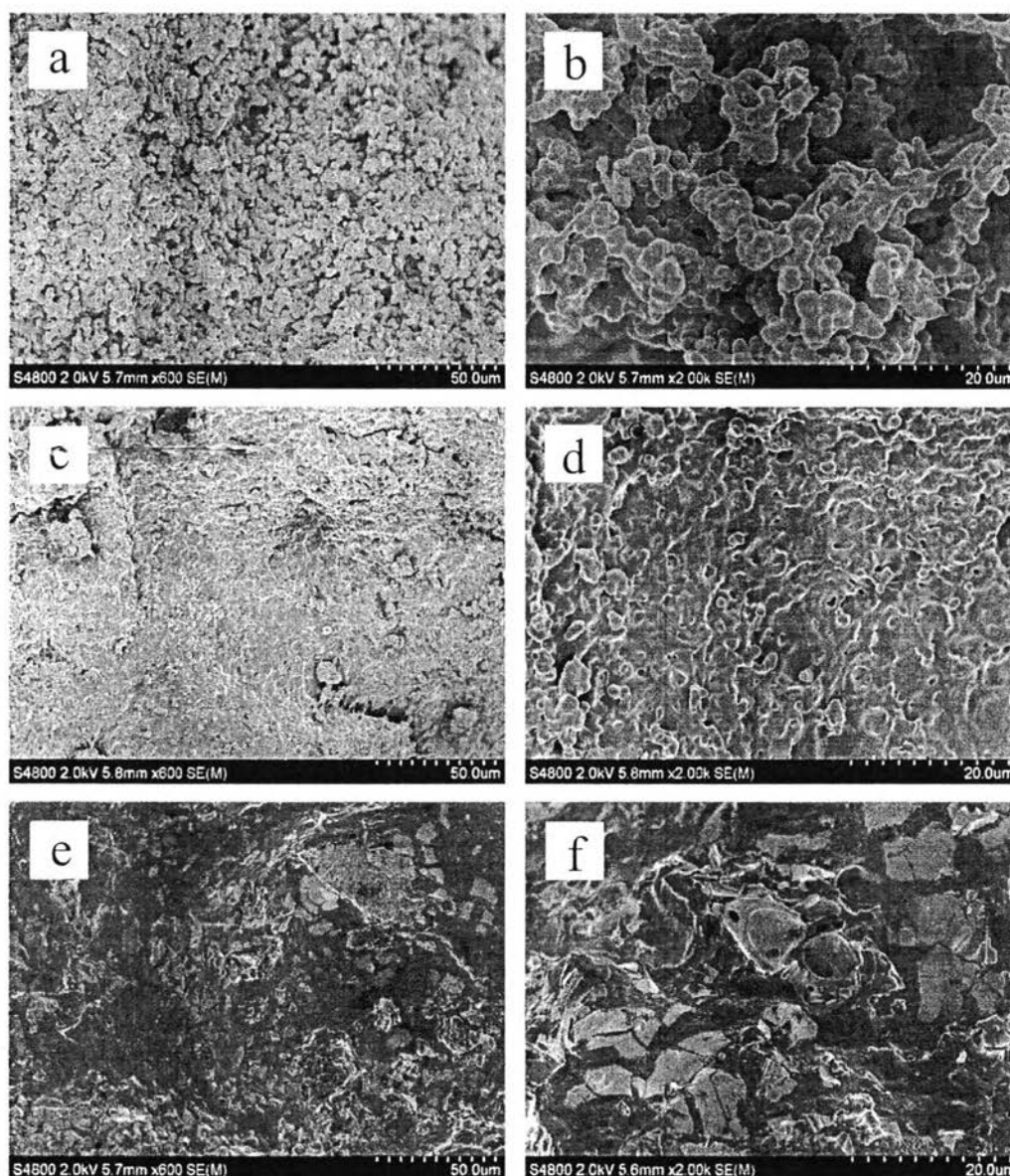
Figure J3 SEM images of (a) DETA-derived PBZ carbon aerogel at 30 wt%, (b) 30 wt%, (c) 35 wt%, (d) 35 wt%, (e) 40 wt%, and (f) 40 wt% of monomer solutions at activating temperature of 800 °C; low magnification for (a), (c), and (e); high magnification for (b), (d), and (f).
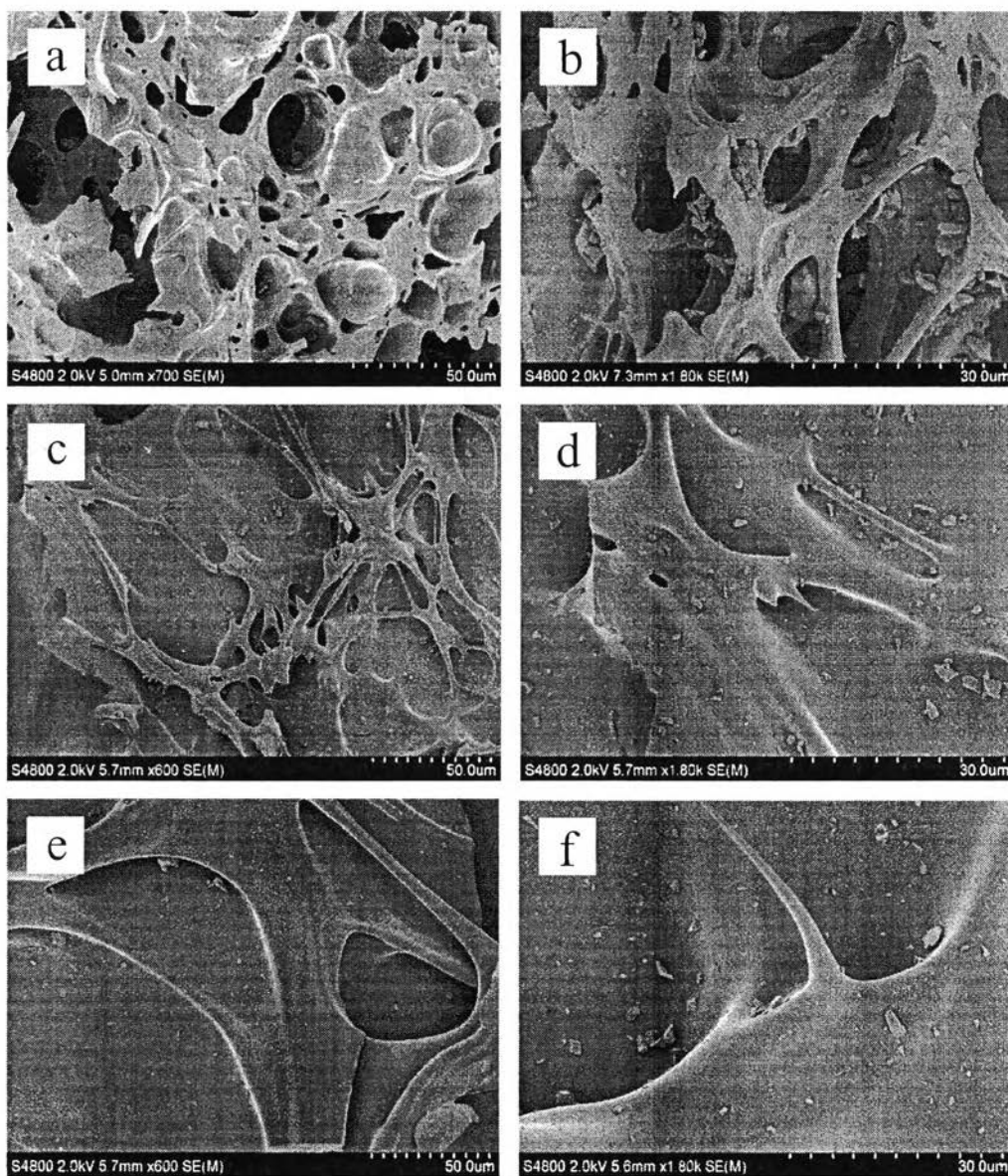
Figure J4 SEM images of (a) PEHA-derived PBZ carbon aerogel at 30 wt%, (b) 30 wt%, (c) 35 wt%, (d) 35 wt%, (e) 40 wt%, and (f) 40 wt% of monomer solutions at activating temperature of 800 °C; low magnification for (a), (c), and (e); high magnification for (b), (d), and (f).
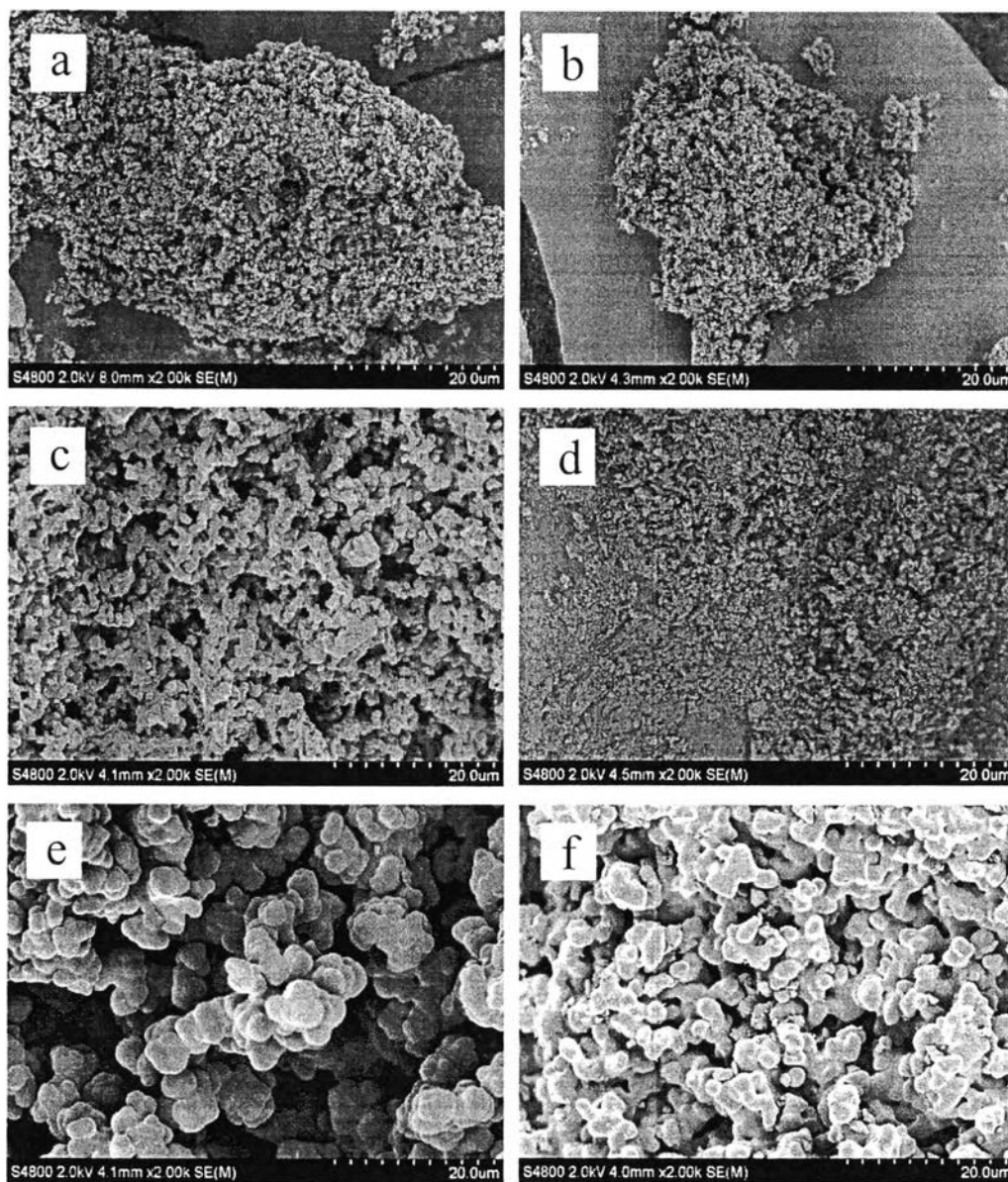
Figure J5 SEM images of (a) activated carbon from DETA-derived PBZ, (b) activated carbon from PEHA-derived PBZ, (c) DETA-derived PBZ carbon aerogel at 30 wt% (d) PEHA-derived PBZ carbon aerogel at 30 wt%, (e) DETA-derived PBZ carbon aerogel at 30 wt% loading non-ionic surfactant, and (f) PEHA-derived PBZ carbon aerogel at 30 wt% loading non-ionic surfactant at activating temperature of 900 °C.

CURRICULUM VITAE

Name: Ms. Nittada Jungsawat

Date of Birth: March 5, 1991

Nationality: Thai

University Education:

2009–2012   Bachelor Degree of Petrochemicals and Polymeric

Materials, Faculty of Engineering Technology,

Silpakorn University, Bangkok, Thailand

Work Experience (trainee):

2012   Position: Process Engineer

Company name: Polyplex (Thailand) Public Co. Ltd

Proceedings:

1. Jungsawat, N.; and Suriyapraphadilok, U. (2015, April 21) Improvement of the surface properties of phenol-diethylenetriamine-based carbon aerogels for carbon dioxide adsorption application. Proceedings of The 6th Research Symposium on Petroleum, Petrochemicals and Advanced Materials and The 21st PPC Symposium on Petroleum, Petrochemicals, and Polymers, Bangkok, Thailand.